Implementation of Non-Ergodic Ground Motion Prediction Equations in Probabilistic Seismic Hazard Analysis for France

Work Package 5 - PSHA

AUTHORS		REVIEW		APPROVAL	
Name	Date	Name	Date	Name	Date
Chih-Hsuan Sung *Norman Abrahamson*		*Chritophe Martin*	*19/02/2021*	Emmanuel Viallet *Public access* ◉ *SIGMA-2 restricted* ○	2021/08/26

Document history

DATE	VERSION	COMMENTS
2020/09/07	0	*Initial version*
2021/02/09	1	*Revision after SIGMA-2 scientific committee review*

Executive Summary

The available earthquake data in the M2 to M5.2 range are used to develop an initial non-ergodic ground-motion model for France. Because most of the magnitudes of the French database are small (Mw = 2.0 − 5.2), the non-ergodic model is developed for the average horizontal Fourier Amplitude Spectral values (called EAS) rather than for the response spectral accelerations. The scaling of PSA depends on the spectral shape, the linear source, path, and site effects will not have the same scaling on the PSA values for small and large magnitudes; however, using the EAS can avoids the scaling issue being affected by differences in the response spectral shape. The non-ergodic EAS model includes source, site, and path terms. In this study, an ergodic EAS ground-motion model (GMM) is first developed to use as a reference model for evaluating the regional differences. A California GMM for the EAS is used to constrain the extrapolation of the GMM outside the magnitude range covered by the French data. A fully non-ergodic GMM is then developed using a method similar method to Landwehr et al (2016), with a modification for anisotropic path effects. The non-ergodic model shows that using the French data set, about 60% of the aleatory variance in the ergodic model is due to systematic source, path, and site effects, consistent with data sets from other regions.

Examples hazard results are shown for eight sites in France for 5 Hz and 1Hz using a non-ergodic version of the program HAZ45. Using a non-ergodic GMM, there is a large reduction in the aleatory standard deviation, but there is also a shift in the median from each source location that can be either positive (large median) or negative (smaller median). The differences between the ergodic and non-ergodic hazard results are larger at 5 Hz than at 1 Hz. At the 1×10^{-4} annual frequency of exceedance, there tends to be a reduction in the hazard using the non-ergodic GMM, but at some sites, there will be an increase in the hazard if there is an increase in the medians for the controlling sources that offsets the reduction in the aleatory standard deviation at the 1×10^{-4} annual frequency of exceedance.

The next step for this task is to complete the verification of the non-ergodic probabilistic seismic hazard analysis (PSHA) codes by comparing hazard results from OpenQuake with those from HAZ45.

Table of content

1. Introduction

As ground-motion data sets have grown over the past decade, there has been a trend of moving from ergodic to non-ergodic ground-motion models (GMMs). For example, the 2008 Next Generation Attenuation West-1 (NGA-W1) GMMs developed for crustal earthquakes (Power et.al., 2008) were fully ergodic models that were applied to all regions within the same broad tectonic category. Six years later, with a much larger data set available, four of the 2014 Next Generation Attenuation West-2 (NGA-W2) GMMs for crustal earthquakes (Abrahamson et. al., 2014; Boore et al, 2014; Campbell and Bozorgnia, 2014; Chou and Youngs, 2014) included regional differences in four terms of the GMMs: constant term, large distance scaling, the V_{S30} scaling, and the basin depth scaling. Within broad regions, there are still regional differences in the median ground motion on a scale of 10s of km. This has led to the development of non-ergodic GMMs in which the median ground motion depends on the coordinates of the source and the site.

Non-ergodic GMMs have a significantly smaller aleatory variability compared to ergodic GMMs. This reduction in the aleatory variability has been seen in many studies with different data sets: Atkinson (2006), Morikawa (2008), Anderson and Uchiyama (2011), Lin et al. (2011), and Lanzano et. al. (2017). These previous studies have shown that for a specific site and earthquake pair, the variance of the aleatory variability is only 30-40% of the ergodic variance, indicating that most of the variability treated as randomness in ergodic GMMs is actually due to systematic source, path, and site effects.

Partially non-ergodic GMMs that only account for the systematic site effects have been developed (e.g., Rodgriez-Marek et al., 2013; Kotha et al., 2016; Sung and Lee, 2019). The single-station sigma approach that has been used in seismic hazard studies for nuclear power plants and dams over the past ten years (e.g, Renault et al., 2010; BCHydro 2012; Coppersmith et al., 2014; Bommer et al., 2015; Geopentech, 2015; Tromans et al., 2019; and NCREE 2018). The reduced aleatory variability for the partially non-ergodic approach is called the single-station standard deviation. Using single-station variance, about 30% - 40% of the variance of the ergodic model is removed as compared to 60-70% for the fully non-ergodic case. The site-specific site effect is then included as an adjustment to the median using either results from analytical site response analysis or residuals from empirical ground-motion data recorded at the site.

For PSHA applications with the single-station standard deviation approach, the hazard is computed for a reference rock site condition with the ergodic GMM for the median and with a reduced standard deviation. The single-station standard deviation approach is straight forward to implement in a PSHA because it only involves changing the standard deviation of the GMM and incorporating the site-specific site effect which applies to all sources.

Fully non-ergodic GMMs account for the systematic source and path effects in addition to the systematic site effect. Because the source and path effects depend on the location of the source and the site, the

coefficients for the non-ergodic GMM depend on the latitude and longitude of the source and the site. This makes implementation of a fully non-ergodic GMM into PSHA more complicated and requires modification to the PSHA software. Under Work Package 5, this study conducts a trial PSHA implementation of a non-ergodic GMM for France.

In this study, there are four main tasks: (1) develop an ergodic GMM for France that serves as the reference model; (2) develop a non-ergodic GMM for France, sampling the epistemic uncertainty in the median; (3) modify the PSHA computer program HAZ45 to implement the non-ergodic GMM; (4) conduct example PSHA calculations.

2. Data Set

2.1 RESIF database

We use the processed ground-motion data from the Réseau Sismologique et géodésique Français (RESIF) data set, which includes more than 6500 recordings from 468 earthquakes recorded at 379 stations in Metropolitan France between 1996 and 2016. This dataset includes data recorded by accelerometric and broadband sensors (RESIF, 1995a, b), including 177 permanent stations (RA and FR network codes) and 202 temporary stations (X7 and YP network codes) in France. The dataset is available as a version-numbered flat file containing the metadata, the response spectra for several damping values, and the Fourier amplitude spectra (Traversa et al., 2020).

Two methods for the conversion to moment magnitude were used based on the year of the earthquake: For earthquakes that occurred in France between 1996 to 2009, the moment magnitude was provided by the Sismicité Instrumentale de l'Hexagone (Si-Hex) project (Cara et al., 2015). For earthquakes that occurred after 2009, the moment magnitude was estimated using the conversion equation proposed by Grunthal et al. (2009). The magnitude conversions are given in the SIGMA2-2019-D3-028 report (Bremaud and Traversa, 2019). **Figure 1** shows a map with the event and station locations in the data set that were selected.

For the ground-motion model, the site conditions are parameterized by the time-averaged shear-wave velocity over the top 30 meters (V_{S30}); however, V_{S30} measurements are not available for most of the stations in the RESIF data set. For the stations without measured V_{S30}, we used the estimates from the global V_{S30} map (https://earthquake.usgs.gov/data/vs30/) of the United States Geological Survey (USGS) which uses the topographic slope as a proxy for the V_{S30} (Wald and Allen, 2007 and Allen and Wald, 2009). **Figure 2** shows the global V_{S30} values from USGS in France and also shows the final V_{S30} values at each station. As we will estimate the site-specific site terms as part of the development of the non-ergodic GMM, using proxies for the for V_{S30} is not a key limitation of the study.

The final subset consists of 6044 recordings from 463 earthquakes with the range of M is from 2.0 to 5.2 (ML 2.4 to 5.6), rupture distance (R_{RUP}) between 2 km to 660 km, and Vs30 is from 171 to 3100 m/s (**Figure 3**). The usable frequency band was set based on the filters applied during the data processing. **Figure 4a** shows the total number of useable records at each frequency and also the number of recordings with and without measured V_{S30} values. **Figure 4b** shows a number of useable records for different moment magnitude (M) ranges. Most of the records are in the M3.0 to M4.0 range. The number of useable records at each frequency is also listed in Table 1.

2.2 EAS Ground-Motion Intensity Measure

To have enough data to constrain the non-ergodic terms, data from small magnitudes are used. But why do we need to use Fourier spectral values instead of PSA values to build the GMM? **Figure5a** shows two theoretical source spectrums are based on the omega-squared spectrum (Aki 1967; Brune, 1970) with the stress drop = 100 bar, kappa = 0.02 sec, and Vs = 3600 m/s, from M3 to M7. One of them contains the site amplification (solid lines), and the site amplification function is shown in **Figure 5b**. This site amplification function is from the B/C boundary of Akinson and Boore (2006) with Vs = 760 m/s. Whether it is at M3 or M7, the linear transfer function is the same. That is, the site amplification function does not depend on the magnitude in the FAS; however, for the response spectrum, the site amplification function does depend on the magnitude. As an example, we used the Random Vibration Theory (RVT) to convert the two FAS in **Figure 5a** to the response spectra as shown in **Figure 5c**. We further calculated the site amplification function from the two response spectrums (ratio of the two spectrums per magnitude) and obtained the magnitude dependence in the PSA amplification function as a function of frequency, shown in **Figure 5d**. The main reason for this difference is that the response spectrum is based on the peak of the oscillator response for each period. Therefore, the non-ergodic model is developed for the Fourier spectral values rather than for the PSA values. The non-ergodic FAS model can be converted to a PSA model in a later step using Random Vibration Theory (RVT), but that task belongs in WP3; it is not part of the current WP5 task.

The intensity measured used in the ground-motion model is the "Effective Amplitude Spectrum" (EAS) defined by Goulet et al. (2018). The EAS is an orientation independent measure of the average horizontal-component Fourier amplitude spectrum (FAS) of the ground acceleration given by

$$EAS(f) = \sqrt{\frac{1}{2}[FAS_{H1}(f)^2 + FAS_{H2}(f)^2]}. \tag{1}$$

in which FASH1(f) and FASH2(f) are the FAS of the two as-recorded orthogonal horizontal components of the ground motion, and f is the frequency in Hz. This definition is used to facilitate the later use of RVT to convert the EAS to response spectral values.

The EAS is also smoothed using the Konno and Ohmachi (1998) smoothing window. The weights and window parameter are set to be consistent with those used by PEER for other data sets (Next Generation Attenuation East and NGA-W2 data sets):

$$W(f) = \left(\frac{sin(b\ log10(f/f_c))}{b\ log10(f/f_c)}\right)^4 \tag{2}$$

in which W is the weight defined at frequency f for a window with center frequency fc, and the window parameter (b) is set to b = 0.033. The general scaling of the EAS for 1 Hz and 5 Hz are shown in **Figure 6** as a function of magnitude and distance.

3. Ergodic EAS Ground-Motion Model

The ergodic EAS model for France is based a simplified form of the Bayless and Abrahamson (2019) empirical EAS GMM for shallow crustal earthquakes in California (called BA19). The magnitude scaling in the BA19 functional form is based on the functional form used by Chiou and Youngs (2014) (called CY14) for their GMM for response spectral values, which is able to model magnitude scaling of strong ground motion over the M3 to M8 range. **Figure 7b** shows the results for magnitude scaling of 0.02, 0.3, and 20Hz, which are based on an omega-squared spectrum (Aki, 1967; Brune 1970) from M3 to M7 (**Figure 7a**). There is the apparent quadratic behavior for magnitude scaling in 0.3 Hz. Because of that, most GMMs adopted the quadratic term to define the magnitude scaling, but there would be an issue that the steeper slope for quadratic terms does not extrapolate well to the small magnitude range. In contrast, the magnitude scaling in the CY14 model is a smooth transition scaling model between a slope at the low magnitudes ($c_{3a}M$) and a slope at the large magnitudes (c_2M) in **Figure 7c** (Chiou et al. 2010). The c_m term sets the break in the magnitude scaling between small and large magnitudes. The c_n term controls how sharp is the break in the magnitude scaling. This model includes the similar behavior of the quadratic term and solving the issue of going steeper for small magnitudes.

The functional form used for the French ergodic GMM includes the magnitude scaling, path scaling, linear site amplification, and depth to the top of the rupture (Z_{TOR}) scaling as shown in equation (3):

$$ln(EAS) = c_1 + c_2(\mathbf{M} - 6) + c_3 ln(1 + e^{c_n(c_M - \mathbf{M})}) + c_4 ln(R_{rup} + c_5 cosh(c_6 max(\mathbf{M} - c_{hm}, 0))) + (c_{4a} -$$

$$c_4)ln(\hat{R}) + c_7 R_{rup} + c_8 ln(min(Vs30, 1000)/1000) + c_9 min(Z_{tor}, 20) + \varepsilon, \tag{3}$$

In which M is the moment magnitude; R_{rup} is the shortest distance from the site to the rupture plane in km; $\hat{R} = \sqrt{R_{rup}^2 + c_{RB}^2}$, c_{RB} is the midpoint of the transition in distance scaling, and was set as 50 km from analyses of NGA data sets (Chiou and Youngs, 2008). V_{S30} is in m/s; Z_{tor} is the depth to the top of the rupture plane in km; and ε is the total residual in naturel logarithm units. For simplicity, the basin-

depth scaling and the non-linear site effects in the BA19 functional form are not included. The French ground-motion data are not reliable at long periods (T>1 sec) for which the basin terms are most important. The amplitudes of the ground motions in the French data set are in the linear range, so the nonlinear site terms are not needed for this study, but the nonlinear site terms should be included in a final model for the EAS for applications to soil sites in a seismic hazard analysis.

In the BA19 model, the scaling at large magnitude is controlled by five terms: c_2, c_5, c_6, c_n, and c_m. The c_2 term is the scaling for large magnitudes. The c_5 and c_6 terms are finite-fault terms for the saturation at short distances. $c_5 \cosh(c_6 \max(M - c_{hm}, 0))$ also like the transition formula, which is varying smoothly from a constant at small magnitudes to large magnitudes. Because there are no data from large magnitude earthquakes in France, the coefficients of the large magnitude scaling for the French ergodic GMM are constrained to the values for the BA19 model (c_2, c_5, c_6, c_n, and c_{hm}). c_3 term is not the scaling for small magnitudes, it is the transition formula mentioned previously in the **Figure 7c**, so c_3 = (c_2 - c_{3a})/c_n (Chiou and Youngs, 2010). For long distances, the $(c_{4a} - c_4)ln(\hat{R})$ term is the transition formula between the S waves and the surface waves. c_{RB} is the midpoint of the transition in distance scaling in the $ln(\hat{R})$. We also follow the CY14's assumption that c_{RB} = 50 km and c_{4a} = −0.5.

In the regression, we used the maximum-likelihood technique based on the random-effects approach (Brillinger and Preisler 1984, 1985; Abrahamson and Youngs, 1992) to estimate the coefficients for the GMM in the statistical software R (Pinheiro et al., 2020). This procedure leads to the separation of total residuals (ε) into between-event residuals (δB), between-site residuals ($\delta S2S$), and within-site residuals (δWS) (Al Atik et al., 2010; Villani and Abrahamson, 2015).

The number of useable recordings decays quickly for frequencies less than 1 Hz. Therefore, the coefficients are only estimated for frequencies greater than or equal to 1 Hz. For frequencies less than 1 Hz (0.1 Hz to 0.9 Hz), we adopt the coefficients from the BA19 model which are only shown in **APPENDIX A**. This approach allows us to move forward with the EAS GMM for France, but it needs to be further evaluated. The resulting ergodic model coefficients from 1 Hz to 23.5 Hz are listed in **Table 1** and are shown in **Figure 8**.

As an example, the residuals for the ergodic GMM for the EAS at 5 Hz are shown in **Figure 9**. There are no significant trends in the between-event residuals with magnitude, in the within-site residuals with distance, or in the between-site residuals with V_{S30}. **Table 1** also shows the standard deviations for these residual components of the French ergodic models from 1 Hz to 23.5 Hz. The standard deviations from 0.1 Hz to 0.9 Hz based on the BA19 model are shown in **APPENDIX A**.

The comparison of the median EAS for the French ergodic model with the BA19 model (without the nonlinear site term or the basin depth term) for the distance scaling and magnitude scaling at 1.0 Hz and 5.0 Hz are shown in **Figure 10**. Overall, the scaling of the EAS is similar between the two regions. The main differences are in the distance scaling at large distances (linear R term) and in the small-

magnitude scaling. For the 5-Hz distance scaling, the attenuation at large distance is lower in France than in California. For the magnitude scaling, there is weaker magnitude scaling in France than in California. Fig. 17 of Ameri et al. (2017) also shows a similar PSA scaling for NGAW2 and French models. Regional differences in median ground motion in France can be seen in the data. For example, we chose eastern France as the target area to plot the between-event residuals (**Figure 11a**). We further split this area into three smaller regions: E1, E2, E3. The probability density distribution of between-event residuals for the combination of three regions is shown in **Figure 11b**, and other individual small regions results are shown in **Figure 11c**, **Figure 11d**, and **Figure 11e**.The results show regional differences in the mean source term (solid lines in **Figure 11b-d**) of up to a factor of 1.22 (0.2 ln units) for the subregions.

4. Non-Ergodic Ground-Motion Model

Using the notation of Al-Atik et al (2010), the median non-ergodic GMM can be written as

$$\mu_{nonerg}(\mathbf{x}, \mathbf{t_e}, \mathbf{t_s}) = \mu_{erg}(\mathbf{x}) + \delta L2L(\mathbf{t_e}) + \delta S2S(\mathbf{t_s}) + \delta P2P(\mathbf{t_e}, \mathbf{t_s}). \tag{4}$$

in which $\mathbf{t_e}$ and $\mathbf{t_s}$ are the coordinates of the earthquake and the site, respectively, $\delta L2L(\mathbf{t_e})$ is adjustment to the source term, $\delta S2S(\mathbf{t_s})$ is the site term, and $\delta P2P(\mathbf{t_e}, \mathbf{t_s})$ is the path term. Below, we relate the non-ergodic terms in equation (4) to the notation of Landwehr et. al. (2016) with modifications for anisotropic linear R scaling used by Abrahamson et. al. (2019).

For the non-ergodic source term, the model is a constant based on the coordinates of earthquake source location, $\mathbf{t_e}$:

$$\delta L2L(\mathbf{t_e}) = \beta_{-1}(\mathbf{t_e}) \tag{5}$$

For the non-ergodic site term, there are two length scales for the constant term, so the model includes two constant terms (one correlated and one uncorrelated) and a spatially correlated change in the V_{S30} scaling based on the coordinates of site location, $\mathbf{t_s}$. The uncorrelated site term is given by $\delta S'_{S2S}$:

$$\delta S2S_S = \beta_0(\mathbf{t_s}) + f_{Vs30}(Vs30; \mathbf{t_s}) + \delta S'_{S2S} \tag{6}$$

For the non-ergodic path term, the linear R scaling is removed from the reference ergodic GMM, the region is broken into a grid of cells, and attenuation through each cell is estimated. The path term is given by

$$\delta P2P(\mathbf{t_e}, \mathbf{t_s}) = \sum_i^{Nc} \theta_{Attn,i} \Delta R_{Rup,i} - \theta_{Attn} R_{Rup} \tag{7}$$

in which the $\Delta R_{Rup,i}$ is the length of the ray (between the source and the site) in the ith cell (**Figure 12**). In the reference ergodic GMM, the linear R scaling coefficient, θ_{Attn}, is constrained to be negative to represent Q effects. The minus in front of $\theta_{Attn}R_{Rup}$ indicates the linear R scaling is removed from the ergodic GMM, so that a constraint on the attenuation ($\theta_{Attn,i} < 0$ for each cell) can be applied to the non-ergodic model, similar to the constraint in the ergodic model.

The total residuals from the ergodic GMM are given by:

$$\varepsilon_{es} = ln(EAS_{es}) - \mu_{erg}(\mathbf{M}, \mathbf{R}, \mathbf{S}, \dots) \tag{8}$$

These total residuals, ε_{es}, are modeled in two steps to estimate the non-ergodic terms: (1) the source and site terms using the Variable Coefficient Model (VCM) via a Gaussian process regression (Landwehr et al., 2016), and (2) the path term of anelastic attenuation per cell from the cell-specific approach using the Bayesian hierarchical model (Kuehn et al., 2019). These two steps are described below.

4.1 Source and Site Terms for the VCM

In the first step, we follow the equations (5) and (6) that depend only on source or site coordinates as the additional parameters to regress the total residuals:

$$\varepsilon_{es} = C_0 + \beta_{-1}(\mathbf{t_e}) + \beta_0(\mathbf{t_s}) + f_{Vs30}(Vs30; \mathbf{t_s}) + \delta S'_{S2S} + \delta B_e + \delta WS_{es} \tag{9}$$

In this model, $f_{V_{S30}}(\mathbf{V_{S30}}; \mathbf{t_s}) = \beta_4(\mathbf{t_s})\ln(\min(\mathbf{V_{S30}}, 1000)/1000)$, C_0 is the intercept that accounts for the change in the implicit weighting for each recording, $\delta S'_{S2S}$ is the zero-correlation length site term, δB_e is the remaining aleatory variability of the event term, and δWS_{es} is the remaining aleatory variability of within-site term. The $\delta S'_{S2S}$ has the same role as δS_{S2S} for the single-station standard deviation approach, but it is computed relative to the site scaling in the VCM model.

The regression approach for the VCM is the Gaussian Process (GP) with a hierarchical Bayesian framework. The Gaussian process is a distribution over a function $f(x)$, its distribution is defined by a mean function and a covariance function:

$$\boldsymbol{f}(\mathbf{x}) \sim GP(0, \kappa(\mathbf{x}, \mathbf{x}')), \tag{10}$$

Because we are fitting the model to the residuals from the ergodic GMM, the mean function is set in 0 and the x = ($\mathbf{t_e}$, $\mathbf{t_s}$) and x' = ($\mathbf{t_e}'$, $\mathbf{t_s}'$) into covariance function. The covariance function model is the joint distribution of all random variables to build the distribution over a function with a continuous domain, such as location of event or site. We set the covariance function (also known as the kernel function) of VCM to be consistent with Landwehr et al. (2016):

$$\kappa_i(\mathbf{x}, \mathbf{x}') = \begin{cases} \theta_j^2 exp\left(-\dfrac{||\mathbf{x}(\mathbf{t_e})-\mathbf{x}'(\mathbf{t_e'})||}{\rho_j^2}\right) & if\ j \in \{-1\} \\ \theta_j^2 exp\left(-\dfrac{||\mathbf{x}(\mathbf{t_s})-\mathbf{x}'(\mathbf{t_s'})||}{\rho_j^2}\right) & if\ j \in \{0,4\} \end{cases}. \tag{11}$$

in which θ_j^2 is the variance (amplitude) and ρ_j^2 is the correlation length (length scale); they are the hyperparameter in the kernel function. We estimate the hyperparameters of the Gaussian process via the marginal likelihood based on the observations. Then, the posterior distribution with mean prediction and standard deviation of the β_{-1}, β_0, and β_4 for each source location and site location are estimated. The resulting hyperparameter of equation (11) from 1.0 Hz to 23.5 Hz are listed in **Table 2** and are shown in **Figure 11**. The hyperparameters from 0.1 Hz to 0.9 Hz are shown in **APPENDIX A**.

Following Landwehr et. al. (2016), the estimate of the variance of epistemic uncertainty (ψ^2) in the median ground motion is given by:

$$\psi^2 = \mathbf{k}_* - \mathbf{k}^{\mathbf{T}}(\mathbf{K} + \sigma_0^2 \mathbf{I})^{-1}\mathbf{k}, \tag{12}$$

$$\mathbf{K} = \begin{bmatrix} K_{1,1} & \cdots & K_{1,n} \\ \vdots & \ddots & \vdots \\ K_{n,1} & \cdots & K_{n,n} \end{bmatrix} \quad and \quad K_{i,l} = \sum_{j=1}^{d} x_{ij}\, x_{lj}\kappa_j(t_i, t_l), \tag{13}$$

$$\mathbf{k} = [k_1, \quad k_2, \quad \cdots, \quad k_{n-1}, \quad k_n] \quad and \quad k_i = \sum_{j=1}^{d} x_{ij}\, x_{*j}\kappa_j(t_i, t_*), \tag{14}$$

$$\mathbf{k}_* = [k_*, \quad k_*, \quad \cdots, \quad k_*, \quad k_*] \quad and \quad k_* = \sum_{j=1}^{d} x_{*j}\, x_{*j}\kappa_j(t_*, t_*), \tag{15}$$

in which

t_* is the latitude and longitude for a new location to estimate the median ground motion

ψ is the standard deviation of epistemic uncertainty for site location, t_*

κ_j is from the equation (11)

I is the identity matrix

σ_0 is the standard deviation of aleatory variability of the ground motion.

To show the adjustment map of source constant (β_{-1}), site constant (β_0), and ln(Vs30) coefficient (β_4), we divide France into cells of size 0.2 × 0.2 degrees. The justification for the selected grid size is discussed later. The mean values of the three non-ergodic coefficients are computed for each cell using either the source location or site location. Maps of the spatially varying mean coefficients are shown in **Figure 14** (constant source term), **Figure15** (constant site term), and **Figure 16** (linear Vs30 term), for 1Hz and 5 Hz. These adjustment terms are zero in regions without data (or with sparse data) and

potentially show the larger (positive) values or smaller (negative) values for cells close to observed events and stations.

The median ground motion using the VCM model is given by

$$\mu_{VCM}(\mathbf{M}, \mathbf{R}, \mathbf{S}, \boldsymbol{\theta}, \mathbf{t}_e, \mathbf{t_s}) = \mu_{erg}(\mathbf{M}, \mathbf{R}, \mathbf{S}) + C_0 + \beta_{-1}(\mathbf{t_e}) + \beta_0(\mathbf{t_s}) + f_{Vs30}(Vs30; \mathbf{t_s}) \tag{16}$$

and the total residuals from the VCM are given by:

$$\eta_{es} = ln(EAS_{es}) - \mu_{VCM}(\mathbf{x}, \boldsymbol{\theta}, \mathbf{t}_e, \mathbf{t_s}) \tag{17}$$

4.2 Path-specific attenuation term

We used the same 0.2 x 0.2 degrees grid size for the path effects. **Figure 17a** shows the ray paths from each source to each station with a useable recording at 5 Hz from that earthquake. The number of rays that pass through each cell is shown in **Figure 17b**, which indicates how well the path effect is constrained for each cell. We apply the cell-specific anelastic attenuation terms to replace an ergodic term in the GMM by fitting the residual shown in equation (17):

$$\eta_{es} = f_{Attn}(\Delta\mathbf{R_{Rup}}_{,i}; \mathbf{cell}_i) + \partial B_e + \partial S2S_s + \partial W_{s,es}. \tag{18}$$

$$f_{Attn}(\Delta\mathbf{R_{Rup}}_{,i}; \mathbf{cell}_i) = \sum_i^{Nc} \theta_{Attn,i}\Delta R_{Rup,i} \tag{19}$$

and δB_e is the remaining variability of the event term, $\delta S2S_s$ is the zero-correlation length site term, δWS_{es} is the remaining variability of within-site term. To avoid nonphysical attenuation coefficients, the $\theta_{Attn,i}$ is constrained to be negative.

We apply the same regression model (Bayesian hierarchical model) as Kuehn et al. (2019) into the cell-specific anelastic attenuation terms. The path terms are assumed to be distributed as a truncated normal distribution. The truncation is used to remove the positive values. All the settings of the prior distributions of variables in the cell-specific model are the same as equation (5) to equation (8) of Kuehn et al. (2019). **Figure 18** shows the mean values of the posterior distribution of the θ_{Attn} per cell at 1.0 Hz and 5.0 Hz. Greater anelastic attenuation coefficients (lower Q) occur in Alps whereas the smaller values (higher Q) in western France Furthermore, **Figure19** shows the other French anelastic attenuation maps: (1) Qs in Figure 5 of Campillo and Plantet (1991) at 6Hz, and (2) the ratio of the absorption quality factor (Qi) and the spatial average of Qi (Qm) in Figure5 of Mayor et al. (2018) at 4 – 8 Hz. These results also show apparent lower Q values in the south-eastern regions and higher Q values in the western areas; however, if the cell did not include any path ray, the cell-specific anelastic attenuation coefficient would use the ergodic anelastic attenuation value (c_7). The standard deviation of the epistemic uncertainty of the $\theta_{Attn,i}$ is captured from the result of the posterior distribution for θ_{Attn}, which are shown in **Figure 20**,

for 5.0 Hz. In the specific-site PSHA calculations, these epistemic uncertainties for each source cell are included on the logic tree. **Table 3** lists the results of mean attenuation, $\mu_{\theta Attn}$, and standard deviation, $\sigma_{\theta Attn}$, for 43 frequencies. The mean attenuation and standard deviation from 0.1 Hz to 0.9 Hz are shown in **APPENDIX A**.

If the chosen grid size is not larger than the correlation length of the hyperparameter, the results will not be sensitive to the grid size. **Figure 21** shows the semi-variogram of non-ergodic source term for the different grid sizes at 5Hz. For this case, the correlation length of the hyperparameter in the GP model is 0.387 degrees. The result shows the consistent trend of the semi-variance when the grid size is smaller than the correlation length. On the contrary, the semi-variance is unstable with the grid size greater than the correlation length. We finally chose the grid size is 0.2 x 0.2 degrees because this given grid size needs to suitable for all non-ergodic terms.

4.3 Residuals & Standard Deviation

The residuals of the ergodic, VCM-non-ergodic, and fully non-ergodic (VCM + path effects) GMMs for 5.0 Hz are shown in **Figure 22**. The results show a significant reduction of the variability of the between-event and between-site residuals for the VCM-non-ergodic model as compared to the ergodic model. Because the VCM-non-ergodic model used in the first step did not include a non-ergodic path term, there is not a significant reduction in the variability for the within-site residual. Including the non-ergodic path term does not significantly change the standard deviation of the between-event or between-site residuals, but it does reduce the standard deviation of the within-site residuals at large distances. The standard deviations of the within-site residuals in different distance bins for the three models are shown in **Figure 23,** for 1.0 Hz and 5.0 Hz. At short distances, the standard deviations of the within-site residuals, φ_{ss}, are similar for the three models, whereas there is a significant decrease in the φ_{ss} at long distances for the non-ergodic GMM, particularly for 5 Hz.

5. Median and Epistemic Uncertainty for Non-Ergodic Model

Because the adjustment terms of a non-ergodic GMM vary by the geographical location, the median predictions at a given site also change depending on event locations. **Figure 24** shows an example of the spatial variation of median EAS predictions by the French non-ergodic and ergodic GMMs for a set of predictor variables M = 5.0, V_{S30} = 2100 m/s, Z_{TOR} = 10 km at 5.0 Hz for SITE 1 in south-eastern France. The ergodic GMM has the same attenuation in all directions, but for the non-ergodic GMM, the attenuation can depend on the direction. **Figure 25** compares the distance scaling of the EAS in different directions for the ergodic and non-ergodic models at 5.0 Hz for three sites (SITE1, SITE2, and SITE4). The largest differences are seen for distances of 100-300 km due to the path effects.

The epistemic uncertainty of the median ground motion for the non-ergodic model is shown in **Figure 26** for SITE 1 and SITE 2 at 5.0 Hz. The results show the lower uncertainty is constrained to locations

where data are available, whereas the uncertainty is increased for the region without data (or with sparse data). Furthermore, all epistemic uncertainties for the SITE 1 are lower than the resulting of SITE 2, which is due to the location of SITE 1 nears the observed data.

We chose SITE 1 and use the same parameters (V_{S30} = 2100 m/s, Z_{TOR}=10 km) to calculate the median EAS spectra at 1.0 Hz to 23.5 Hz. We chose two target sources which have the similar source-site distance. The first target source (Source 1, 43.7°N, 2.7°E) is located west of the site at a distance of 246.8 km, and the second source (Source 2, 45.9°N, 5.7°E) is located north of the site at a distance of 247 km (**Figure 27**). Examples of the median EAS spectra from the non-ergodic and ergodic models from M3 to M8 are shown in **Figure 28**. For Source 1, the ergodic and non-ergodic models have similar Fourier spectra, only a slight reduction on lower frequencies and a slight increase on higher frequencies for the non-ergodic model. (**Figure 28a**). Source 2 shows a significant difference at frequencies greater than 2 Hz between non-ergodic and ergodic models (**Figure 28b**). **Figure 29a** and **Figure 29b** show the epistemic uncertainties of the non-ergodic model at all frequencies for Source 1 and Source 2, respectively. Source 2 has a smaller epistemic uncertainty than Source 1 due to the available data closed.

Figure 30 and **Table 4** show the standard deviations terms for the ergodic and non-ergodic GMM for each frequency: total, between-event, between-site, and within-site standard deviations. There is a significant reduction of the aleatory variability for the non-ergodic model. For example, at 5 Hz, the ergodic aleatory standard deviation is 0.94, the partially non-ergodic aleatory standard deviation (the single station standard deviation) is 0.80, and the full non-ergodic aleatory standard deviation is 0.59. This corresponds to a 60% reduction in variance from the ergodic to the non-ergodic GMM and is consistent with the results from active regions discussed in the introduction. For the 0.1 to 0.9 H are shown in **APPENDIX A**.

6. PSHA Implementation

For PSHA implementation of the non-ergodic approach, the site/source specific adjustment along with the standard deviation of epistemic uncertainty in the adjustment needs to be included (e.g., **Figure 26**). The current approach is to precompute the net adjustment term (sum of the source, path, and site terms) for each source location for a single site location. We randomly sample 100 different adjustments from the distribution based on the epistemic uncertainty that was implied by the varying coefficient model and cell-specific approach. **Figure 31** shows the two samples of 100 maps for sampled adjustments. That is, in PSHA code, we will add these adjustments (constants per grid) to the ergodic model; there is a logic tree with 100 branches of the non-ergodic terms for the GMM that are equally weighted (**Figure 32**).

For the site terms, a single non-ergodic term is estimated for each realization. The source and path non-ergodic terms are sampled to capture the variance and the correlations of the terms. The net adjustment

is the sum of the source, path, and site terms. By precomputing the net adjustment terms, fewer changes are required for the PSHA program. The main change is that the adjustment terms depend on the latitude and longitude of the source.

The following is the formula for the ergodic probability of exceeding any PGA level using knowledge of the median ground motion (μ_{erg}) and ergodic aleatory standard deviation (σ_{erg}) in the units:

$$P(Y > Z|M,R) = 1 - \Phi\left(\frac{ln(z) - \mu_{erg}(M,R,T)}{\sigma_{erg}(M,R,T)}\right)... \quad\quad .....(20)$$

Where the Y is the ground-motion parameter of interest, and $P(Y > Z|M,R)$ is the conditional probability that Y is larger than z for a given magnitude, distance, and other relevant parameters. Φ() is the cumulative distribution function of a standard normal distribution. But for non-ergodic GMMs, the latitude and longitude of each source needs to be passed to the GMM subroutine and the appropriate adjustment factor interpolated from the pre-calculated values.

$$P(Y > Z|M,R) = 1 - \Phi\left(\frac{ln(z) - \left(\mu_{erg}(M,R,T) + \Delta\mu_{ne}(Lat_e, Lon_e, Lat_s, Lon_s, M, T)\right)}{\sigma_{ne}(M,R,T)}\right),.......(21)$$

The HAZ45 code runs the hazard for a single site, so the $\Delta\mu_{ne}$ is a table of values for different source locations and magnitudes for the selected site, and the σ_{ne} is the non-ergodic aleatory standard deviaiton. Multiple realizations are included to capture the epistemic uncertainty in the non-ergodic terms. **Figure 33** shows the map of the locations of the sites which we selected to randomly sample the adjustments, and **Table 5** shows the latitude, longitude, Vs30, and non-ergodic site terms for each site. **Figure 34** shows the mean adjustment over the 100 realization for SITE 1 and SITE 2 per source grid. For sites without local data (e.g., SITE 2), the mean values in the maps are close to zero. For sites will location data to constrain the non-ergodic terms (e.g., SITE 1), the mean can be close to zero or different from zero depending on the data. The mean adjustment for other six sites is show in **APPENDIX B**. For standard deviation of the 100 realization for the same sites is shown in **Figure 35** and **APPENDIX C**. The epistemic uncertainties range from 0.15 for regions with local data to 0.7 for regions without local data. It should be similar to the previous epistemic uncertainty map (**Figure 26**) because we adopted these epistemic uncertainties to generate the samples (adjustments) for each cell.

The changes required to implement the non-ergodic GMMs have been implemented into HAZ45 and is currently being implemented into OpenQuake (OQ). Example hazard results using the HAZ45 software are shown below. The seismic source model is the EDF zoning (Drouet et al., 2020)

Figure 36 to **Figure 41** compares the hazard using the ergodic EAS GMM with the hazard from the 100 samples of the non-ergodic adjustment terms for eight sites. SITE1, SITE5 to SITE8 are all close to the local data, so they would have data to constrain the adjustments for the site term. For the non-ergodic

GMM, the aleatory variability is reduced. If only the aleatory variability is reduced, then the non-ergodic hazard curves would be much steeper than the ergodic hazard curves; however, the adjustments vary spatially, which acts like additional variability in the total hazard (summed over all source locations). So, the non-ergodic hazard curves are not as steep as would be the case if the adjustment was the same for all source locations, as is the case with the partially non-ergodic single-station standard deviation approach. The mean hazard also samples the epistemic uncertainty from the 100 realizations which will also flatten the slope of the mean hazard curve. The effect of the epistemic uncertainty on the slope of the hazard curve can be seen by comparing the slope from the mean hazard and the slope from the median hazard.

For SITE 1 (southeastern France, **Figure 36**), the mean hazard curves for the ergodic and non-ergodic GMMs are similar for 1 Hz, but there is a large reduction in the mean non-ergodic hazards for 5 Hz. At an annual frequency of exceedance of 1×10^{-4}, there is a factor of 2 reduction in the ground France motion, and the 95th fractile from the non-ergodic hazard is close to the mean ergodic hazard. The slope of the median hazard (dashed blue line) is steeper than the slope of the mean hazard.

For SITE 2 (central – western France, **Figure 37**), SITE 3 (northwestern France, **Figure 38**), and SITE 4 (northern France, **Figure 39**), the 1-Hz mean hazard and 5-Hz mean hazard are similar the mean ergodic hazard results. These sites have wider range of the fractile than SITE 1 is dues to the higher epistemic uncertainties for the adjustments.

Ameri et al. (2017) showed a factor 2 reduction in the PSA ground motion in the uniform hazard spectra at a 10,000-yr return period when they adopted the partially non-ergodic model. However, the hazard will not be reduced/increased at all sites. To demonstrate this, we selected four additional sites (SITE 5 to SITE 8, **Figure 40** to **Figure 41**) for which the non-ergodic model leads to hazard that is larger/lower than then ergodic hazard at the 1×10^{-4} annual frequency of exceedance. For SITE 5 (eastern France), the 1-Hz ground motion from the mean non-ergodic hazard at the 1×10^{-4} annual frequency of exceedance is about a factor of 1.75 larger than the ground motion at the same annual frequency of exceedance for the ergodic model. For SITE 6 (southern France), the 5-Hz ground-motion from the mean non-ergodic hazard is about 1.5 larger than the 5-Hz ground motion from the ergodic model for the 1×10^{-4} annual frequency of exceedance. For SITE 7 (northwestern France), there is a factor of 1.8 reduction at the 1×10^{-4} annual frequency of exceedance of the 1-Hz ground motion from the mean non-ergodic hazard. For SITE 8 (eastern France), the 5-Hz ground-motion is about 2 reduction from the mean non-ergodic hazard at the 1×10^{-4} annual frequency of exceedance. SITE 7 has higher epistemic uncertainty for the adjustments so that the fractile is wider than others.

We conducted an initial the verification of the ergodic and non-ergodic PSHA codes by comparing the hazard results from OQ with HAZ45 for SITE 1 on 5Hz in **Figure 42**. The OQ's results is from Marco Pagani. The result show that the consistent hazard level for both models.

7. Conclusions

Traditionally, GMMs used in PSHA have been based on the ergodic assumption (Anderson and Brune, 1999). The move to non-ergodic GMMs will lead to GMMs that have a better physical basis and provide more accurate estimates of the hazard in regions with local data. In regions with little local data, non-ergodic GMMs can still be used. In this case, the mean hazard will approximate the ergodic mean hazard, but the uncertainty range will be broader and will provide a better estimate of the uncertainty and also show the value of collecting local ground-motion data.

The non-ergodic GMM for EAS develop in this study can be extended to response spectral values. Before doing so, the extrapolation to low frequencies should be revised. Because the available data ground-motion from France were not reliable at low frequencies, the current model assumed that the low-frequency scaling from the BA19 model is applicable to France at frequencies less than 1 Hz. This can be improved. It may be possible to use the hyperparameters for low frequencies from the California models and then estimate the non-ergodic terms using the French data.

Using a non-ergodic GMM, there is a large reduction in the aleatory standard deviation, but there is also a shift in the median from each source location that can be either positive (large median) or negative (smaller median). At the 1×10^{-4} annual frequency of exceedance, there tends to be a reduction in the hazard using the non-ergodic GMM, but at some sites, there will be an increase in the hazard if there is an increase in the medians for the controlling sources that offsets the reduction in the aleatory standard deviation at the 1×10^{-4} annual frequency of exceedance.

There is a need to verify the PSHA programs for implementing non-ergodic GMMs. The next step for this task is to conduct the verification of the non-ergodic PSHA codes by comparing hazard results from OpenQuake with those from HAZ45. The initial comparison shows that the two PSHA programs lead to consistent hazard estimates for both the ergodic and non-ergodic GMMs.

8. References

Abrahamson, N. A., and R. R. Youngs (1992). A stable algorithm for regression analyses using the random effects model, Bull. Seism. Soc. Am. 82 505-510.

Abrahamson, N. A., W. J. Silva, and R. Kamai (2014). Summary of the ASK14 ground motion relation for active crustal regions, Earthquake Spectra 30, no. 3, 1025–1055, doi: 10.1193/070913EQS198M.

Abrahamson, N. A., N. M. Kuehn, M. Walling, and N. Landwehr (2019). Probabilistic Seismic Hazard Analysis in California Using Non-ergodic Ground-Motion Models, Bull. Seism. Soc. Am. 109 (4), 1235–1249, doi: 10.1785/0120190030

Al Atik, L., N. A. Abrahamson, F. Cotton, F. Scherbaum, J. J. Bommer, and N. Kuehn (2010). The variability of ground-motion prediction models and its components, Seismol. Res. Lett. 81, no. 5, 794–801.

Allen, T. I., and Wald, D. J., 2009, On the use of high-resolution topographic data as a proxy for seismic site conditions (Vs30), Bulletin of the Seismological Society of America, 99, no. 2A, 935-943.

Ameri, G., F. Hollender, V. Perron, and C. Martin (2017). Site-specific partially non-ergodic PSHA for a hard-rock critical site in southern France: adjustment of ground motion prediction equations and sensitivity analysis, Bull Earthquake Eng, (15), 4089–4111.

Ameri, G., S. Drouet, P. Traversa, D. Bindi, and F. Cotton (2017). Toward an empirical ground motion prediction equation for France: accounting for regional differences in the source stress parameter, Bull Earthquake Eng, (15), 4681–4717

Anderson, J., and J. N. Brune (1999). Methodology for using precarious rocks in Nevada to test seismic hazard models, Bull. Seism. Soc. Am., 89, 456–467.

Anderson, J. G., and Y. Uchiyama (2011). A methodology to improve ground-motion prediction equations by including path corrections, Bull. Seismol. Soc. Am. 101, 1822–1846.

Atkinson, G.M. (2006). Single-station sigma, Bull. Seism. Soc. Am., 96, 446–455.

Bayless, J and N. A. Abrahamson (2019) Summary of the BA18 Ground-Motion Model for Fourier Amplitude Spectra for Crustal Earthquakes in California, Bulletin of the Seismological Society of America, 109 (5), 2088–2105.

BC Hydro (2012). Dam safety probabilistic seismic hazard analysis (PSHA) model, Technical Report, Report No. E658, Vancouver, British Columbia.Bommer, J. J., K. J. Coppersmith, R. T. Coppersmith, K. L. Hanson, A. Mangongolo, J. Neveling, E. M. Rathje, A. Rodriguez-Marek, F. Scherbaum, R. Shelembe, P. J. Sta_ord, and F. O. Strasser (2015). A SSHAC Level 3 Probabilistic Seismic Hazard Analysis for a New-Build Nuclear Site in South Africa. Earthq. Spectra 31(2), 661-698. doi: 10.1193/060913EQS145M.

Boore, D. M., J. P. Stewart, E. Seyhan, and G. M. Atkinson (2014). NGAWest2 equations for predicting PGA, PGV, and 5% damped PSA for shallow crustal earthquakes, Earthq. Spectra 30, no. 3, 1057–1085, doi: 10.1193/070113EQS184M.

Bremaud, V., and P. Traversa (2019). Determination of GMPEs based on different intensity measures, SIGMA2-2019-D3-028.

Brillinger, D. R., and H. K. Preisler (1984). An exploratory analysis of the Joyner-Boore attenuation data, Bull. Seism. Soc. Am. 74 1441-1450.

Brillinger, D. R., and H. K. Preisler (1985). Further analysis of the Joyner-Boore attenuation data, Bull. Seism. Soc. Am. 75 611-614.

Campbell, K. W., and Y. Bozorgnia (2014). NGA-West2 ground motion model for the average horizontal components of PGA, PGV, and 5% damped linear acceleration response spectra, Earthq. Spectra 30, no. 3, 1087–1115, doi: 10.1193/062913EQS175M.

Campillo M, Plantet J (1991) Frequency dependence and spatial distribution of seismic attenuation in France: experimental results and possible interpretations. Phys Earth Planet Inter 67(1):48–64.

Cara, M., Y. Cansi, A. Schlupp, P. Arroucau, N. Béthoux, E. Beucler, S. Bruno, M. Calvet, S. Chevrot, A. Deboissy, et al. (2015). SI-Hex: A new catalogue of instrumental seismicity for metropolitan France, Bull. Soc. Géol. France 186, no. 1, 3–19.

Chiou, B. S.-J., R. B. Darragh, N. Gregor, and W. J. Silva (2008). NGA project strong-motion database, Earthq. Spectra 24, no. 1, 23–44.

Chiou B.S.-J., Youngs R.R., Abrahamson N.A, Addo K. (2010). Ground-motion attenuation model for small-tomoderate shallow crustal earthquakes in California and its implications on regionalization of ground-motion prediction models, Earthq. Spectra, 26: 907–926.

Chiou, B., and R. R. Youngs (2014). Update of the Chiou and Youngs NGA model for the average horizontal component of peak ground motion and response spectra, Earthquake Spectra 30(3) 1117-1153.

Coppersmith, K., J. J. Bommer, K. Hanson, R. Coppersmith, J. Unruh, L. Wolf, R. Youngs, L. Al Atik, A. Rodriguez-Marek, and G. Toro (2014). Hanford sitewide probabilistic seismic hazard analysis. Technical Report Prepared for the U.S. Department of Energy Under Contract DE-AC06076RL01830, and Energy Northwest, Pacifc Northwest National Lab Report PNNL-23361, November.

Drouet, S., G. Ameri, K. L. Dortz, R. Secanell, and G. Senfaute (2020). A probabilistic seismic hazard map for the metropolitan France, Bulletin of Earthquake Engineering, 18, 1865–1898.

Geopentech (2015). Southwestern United States ground motion characterization SSHAC level 3 - Technical Report Rev. 2, March 2015. Technical report.

Goulet, C. A., A. Kottke, D. M. Boore, Y. Bozorgnia, J. Hollenback, T. Kishida, A. Der Kiureghian, O. J. Ktenidou, N. M. Kuehn, E. M. Rathje, et al. (2018). Effective amplitude spectrum (EAS) as a metric for ground motion modeling using Fourier amplitudes, 2018 Seismology of the Americas Meeting, Miami, Florida, 14–17 May 2018.

Grünthal, G., D. Stromeyer, and R. Wahlström (2009). Harmonization check of Mw within the central, northern, and northwestern European earthquake catalogue (CENEC), J. Seismol. 13, no. 4, 613–632.

Konno, K., and T. Ohmachi (1998). Ground-motion characteristics estimated from spectral ratio between horizontal and vertical components of microtremor, Bull. Seismol. Soc. Am. 88, 228–241.

Kotha, S. R., D. Bindi, and F. Cotton (2016). Partially non-ergodic region specific GMPE for Europe and Middle-East, Bull. Earthq. Eng. 14, no. 4, 1245–1263,

Kuehn, N. M., N. A. Abrahamson, and M. A. Walling (2019). Incorporating non-ergodic path effects into the NGA-West2 ground-motion prediction equations, Bull. Seismol. Soc. Am. 109, no. 2, 575–585

Landwehr, N., N. M. Kuehn, T. Scheffer, and N. Abrahamson (2016). A non-ergodic ground-motion model for California with spatially varying coefficients, Bull. Seismol. Soc. Am. 106, no. 6, 2574–2583.

Lanzano, G., M. D'Amico, C. Felicetta, L. Luzi, and R. Puglia (2017). Update of the single-station sigma analysis for the Italian strong-motion stations, Bull. Earthq. Eng., 6, 2411–2428.

Lin, P.-S., B. Chiou, N. Abrahamson, M. Walling, C.-T. Lee, and C.-T. Cheng (2011). Repeatable source, site, and path effects on the standard deviation for empirical ground-motion prediction models, Bull. Seismol. Soc. Am., 101, 2281–2295.

Mayor, J., P. Traversa, and M. Calvet (2018). Tomography of crustal seismic attenuation in Metropolitan France: implications for seismicity analysis, 16, pages2195–2210.Morikawa, N., Kanno, T., A. Narita, H. Fujiwara, T. Okumura, Y. Fukushima, and A. Guerpinar (2008). Strong motion uncertainty determined from observed records by dense network in Japan, J. Seismol., 12, 529–546.

National Center for Research on Earthquake Engineering (NCREE) (2018), Web page for reevaluation of probabilistic seismic hazard of nuclear facilities in Taiwan using SSHAC level 3 methodology project, available at http://sshac.ncree.org.tw.

Pinheiro, J., D. Bates, S. DebRoy, D. Sarkar, and the R Core Team (2020). nlme: Linear and nonlinear mixed effects models, R package version 3.1-145.

Power, M., B. Chiou, N. Abrahamson, Y. Bozorgnia, T. Shantz, and C. Roblee (2008). An overview of the NGA project, Earthq. Spectra 24 (1), 3–21.

Renault, P., S. Heuberger, and N. A. Abrahamson (2010). PEGASOS Refinement Project: An improved PSHA for Swiss nuclear power plants. In Proceedings of 14ECEE-European Conference of Earthquake Engineering, pp. Paper ID 991.

Réseau Sismologique et géodésique Français (RESIF) (1995a). RESIFRAP French Accelerometric Network, RESIF – Réseau Sismologique et géodésique Français, doi: 10.15778/RESIF.RA.

Réseau Sismologique et géodésique Français (RESIF) (1995b). RESIF-RLBP French Broad-band Network, RESIF-RAP strong motion network and other seismic stations in metropolitan France; RESIF - Réseau Sismologique et géodésique Français, doi: 10.15778/ RESIF.FR.

Sung, C. H., and C. T., Lee (2019). Improvement of the Quantification of Epistemic Uncertainty Using Single-Station Ground-Motion Prediction Equations, Bull. Seism. Soc. Am., 109 (4): 1358–1377.

Traversa, P., E. Maufroy, F. Hollender, V. Perron, V. Bremaud, H. Shible, S. Drouet, P. Guéguen, M. Langlais, D. Wolyniec, C. Péquegnat, and I. Douste-Bacque (2020). RESIF RAP and RLBP Dataset of Earthquake Ground Motion in Mainland France, Seismological Research Letters, 91 (4): 2409–2424.

Tromans, I. J., G. Aldama-Bustos, J. Douglas, A. Lessi-Cheimariou, S. Hunt, M. Davi, R. M. W. Musson, G. Garrard, F. O. Strasser, and C. Robertson (2019). Probabilistic seismic hazard assessment for Francea new-build nuclear power plant site in the UK. Bull. Earthquake Eng. 17(1), 1-36. doi: 10.1007/s10518-018-0441-6.

Villani, M. A., and N. Abrahamson (2015). Repeatable site and path effects on the ground-motion sigma based on empirical data from southern California and simulated waveforms from the cybershake platform, Bull. Seismol. Soc. Am. 105, doi: 10.1785/0120140359.

Wald, D. J., and Allen, T. I.,2007, Topographic slope as a proxy for seismic site conditions and amplification, Bulletin of the Seismological Society of America, 97, no. 5, 1379-1395.

Table 1 Coefficients for the ergodic EAS model for France

Freq	N	c_1	c_2	c_3	c_4	c_5	c_6	c_7	c_8	c_9	c_n	c_m	c_{hm}	σ_T	τ	ϕ_{S2S}	φ_{SS}
1	4815	-3.831	1.27	-0.339	-2.165	7.5813	0.4519	-0.0037	-1.2200	-0.0024	3.714	5.616	3.811	1.025	0.600	0.569	0.523
1.1	5056	-3.754	1.27	-0.328	-2.165	7.5811	0.4522	-0.0037	-1.2237	-0.0035	3.857	5.980	3.806	1.052	0.627	0.619	0.514
1.2	5166	-3.891	1.27	-0.307	-2.165	7.58101	0.4525	-0.0038	-1.2358	-0.0034	4.007	5.850	3.801	1.053	0.625	0.631	0.514
1.3	5316	-3.77	1.27	-0.300	-2.165	7.5808	0.4529	-0.0040	-1.2095	-0.0054	4.172	5.80	3.796	1.01	0.629	0.562	0.502
1.5	5495	-3.872	1.27	-0.261	-2.165	7.5800	0.4541	-0.0042	-1.1919	-0.0020	4.561	5.650	3.780	0.995	0.609	0.559	0.503
1.6	5544	-3.855	1.27	-0.247	-2.165	7.5795	0.4548	-0.0044	-1.1789	-0.0007	4.788	5.580	3.771	0.971	0.596	0.529	0.505
1.7	5638	-3.928	1.27	-0.226	-2.165	7.5790	0.4554	-0.0044	-1.1685	-0.0015	5.038	5.520	3.761	0.94	0.553	0.521	0.499
1.8	5686	-4.053	1.27	-0.208	-2.165	7.5784	0.4561	-0.0045	-1.1667	0.0041	5.314	5.400	3.752	0.935	0.544	0.519	0.496
2	5727	-4.012	1.27	-0.182	-2.165	7.5779	0.4568	-0.0047	-1.1627	0.0058	5.619	5.373	3.743	0.923	0.535	0.505	0.499
2.1	5770	-3.948	1.27	-0.173	-2.165	7.5769	0.4578	-0.0049	-1.1492	0.0086	5.957	5.349	3.731	0.898	0.514	0.495	0.493
2.2	5847	-3.885	1.27	-0.164	-2.165	7.5756	0.4589	-0.0050	-1.1532	0.0072	6.332	5.325	3.717	0.898	0.505	0.491	0.503
2.4	5879	-3.887	1.27	-0.147	-2.165	7.5742	0.4600	-0.0051	-1.1125	0.0074	6.746	5.303	3.702	0.9	0.484	0.492	0.504
2.6	5920	-3.892	1.27	-0.132	-2.165	7.5721	0.4612	-0.0053	-1.0669	0.0090	7.207	5.282	3.687	0.877	0.451	0.489	0.489
2.8	5931	-3.883	1.27	-0.120	-2.165	7.5689	0.4626	-0.0055	-1.0355	0.0114	7.722	5.264	3.670	0.87	0.453	0.488	0.487
3	5961	-3.884	1.27	-0.108	-2.165	7.5657	0.4640	-0.0055	-1.0091	0.0122	8.292	5.247	3.653	0.87	0.453	0.504	0.49
3.2	5978	-3.837	1.27	-0.098	-2.165	7.5624	0.4654	-0.0058	-0.9832	0.0128	8.910	5.233	3.636	0.876	0.448	0.506	0.489
3.4	5990	-3.803	1.27	-0.089	-2.165	7.5583	0.4668	-0.0060	-0.9152	0.0137	9.572	5.220	3.618	0.872	0.429	0.495	0.502
3.6	5994	-3.842	1.27	-0.078	-2.165	7.5513	0.4684	-0.0062	-0.8605	0.0167	10.278	5.208	3.600	0.872	0.42	0.495	0.498
4	6001	-3.858	1.27	-0.069	-2.165	7.5444	0.4699	-0.0063	-0.8213	0.0197	11.034	5.198	3.582	0.885	0.416	0.508	0.498
4.2	6005	-3.885	1.27	-0.062	-2.165	7.5333	0.4715	-0.0065	-0.7891	0.0221	11.831	5.189	3.563	0.892	0.423	0.51	0.502
4.5	6008	-3.954	1.27	-0.054	-2.165	7.5196	0.4730	-0.0067	-0.7655	0.0255	12.654	5.181	3.544	0.904	0.434	0.51	0.51
4.8	6006	-4.028	1.27	-0.046	-2.165	7.5058	0.4745	-0.0069	-0.7414	0.0289	13.487	5.173	3.526	0.921	0.437	0.511	0.519
5	5992	-4.042	1.27	-0.041	-2.165	7.4877	0.4760	-0.0072	-0.6994	0.0318	14.314	5.165	3.507	0.94	0.439	0.509	0.53
5.5	5983	-4.061	1.27	-0.037	-2.165	7.4619	0.4773	-0.0074	-0.6567	0.0353	15.131	5.157	3.487	0.964	0.444	0.523	0.544
6	5953	-4.096	1.27	-0.034	-2.165	7.4358	0.4787	-0.0075	-0.6379	0.0369	15.931	5.148	3.468	0.98	0.46	0.538	0.553
6.3	5938	-4.181	1.27	-0.030	-2.165	7.3948	0.4798	-0.0076	-0.6132	0.0402	16.685	5.139	3.447	0.988	0.468	0.549	0.557
6.8	5906	-4.253	1.27	-0.027	-2.165	7.3477	0.4809	-0.0078	-0.6005	0.04401	17.354	5.128	3.424	1.003	0.478	0.557	0.564
7.2	5875	-4.288	1.27	-0.026	-2.165	7.2768	0.4818	-0.0080	-0.5663	0.0473	17.911	5.117	3.396	1.025	0.49	0.57	0.571
7.8	5809	-4.351	1.27	-0.024	-2.165	7.2060	0.4827	-0.0082	-0.5365	0.0486	18.345	5.105	3.369	1.044	0.501	0.578	0.575
8.3	5764	-4.423	1.27	-0.021	-2.165	7.1352	0.4836	-0.0084	-0.5048	0.0489	18.653	5.094	3.341	1.07	0.528	0.595	0.582
9	5671	-4.484	1.27	-0.019	-2.165	7.0217	0.4843	-0.0086	-0.4773	0.0495	18.835	5.083	3.302	1.091	0.551	0.621	0.592
9.5	5606	-4.558	1.27	-0.018	-2.165	6.9069	0.4849	-0.0089	-0.4628	0.0523	18.890	5.073	3.264	1.115	0.573	0.634	0.608
10	5466	-4.599	1.27	-0.017	-2.165	6.8004	0.4855	-0.0090	-0.4611	0.0538	18.827	5.068	3.227	1.141	0.584	0.66	0.618
11	5384	-4.653	1.27	-0.016	-2.165	6.7103	0.4859	-0.0092	-0.4415	0.0577	18.673	5.066	3.196	1.167	0.622	0.661	0.627
12	5215	-4.727	1.27	-0.015	-2.165	6.6201	0.4864	-0.0095	-0.4233	0.0590	18.473	5.065	3.165	1.18	0.642	0.674	0.624
13.5	4934	-4.883	1.27	-0.013	-2.165	6.4551	0.4872	-0.0100	-0.3668	0.0621	18.028	5.062	3.109	1.223	0.69	0.706	0.637
14.5	4801	-5.022	1.27	-0.012	-2.165	6.4551	0.4874	-0.0102	-0.3204	0.0656	17.800	5.061	3.107	1.252	0.701	0.716	0.653
15.5	4593	-5.095	1.27	-0.010	-2.165	6.4551	0.4876	-0.0105	-0.2782	0.0650	17.588	5.060	3.106	1.271	0.704	0.746	0.654

16.5	4466	-5.214	1.27	-0.010	-2.165	6.4551	0.4878	-0.0108	-0.2811	0.0668	17.388	5.059	3.104	1.291	0.725	0.756	0.662
18	4303	-5.288	1.27	-0.009	-2.165	6.4551	0.4880	-0.0108	-0.2645	0.0606	17.174	5.059	3.103	1.303	0.724	0.757	0.665
20	4184	-5.515	1.27	-0.006	-2.165	6.4551	0.4882	-0.0110	-0.2151	0.0646	16.959	5.059	3.102	1.341	0.745	0.771	0.686
22	3774	-5.725	1.27	-0.003	-2.165	6.4551	0.4885	-0.0114	-0.0900	0.0606	16.529	5.061	3.100	1.374	0.717	0.786	0.714
23.5	3447	-5.941	1.27	0.0018	-2.165	6.4551	0.4886	-0.0114	-0.0561	0.0600	16.3134	5.063	3.099	1.383	0.708	0.802	0.712

N = number of records

σ_T = total standard deviation

τ = Between-event standard deviation

ϕ_{S2S} = Between-site standard deviation

φ_{SS} = Within-site standard deviation

Table 2. Hyperparameters for the VCM

Freq	θ_{-1}	θ_0	θ_4	ρ_{-1}	ρ_0	ρ_4
1	3.92E-01	3.71E-01	1.49E-01	4.25E-01	9.04E-01	4.68E-01
1.1	4.22E-01	3.71E-01	1.47E-01	5.09E-01	8.92E-01	5.23E-01
1.2	4.11E-01	3.97E-01	1.48E-01	4.22E-01	8.16E-01	4.97E-01
1.3	3.87E-01	3.79E-01	1.50E-01	4.22E-01	9.44E-01	4.86E-01
1.5	4.84E-01	3.62E-01	1.51E-01	3.85E-01	1.27E+00	4.74E-01
1.6	4.58E-01	3.63E-01	1.50E-01	2.45E-01	9.07E-01	5.53E-01
1.7	4.40E-01	3.83E-01	1.52E-01	2.56E-01	1.09E+00	5.15E-01
1.8	4.31E-01	3.51E-01	1.52E-01	2.42E-01	8.51E-01	4.69E-01
2	3.93E-01	3.08E-01	1.52E-01	2.50E-01	1.04E+00	5.57E-01
2.1	3.90E-01	2.77E-01	1.51E-01	2.89E-01	1.11E+00	5.60E-01
2.2	3.60E-01	2.92E-01	1.51E-01	2.76E-01	8.42E-01	5.23E-01
2.4	3.61E-01	3.01E-01	1.50E-01	3.71E-01	5.68E-01	4.94E-01
2.6	3.64E-01	2.95E-01	1.50E-01	3.59E-01	4.50E-01	4.85E-01
2.8	4.02E-01	2.85E-01	1.49E-01	3.12E-01	3.07E-01	4.74E-01
3	3.87E-01	2.88E-01	1.50E-01	2.34E-01	2.56E-01	4.74E-01
3.2	4.07E-01	2.64E-01	1.52E-01	2.44E-01	2.70E-01	5.03E-01
3.4	3.85E-01	2.41E-01	1.50E-01	2.49E-01	2.41E-01	4.72E-01
3.6	3.58E-01	1.82E-01	1.50E-01	3.11E-01	3.44E-01	4.77E-01
4	3.22E-01	2.28E-01	1.50E-01	3.73E-01	2.91E-01	5.45E-01
4.2	3.45E-01	2.06E-01	1.46E-01	3.55E-01	2.88E-01	4.65E-01
4.5	3.85E-01	2.09E-01	1.50E-01	3.29E-01	2.86E-01	5.09E-01
4.8	3.91E-01	2.27E-01	1.49E-01	3.32E-01	3.16E-01	4.70E-01
5	3.72E-01	2.99E-01	1.54E-01	4.36E-01	3.11E-01	4.43E-01
5.5	3.76E-01	3.47E-01	1.50E-01	4.46E-01	3.33E-01	4.84E-01
6	3.81E-01	3.79E-01	1.49E-01	4.79E-01	3.90E-01	4.76E-01
6.3	3.97E-01	4.13E-01	1.53E-01	4.66E-01	4.11E-01	5.42E-01
6.8	3.90E-01	4.53E-01	1.48E-01	4.37E-01	4.07E-01	4.72E-01
7.2	4.07E-01	4.61E-01	1.50E-01	4.43E-01	4.23E-01	5.78E-01
7.8	4.33E-01	4.70E-01	1.50E-01	4.98E-01	4.32E-01	5.54E-01
8.3	4.56E-01	4.92E-01	1.49E-01	5.14E-01	4.59E-01	5.13E-01
9	4.87E-01	5.40E-01	1.49E-01	5.06E-01	5.26E-01	4.37E-01
9.5	5.14E-01	5.60E-01	1.51E-01	5.41E-01	5.74E-01	4.60E-01
10	5.49E-01	5.79E-01	1.51E-01	5.82E-01	5.98E-01	5.06E-01
11	5.80E-01	6.08E-01	1.52E-01	5.94E-01	5.57E-01	5.00E-01
12	6.22E-01	6.34E-01	1.50E-01	6.58E-01	6.01E-01	5.76E-01
13.5	6.59E-01	7.09E-01	1.52E-01	7.63E-01	4.68E-01	4.78E-01
14.5	6.87E-01	7.33E-01	1.50E-01	7.69E-01	4.22E-01	5.19E-01

15.5	6.83E-01	7.28E-01	1.51E-01	8.33E-01	4.00E-01	5.03E-01
16.5	7.06E-01	7.40E-01	1.51E-01	8.55E-01	4.08E-01	5.29E-01
18	7.01E-01	7.52E-01	1.49E-01	9.57E-01	4.23E-01	5.08E-01
20	7.32E-01	7.52E-01	1.48E-01	9.33E-01	4.27E-01	4.69E-01
22	7.43E-01	7.69E-01	1.51E-01	9.58E-01	4.15E-01	4.62E-01
23.5	7.13E-01	7.83E-01	1.49E-01	8.45E-01	4.67E-01	4.34E-01

Table 3. Mean and Standard Deviation of Posterior Distribution of θ_{ANTT}

Freq (Hz)	$\mu(\theta_{ANTT})$	$std(\theta_{ANTT})$
1	-3.76E-03	1.19E-03
1.1	-3.68E-03	1.14E-03
1.2	-3.89E-03	1.21E-03
1.3	-4.02E-03	1.27E-03
1.5	-4.21E-03	1.38E-03
1.6	-4.39E-03	1.44E-03
1.7	-4.36E-03	1.42E-03
1.8	-4.49E-03	1.48E-03
2	-4.70E-03	1.57E-03
2.1	-4.93E-03	1.66E-03
2.2	-5.02E-03	1.73E-03
2.4	-5.14E-03	1.77E-03
2.6	-5.16E-03	1.79E-03
2.8	-5.31E-03	1.88E-03
3	-5.43E-03	1.91E-03
3.2	-5.57E-03	1.95E-03
3.4	-5.77E-03	2.02E-03
3.6	-5.97E-03	2.13E-03
4	-6.12E-03	2.17E-03
4.2	-6.18E-03	2.21E-03
4.5	-6.41E-03	2.28E-03
4.8	-6.65E-03	2.38E-03
5	-7.00E-03	2.52E-03
5.5	-7.29E-03	2.64E-03
6	-7.39E-03	2.69E-03
6.3	-7.57E-03	2.80E-03
6.8	-7.80E-03	2.88E-03
7.2	-8.05E-03	2.96E-03
7.8	-8.22E-03	3.04E-03
8.3	-8.43E-03	3.13E-03
9	-8.69E-03	3.20E-03
9.5	-8.93E-03	3.32E-03
10	-9.10E-03	3.37E-03
11	-9.38E-03	3.45E-03
12	-9.57E-03	3.52E-03
13.5	-1.00E-02	3.63E-03
14.5	-1.03E-02	3.71E-03
15.5	-1.06E-02	3.81E-03
16.5	-1.09E-02	3.99E-03
18	-1.10E-02	3.93E-03
20	-1.11E-02	3.97E-03
22	-1.15E-02	4.02E-03
23.5	-1.15E-02	3.86E-03

Table 4. Component of the Standard Deviation of Non-ergodic Ground Motion Models

Freq (Hz)	$\sigma_{Total,nonerg}$	$\tau_{non-erg}$	$\phi_{S2S,non-erg}$	$\varphi_{SS,non-erg}$
1	0.868	0.476	0.506	0.521
1.1	0.881	0.490	0.525	0.511
1.2	0.881	0.467	0.548	0.508
1.3	0.853	0.489	0.490	0.499
1.5	0.786	0.344	0.504	0.496
1.6	0.784	0.372	0.480	0.496
1.7	0.742	0.325	0.451	0.492
1.8	0.758	0.341	0.469	0.488
2	0.793	0.394	0.485	0.489
2.1	0.776	0.382	0.476	0.479
2.2	0.784	0.412	0.455	0.487
2.4	0.762	0.386	0.445	0.484
2.6	0.722	0.344	0.429	0.468
2.8	0.702	0.302	0.430	0.465
3	0.724	0.328	0.443	0.469
3.2	0.725	0.307	0.464	0.465
3.4	0.737	0.300	0.475	0.477
3.6	0.768	0.321	0.514	0.471
4	0.773	0.354	0.500	0.471
4.2	0.774	0.333	0.513	0.475
4.5	0.766	0.309	0.513	0.478
4.8	0.762	0.308	0.505	0.480
5	0.746	0.337	0.455	0.486
5.5	0.739	0.334	0.434	0.496
6	0.743	0.343	0.426	0.503
6.3	0.732	0.335	0.410	0.505
6.8	0.720	0.335	0.384	0.508
7.2	0.727	0.326	0.397	0.514
7.8	0.728	0.320	0.403	0.515
8.3	0.739	0.323	0.413	0.521
9	0.740	0.311	0.412	0.530
9.5	0.751	0.315	0.418	0.539
10	0.768	0.315	0.438	0.547
11	0.765	0.316	0.423	0.553
12	0.755	0.299	0.418	0.553
13.5	0.742	0.315	0.368	0.562
14.5	0.749	0.311	0.365	0.575
15.5	0.771	0.320	0.401	0.576
16.5	0.778	0.319	0.406	0.582
18	0.784	0.320	0.400	0.594
20	0.809	0.312	0.423	0.615
22	0.843	0.323	0.443	0.641
23.5	0.865	0.314	0.468	0.656

Table 5. Geographical coordinates and site terms for the example sites.

No.	Latitude	Longitude	V_{S30} (m/s)	β_0(1Hz)	β_0(5Hz)	f_{Vs30}(1Hz)	f_{Vs30}(5Hz)
Site1	43.6748°N	5.7664°E	2100	0.1632	-0.1591	0	0
Site2	47.2294 °N	0.1673°W	1020	-0.1660	-0.0029	0	0
Site3	49.5379°N	1.8754°W	1900	-0.1877	-7.58E-04	0	0
Site4	48.5164°N	3.5185°E	765	-0.0217	-5.28E-06	2.49E-05	-8.75E-06
Site5	45.4°N	5.4°E	900	0.6591	-	-0.0001	-
Site6	42.2°N	1.0°E	783	-	0.5003	-	0.0004
Site7	48.0°N	2.0°W	285	-0.6690	-	0.0023	-
Site8	45.2°N	6.0°E	900	-	-0.2246	-	-0.0007
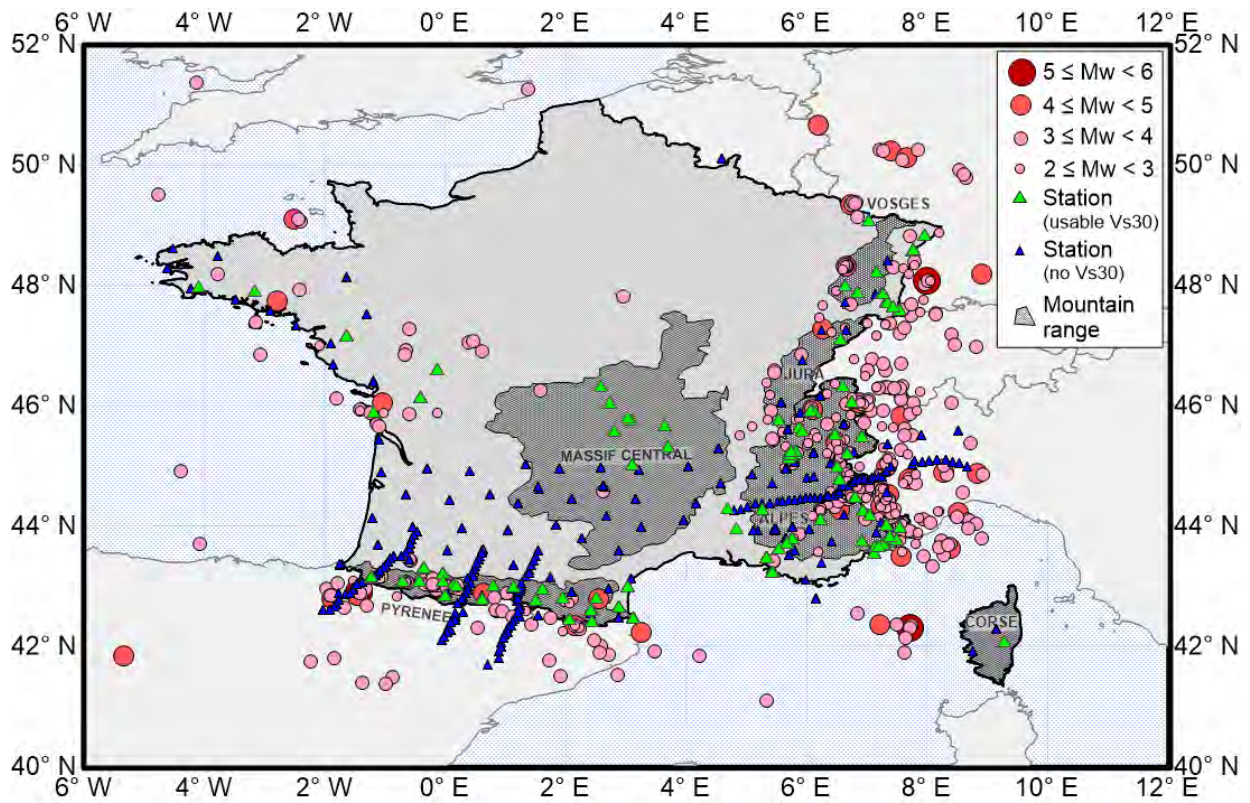
Figure 1. Map showing locations of the strong-motion stations and crustal earthquakes of France used in this study. The circles indicate the earthquake epicenters and the triangles indicate the locations of the stations.
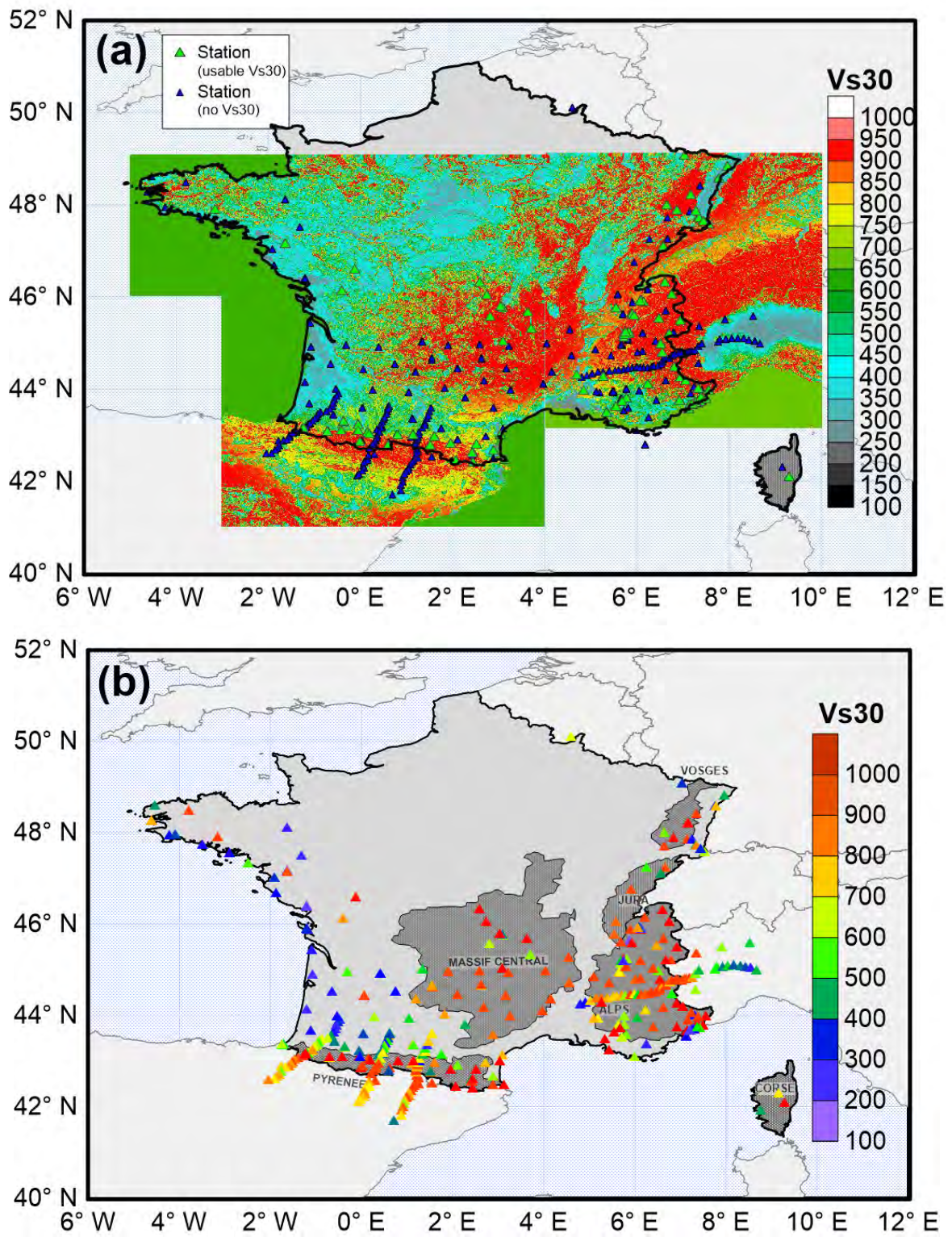
Figure 2. (a) global Vs30 values form USGS in France, and (b) final chosen Vs30 per station.
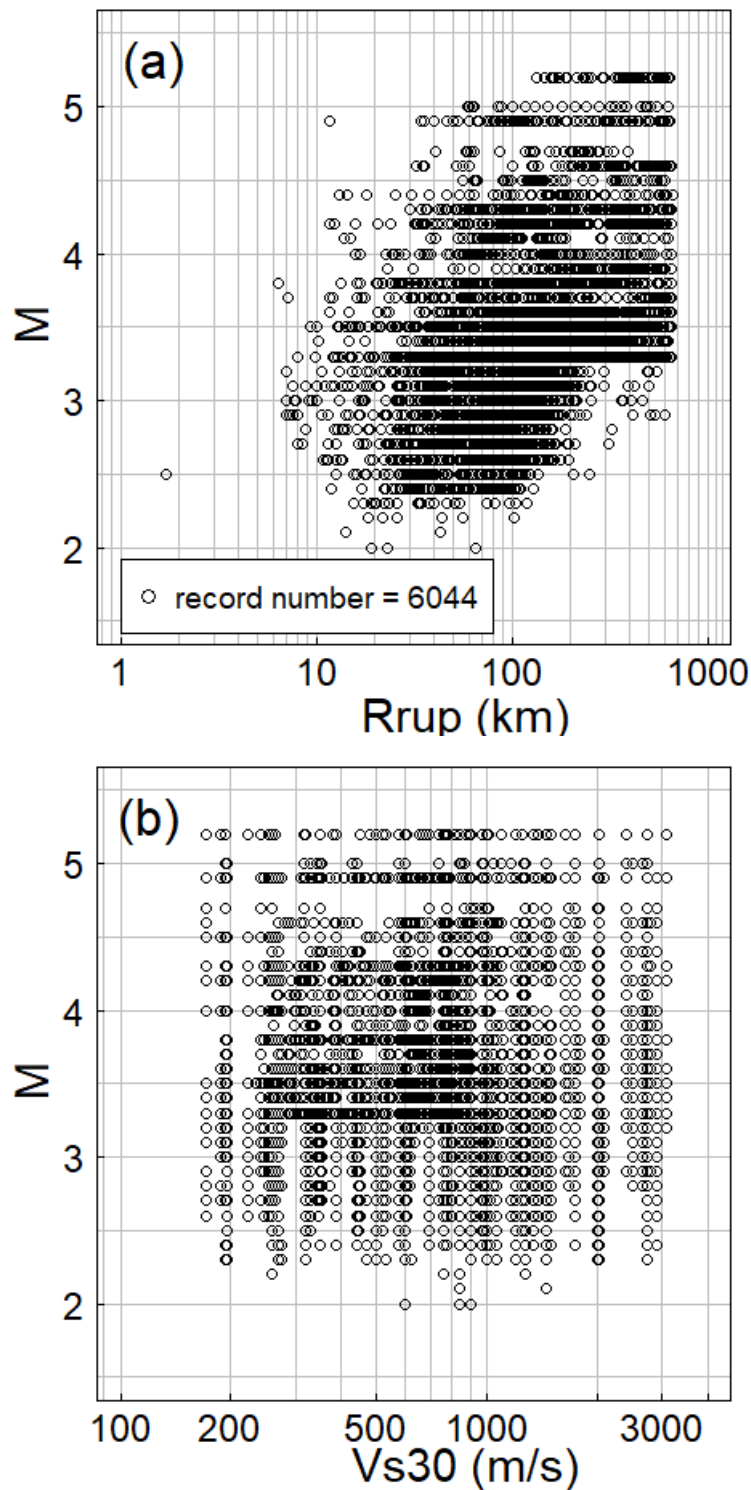
Figure 3. (a) Magnitude-distance and (b) magnitude-Vs30 distribution for RESIF database.
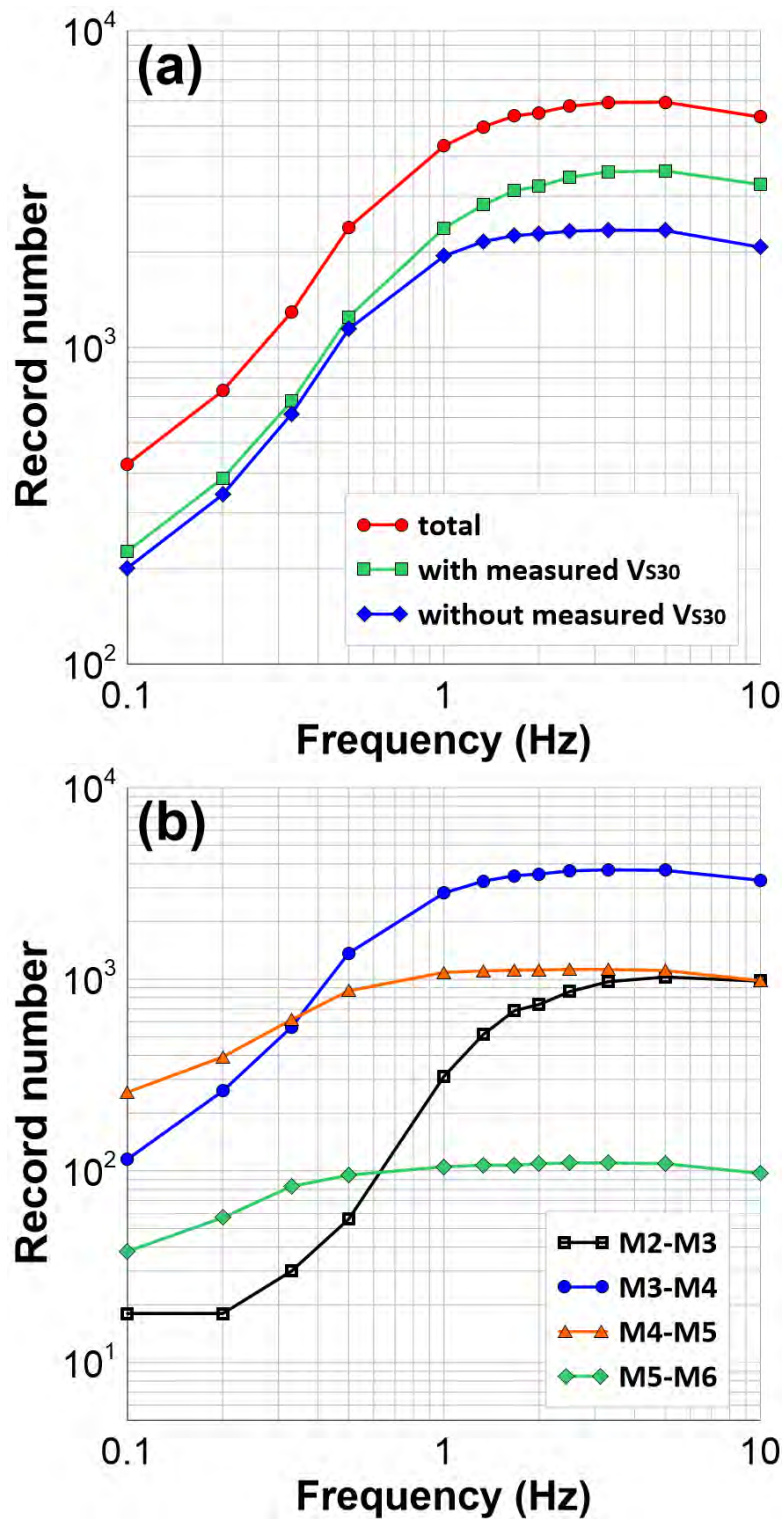
Figure 4. (a) the number of the original record with measured Vs30 (green) and without measured Vs30 (blue), red line is the final number of records after adding the global Vs30 of the USGS, (b) the number of records for different magnitude ranges.
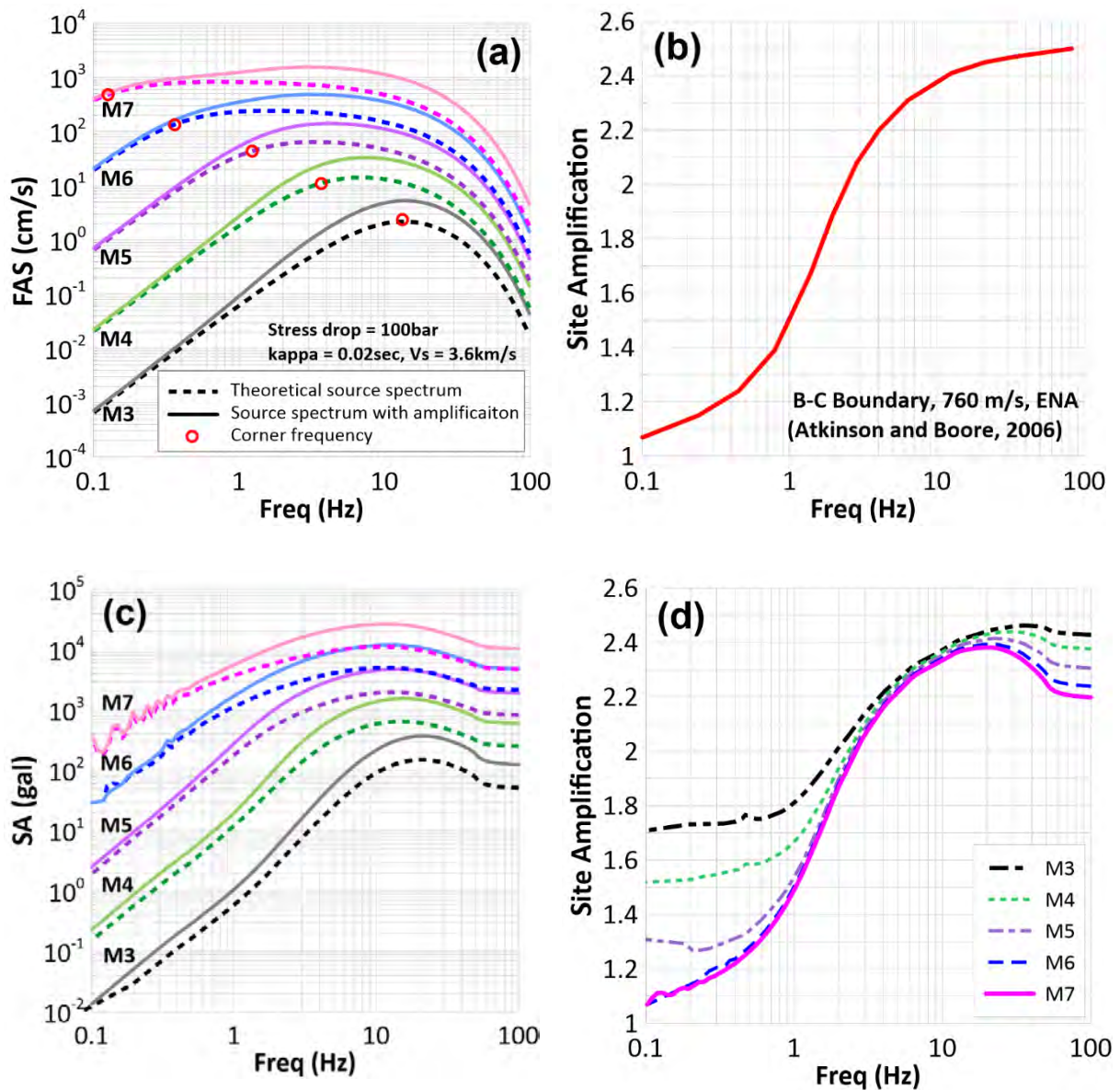
Figure 5. (a) two theoretical source spectrums are based on the omega-squared spectrum (Aki 1967; Brune, 1970) from M3 to M7, solid lines mean the spectrums contain the site amplification. (b) the site amplification function based on the B/C boundary of Akinson and Boore (2006). (c) two response spectrums are converted from FAS via RVT. (d) the site amplification function from the two response spectrums (ratio of the two spectrums per magnitude).
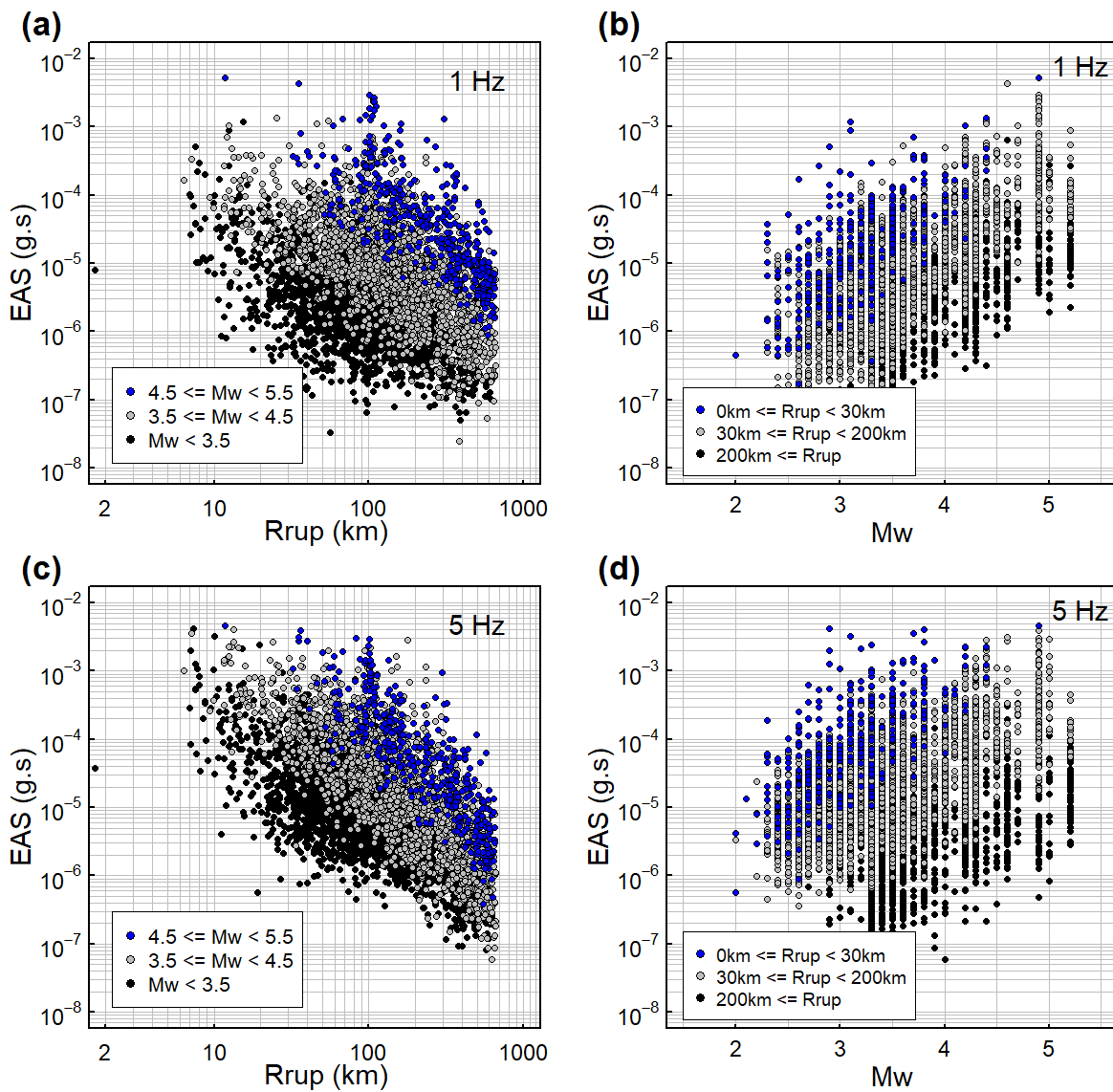
Figure 6. Distribution of EAS as function of magnitude and distance, for 1.0 Hz and 5.0 Hz.
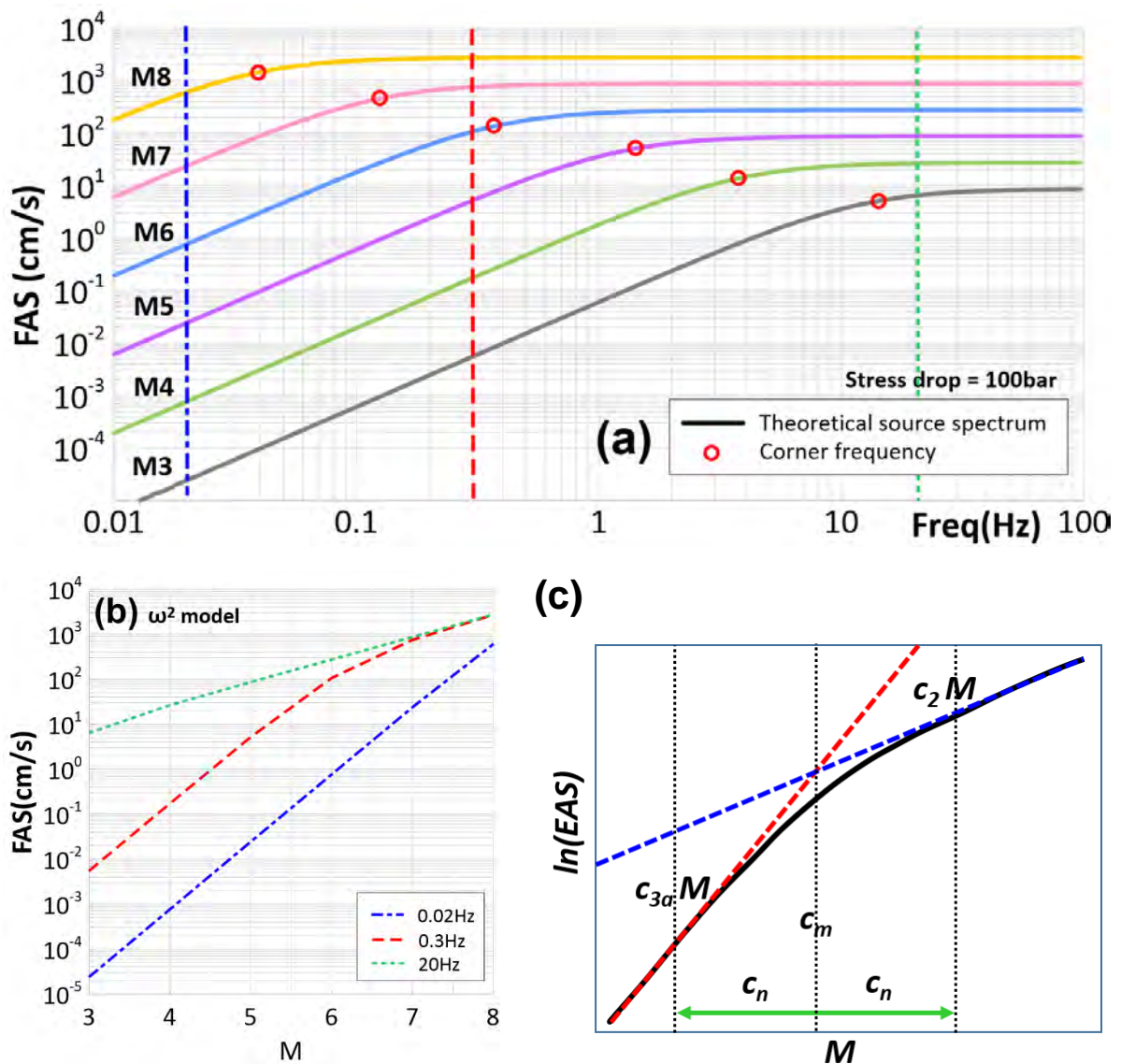
Figure 7. (a) an omega-squared spectrum (Aki, 1967; Brune 1970) from M3 to M7, (b) the results for magnitude scaling of 0.02, 0.3, and 20Hz, and (c) a smooth transition scaling model between a slope at the low magnitudes ($c_{3a}M$) and a slope at the large magnitudes (c_2M) in CY14 model.
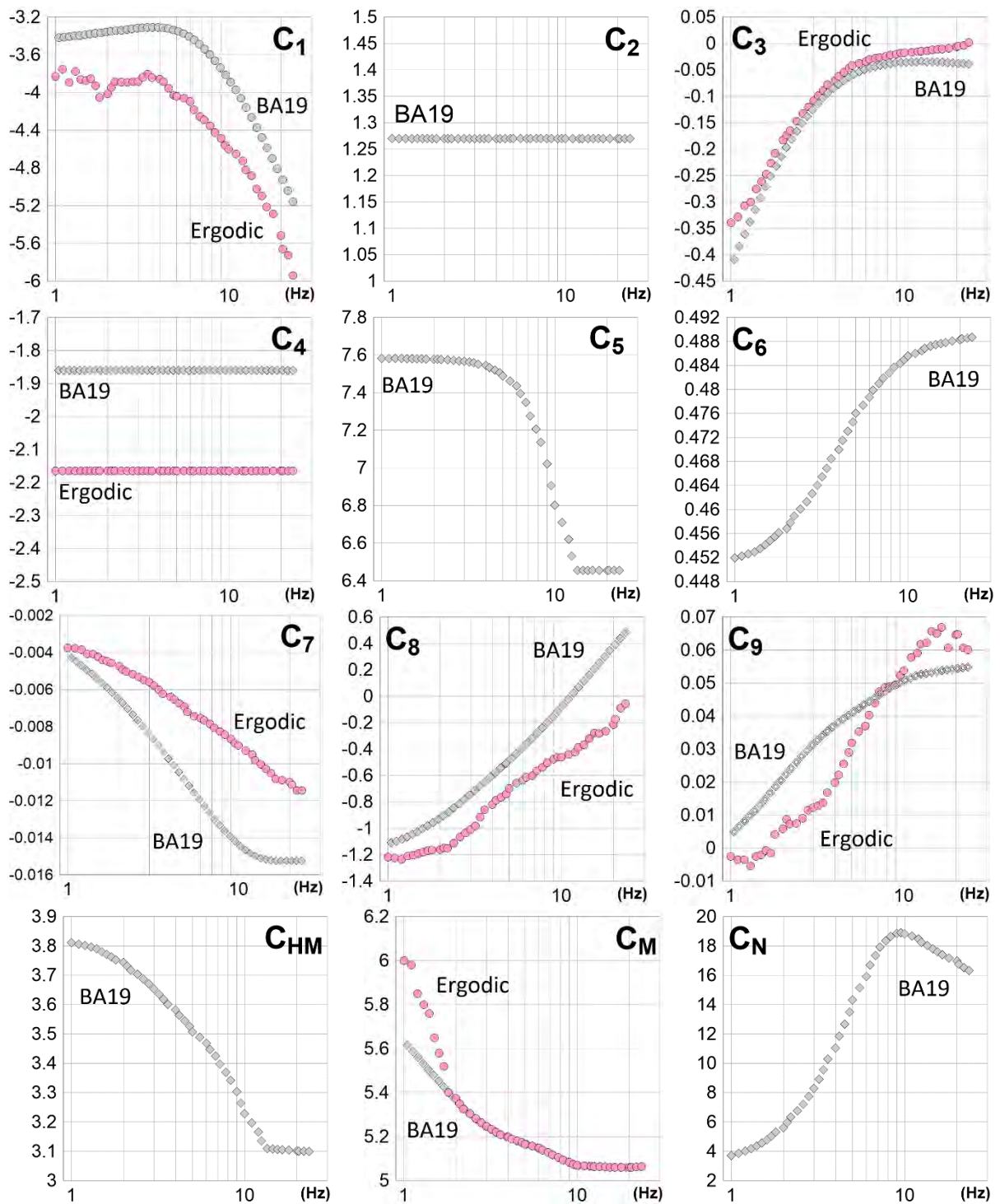
Figure 8. Coefficients of ergodic ground motion models. Gray points are the coefficients of BA19, pink points are the results of the French ergodic model.
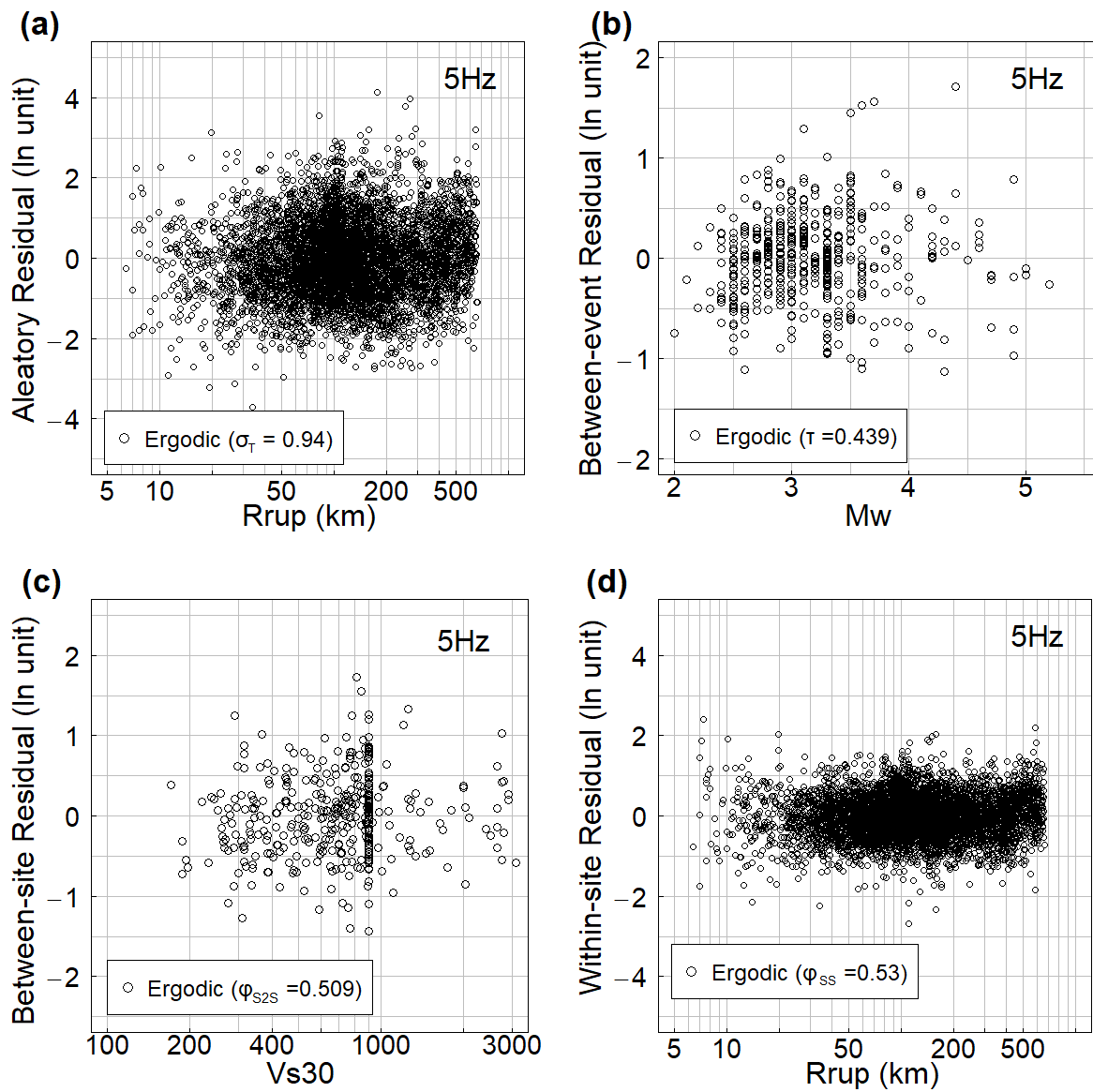
Figure 9. (a) aleatory, (b) between-event, (c) between-site, and (d) within-site residuals of the ergodic GMM for 5.0 Hz.
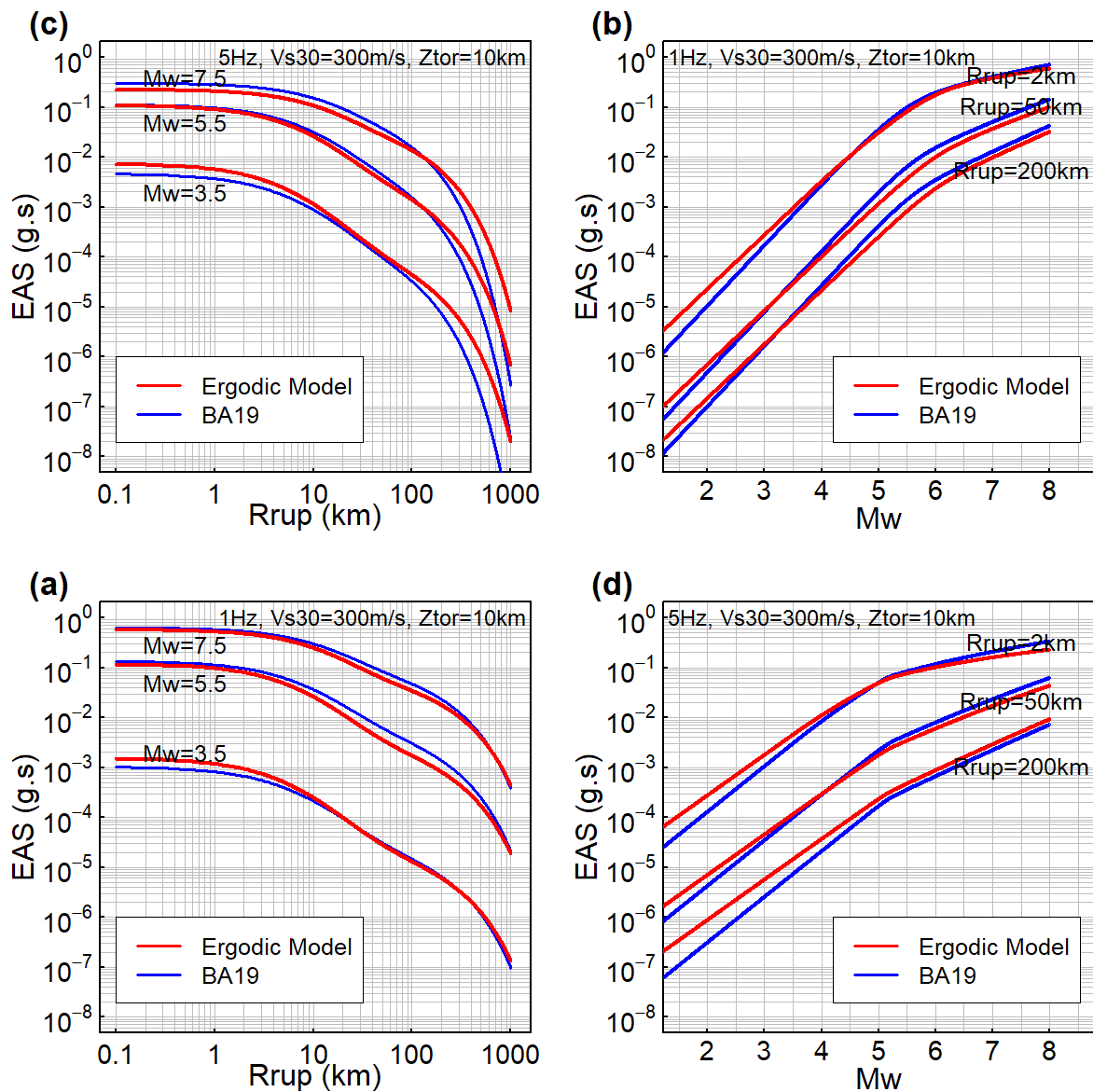
Figure 10. The median EAS as function of magnitude and distance, for 1.0 Hz and 5.0 Hz
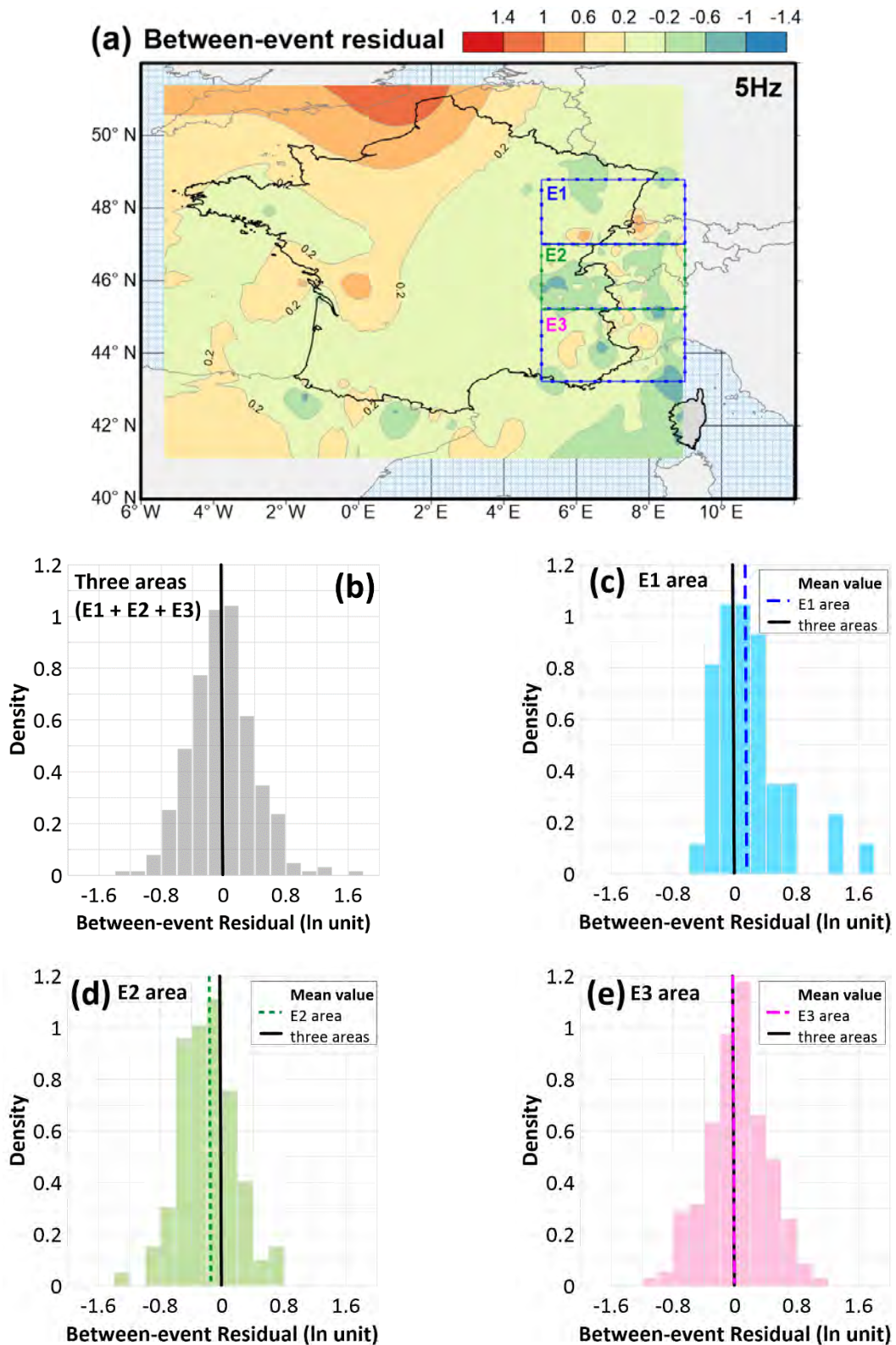
Figure 11. (a) the regional difference effect of the between-event residuals at 5.0 Hz. probability density function and mean values for (b) the combination of three areas, (c) E1 area, (d) E2 area, and (e) E3 area.
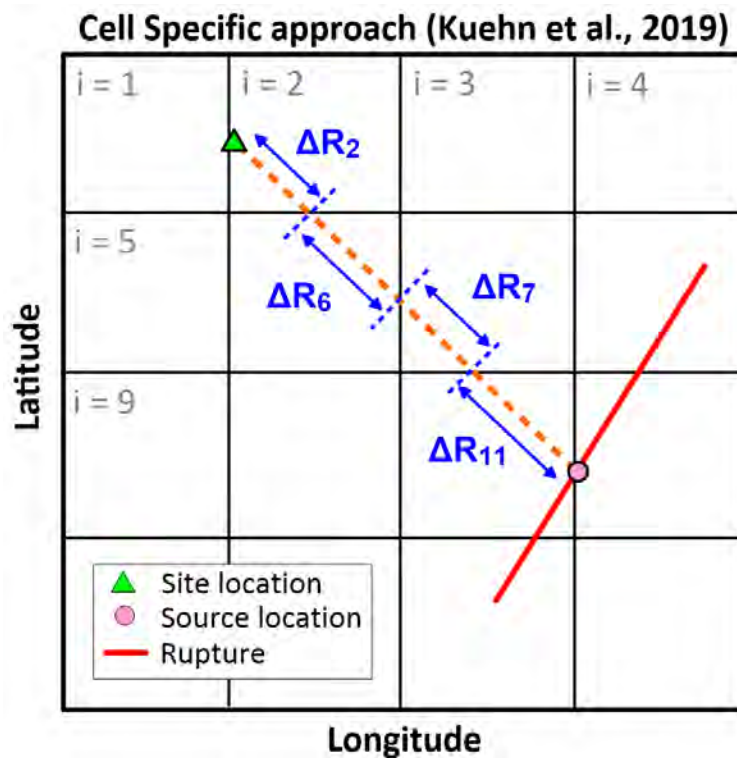
Figure12 Schematic showing how the length of the ray in the ith cell are calculated for the regression of the cell-specific attenuation coefficients (Kuehn et al., 2019).
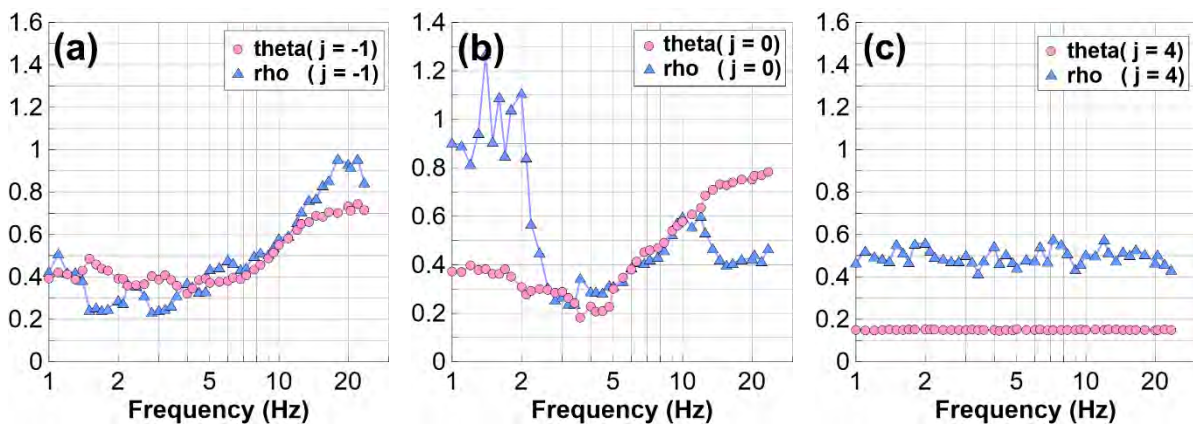
Figure 13. Hyperparameter of kernel function for frequencies: (a) θ_{-1} and ρ_{-1}, (b) θ_0 and ρ_0, (c) θ_4 and ρ_4 in the VCM.
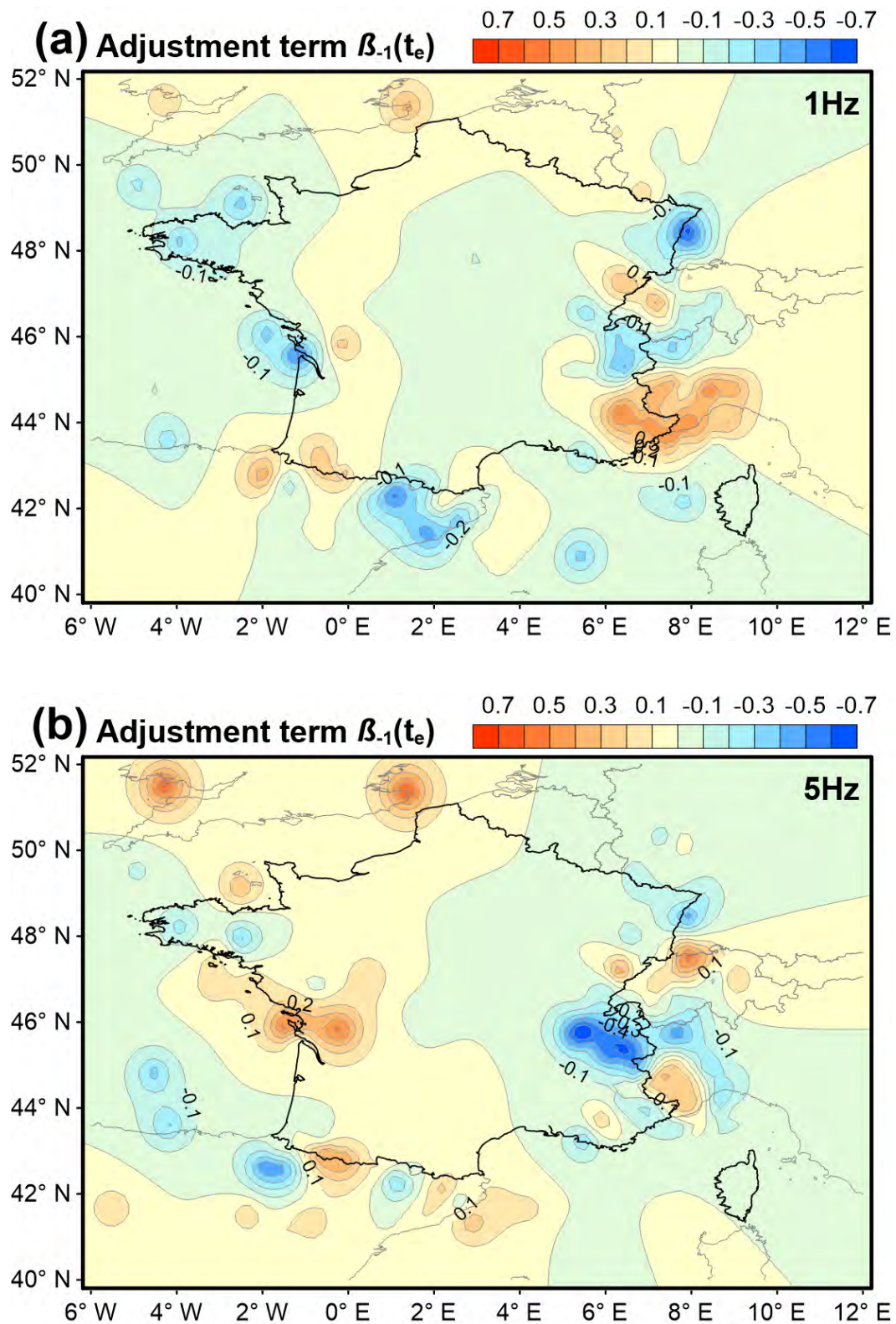
Figure 14. Spatially varying adjustment of constant event term (β_{-1}) for 1Hz and 5Hz.
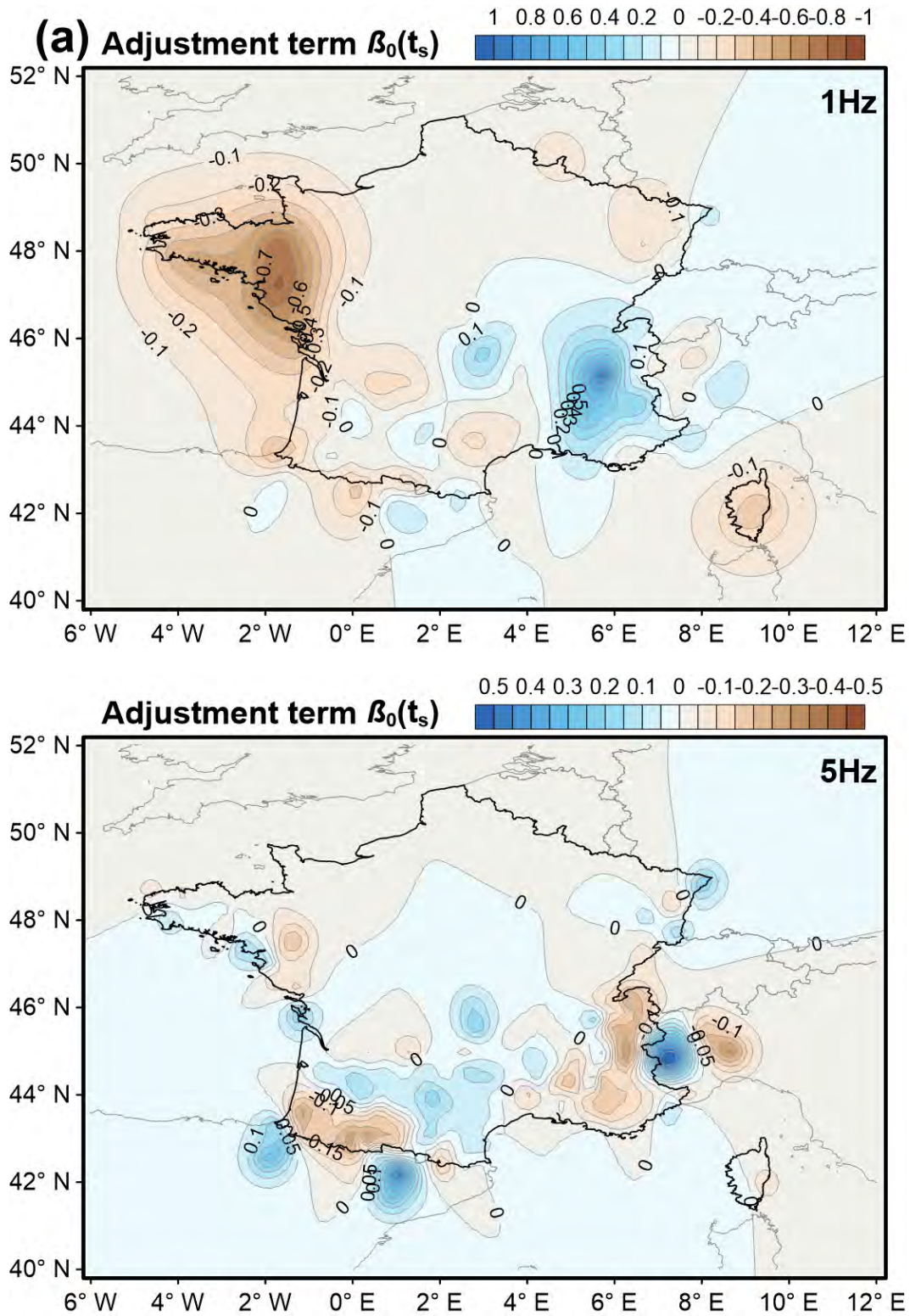
Figure 15. Spatially varying adjustment of constant source term (β_0) for 1Hz and 5Hz.
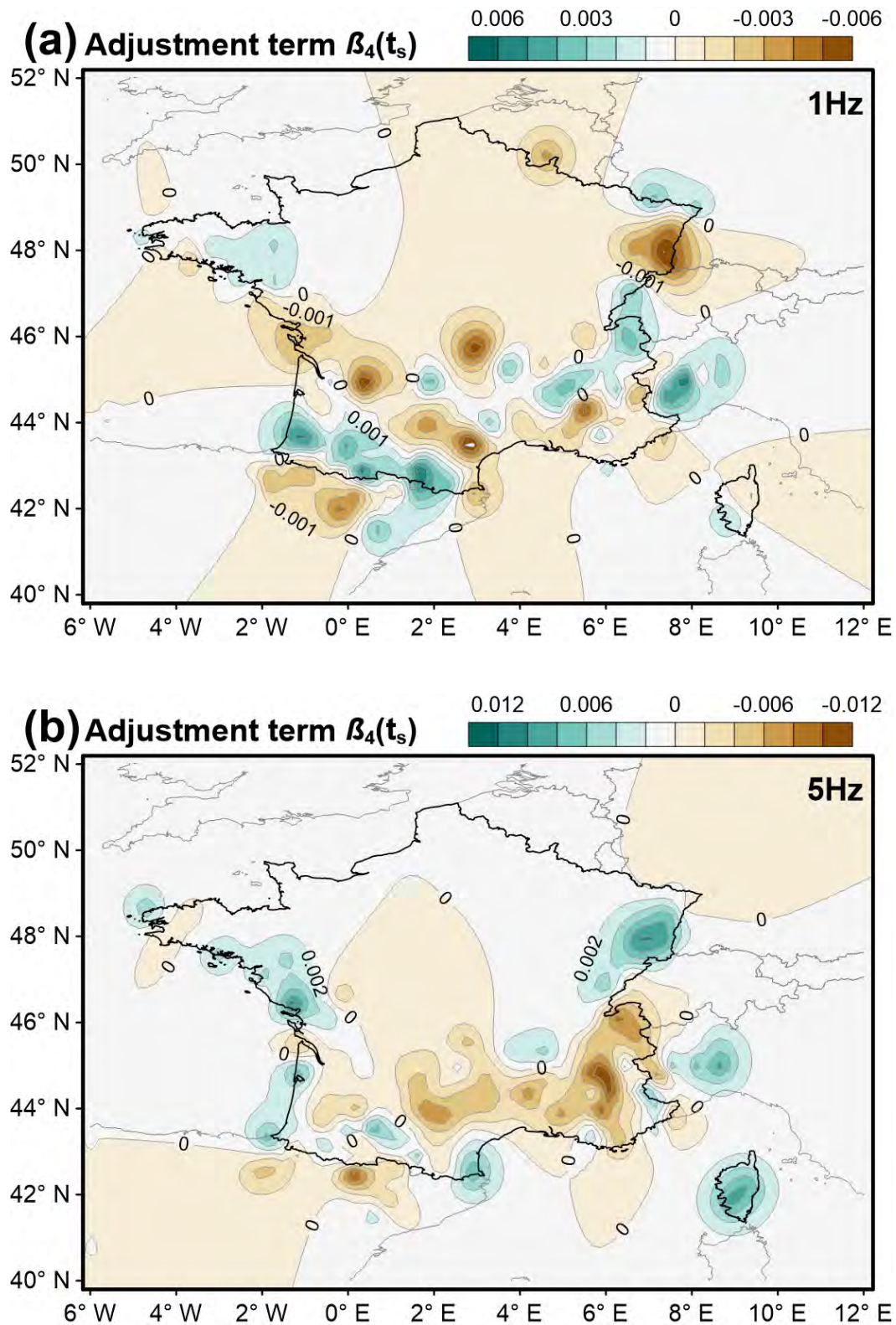
Figure 16. Spatially varying adjustment of linear-Vs30 scaling term (β_4) for 1Hz and 5Hz.
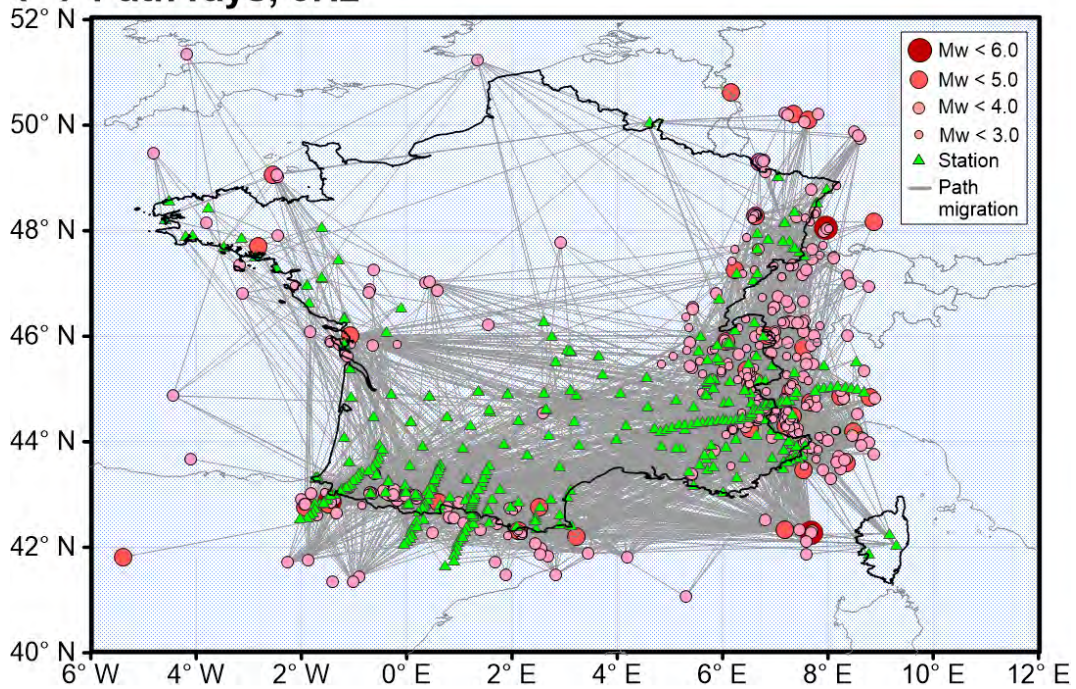
Figure 17. (a) Map of path rays with stations and earthquakes at 5.0 Hz, each gray line shows the path from the earthquake to the recording station. (b) Number of paths per cell, the cell size is 0.2 times 0.2 degrees.
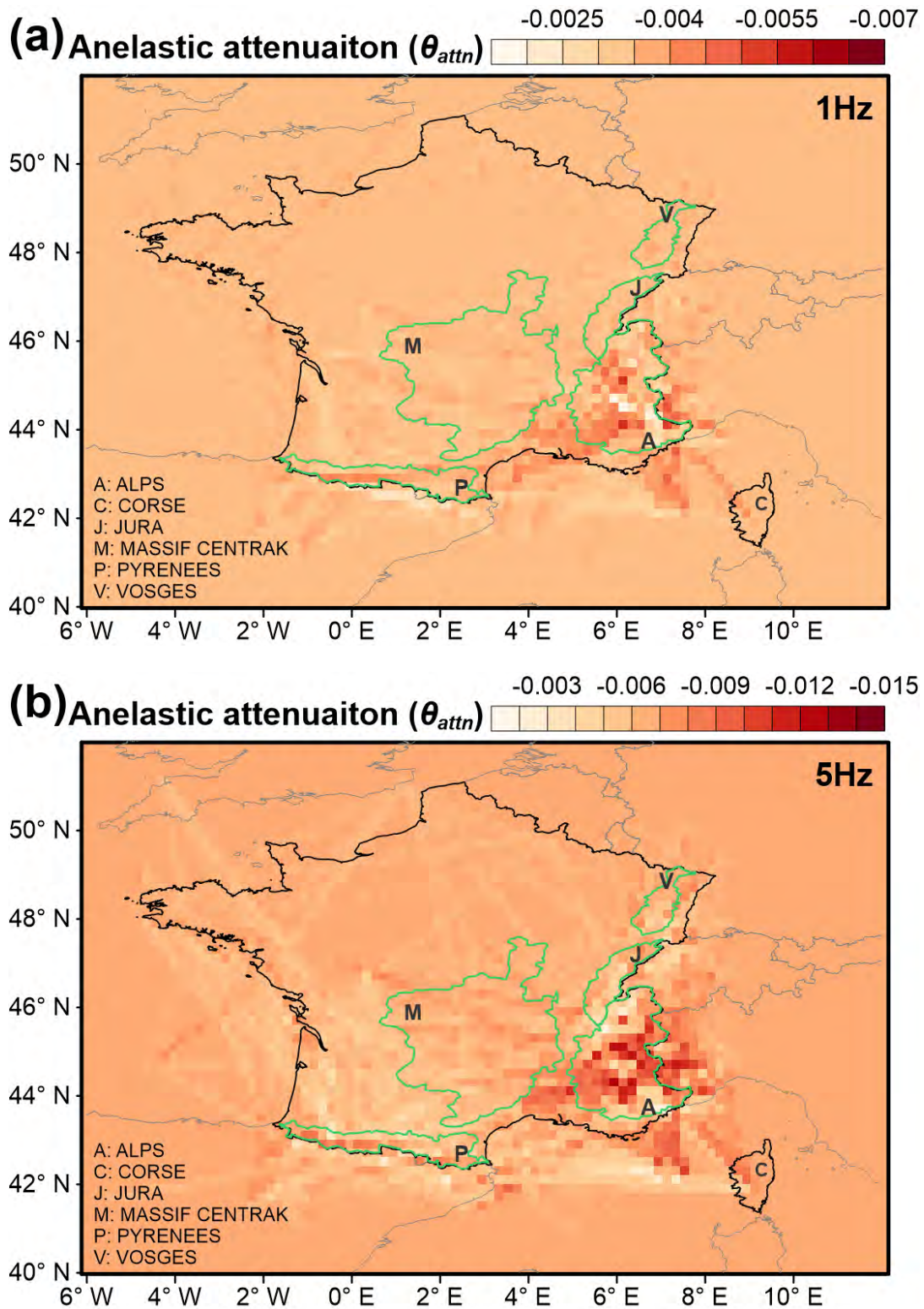
Figure 18. Mean values of the posterior distribution of the θ_{Attn} per cell, for (a) 1.0 Hz and (2) 5.0 Hz. Green lines are mountain regions.
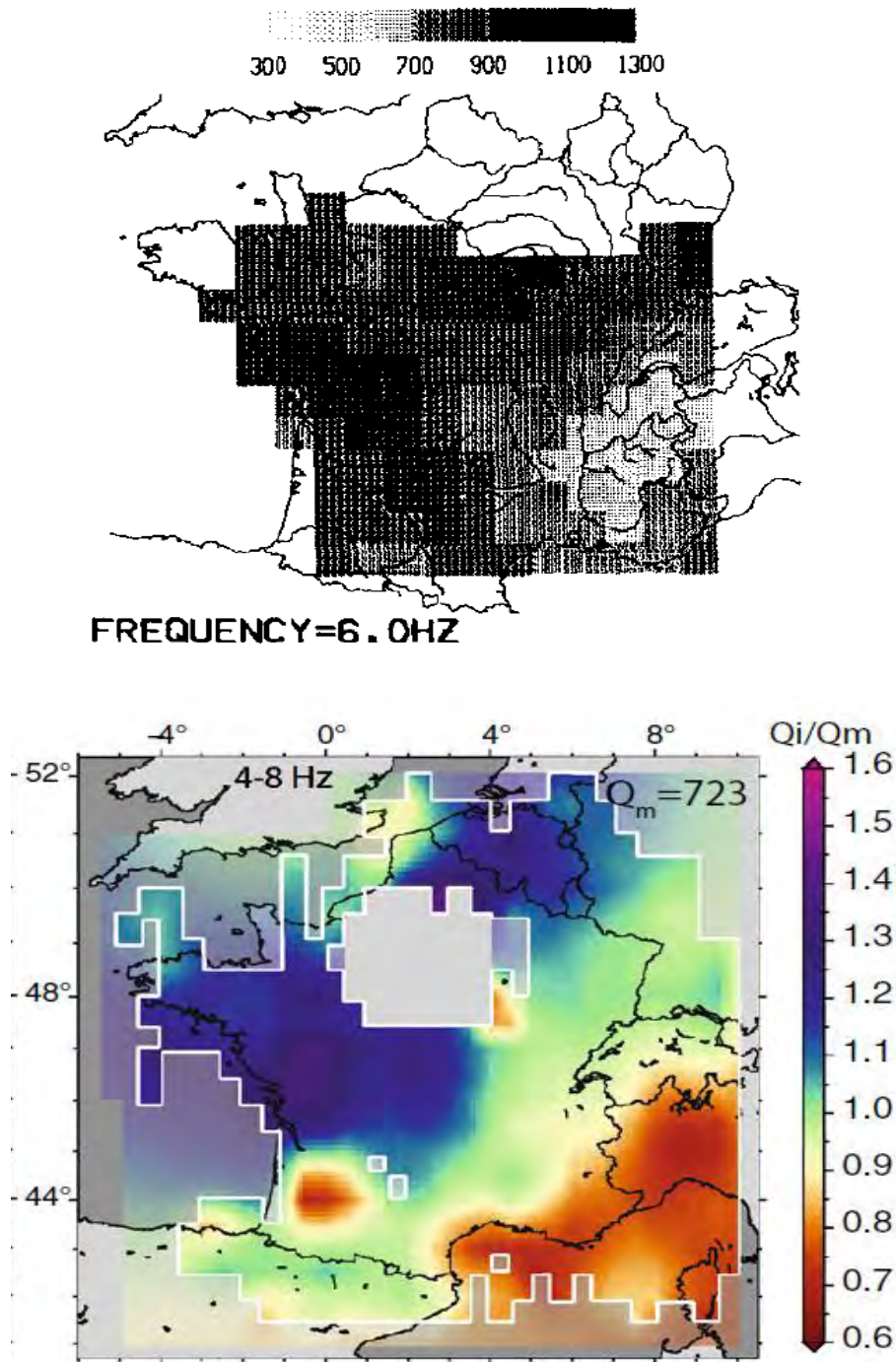
Figure 19. (a) the Qs in Figure 5 of Campillo and Plantet (1991) at 6Hz, and (2) the ratio of the absorption quality factor (Qi) and the spatial average of Qi (Qm) in Figure5 of Mayor et al. (2018) at 4 – 8 Hz.
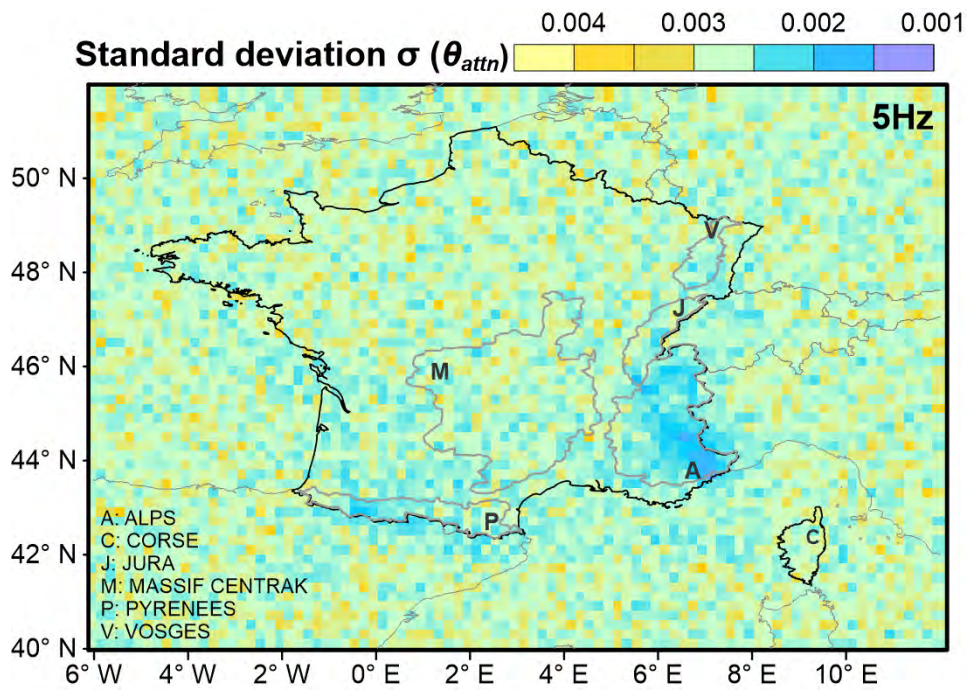
Figure 20. Standard deviation of the posterior distribution of the θ_{Attn} per cell for 5.0 Hz
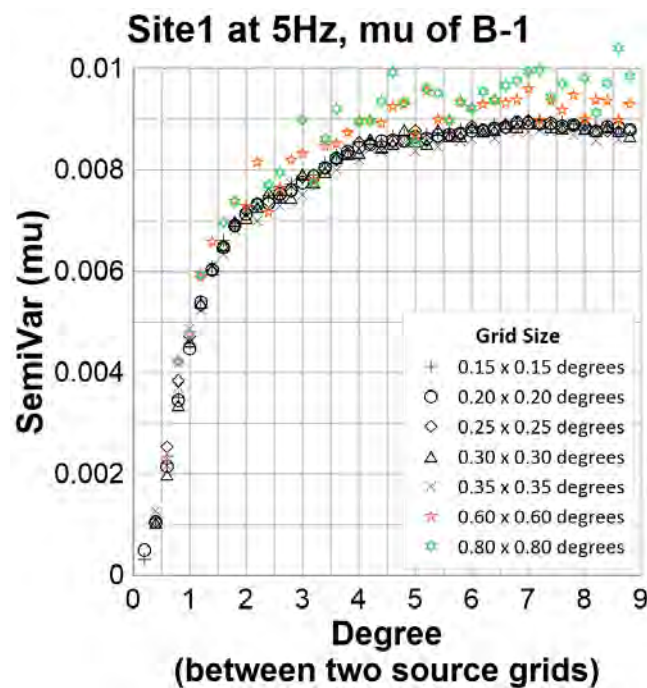
Figure 21. the semi-variogram of the non-ergodic source term (e.g., Figure 14b) for the different grid sizes at 5Hz.
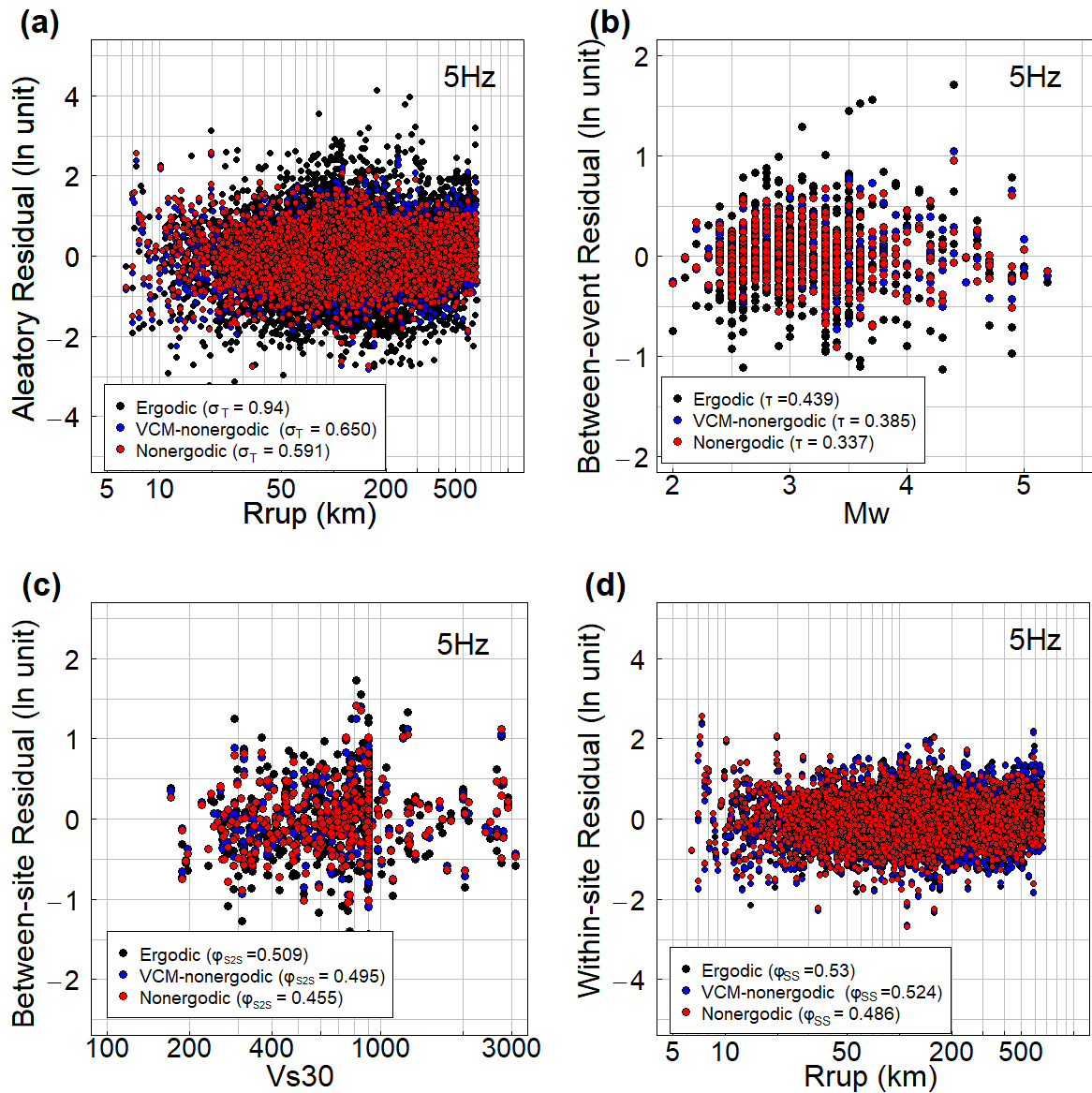
Figure 22. Residual of the ergodic GMM (black circles), VCM-non-ergodic GMM (blue circles), and non-ergodic GMM (red circles) for 5.0 Hz.
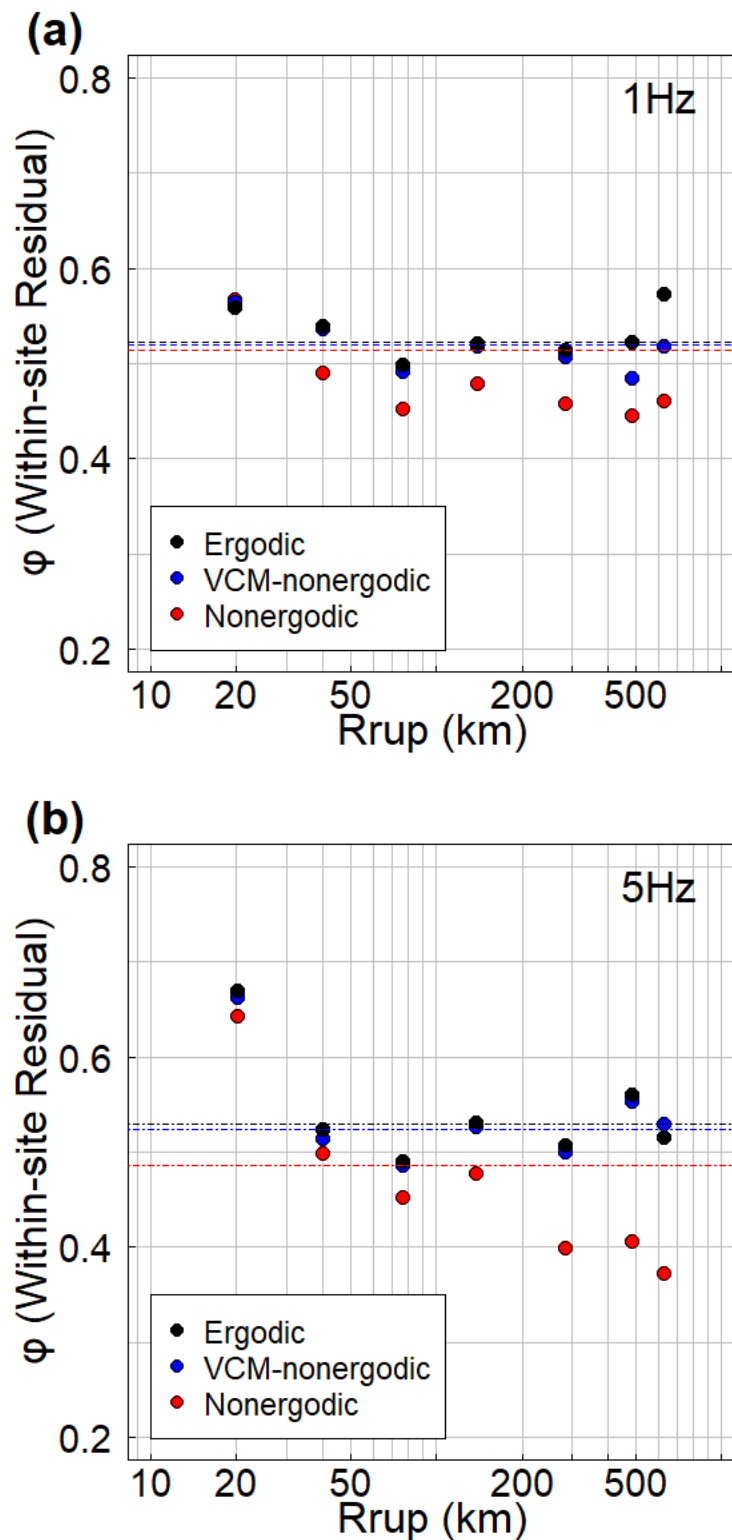
Figure 23. the standard deviations of the within-site residuals in different distance bins for the three models for ergodic, VCM-non-ergodic, and non-ergodic GMMs for (1) for 1.0 Hz, and (2) for 5.0 Hz. Dashed lines are within-site standard deviation for each GMM.
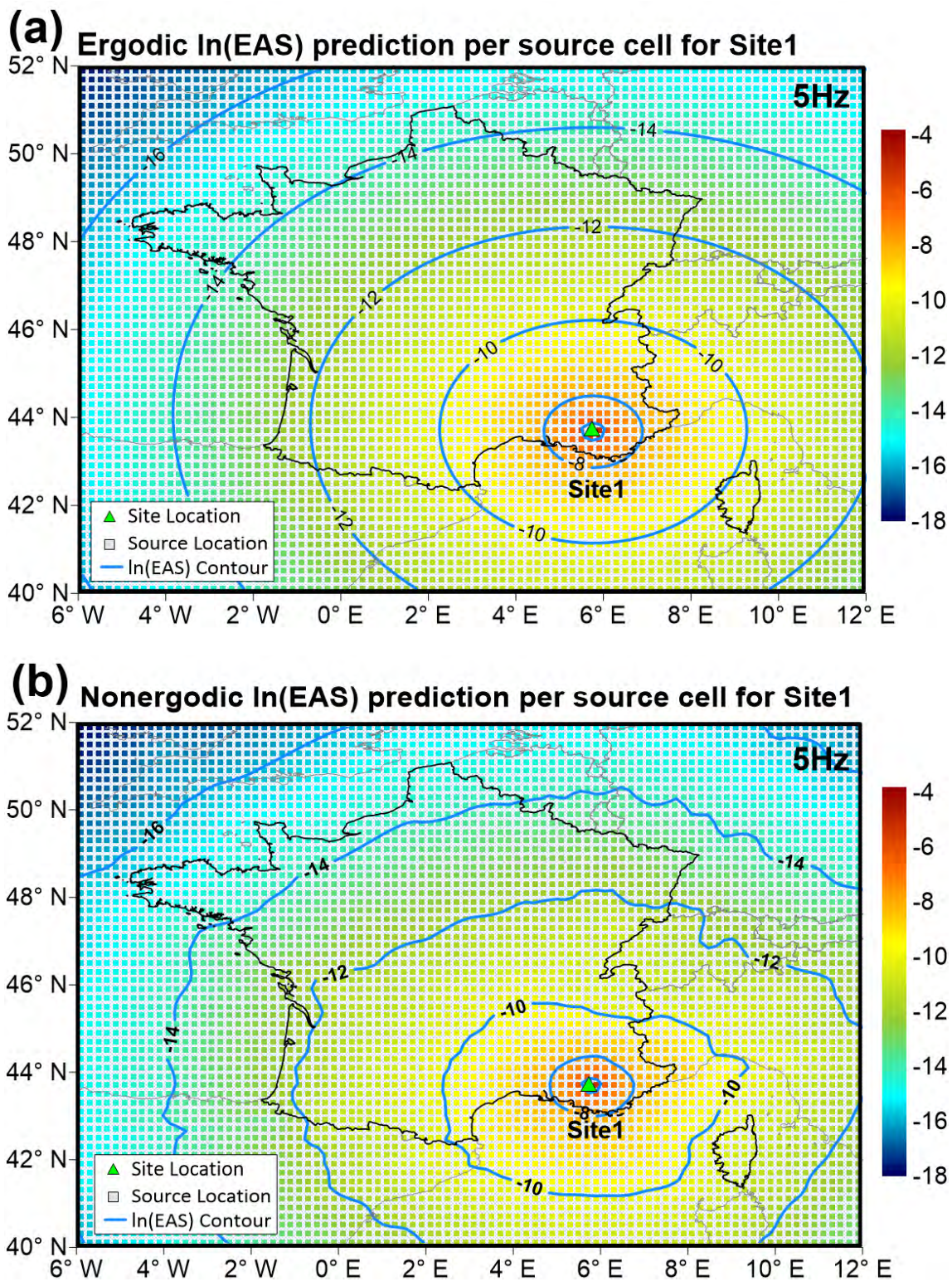
Figure 24. Median EAS predictions at Site1 for (a) the French ergodic model, and (b) the French non-ergodic model at 5.0 Hz.
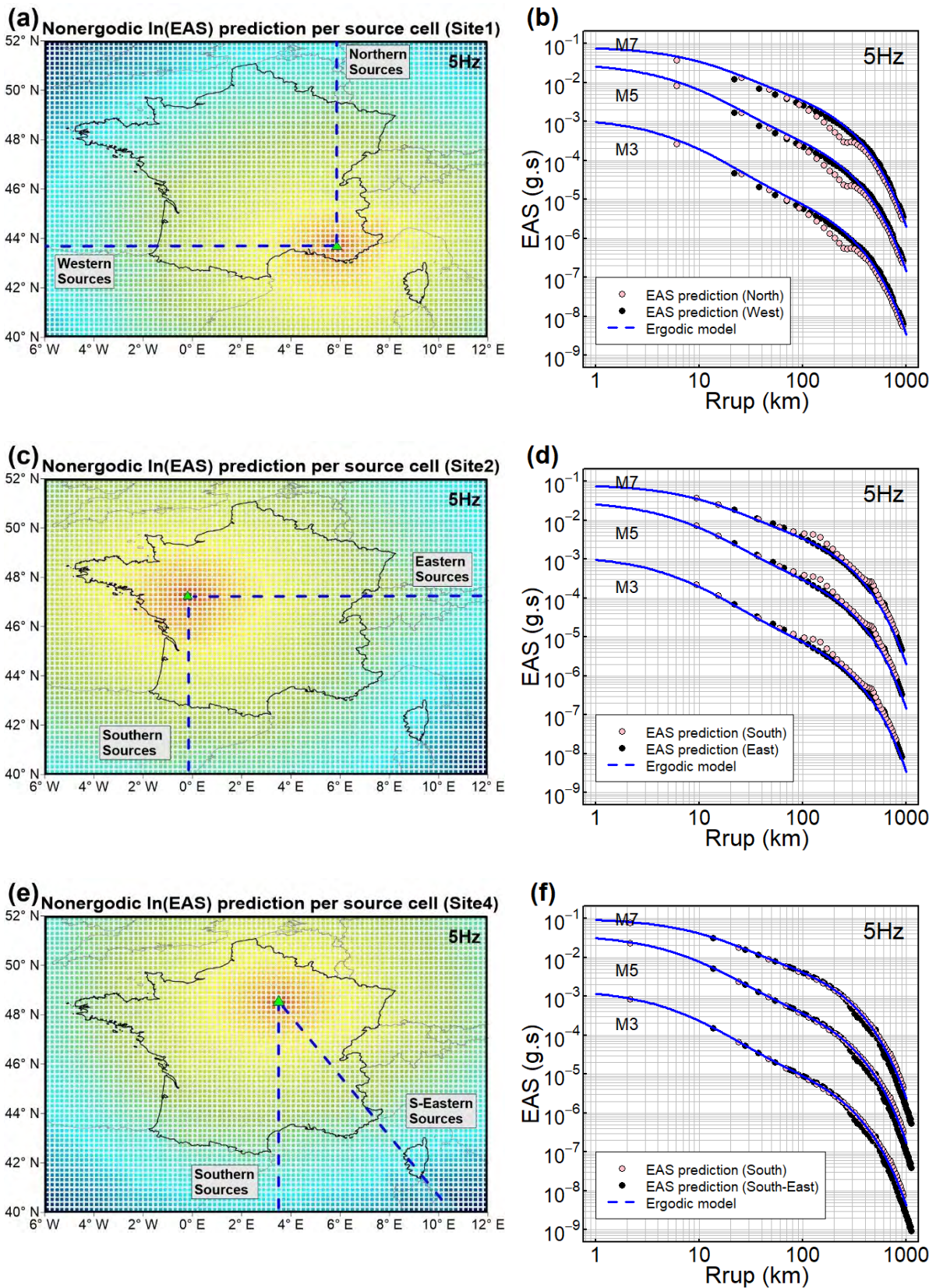
Figure 25. Distance scaling of the EAS prediction of ergodic and non-ergodic models at the given site for 5.0 Hz.
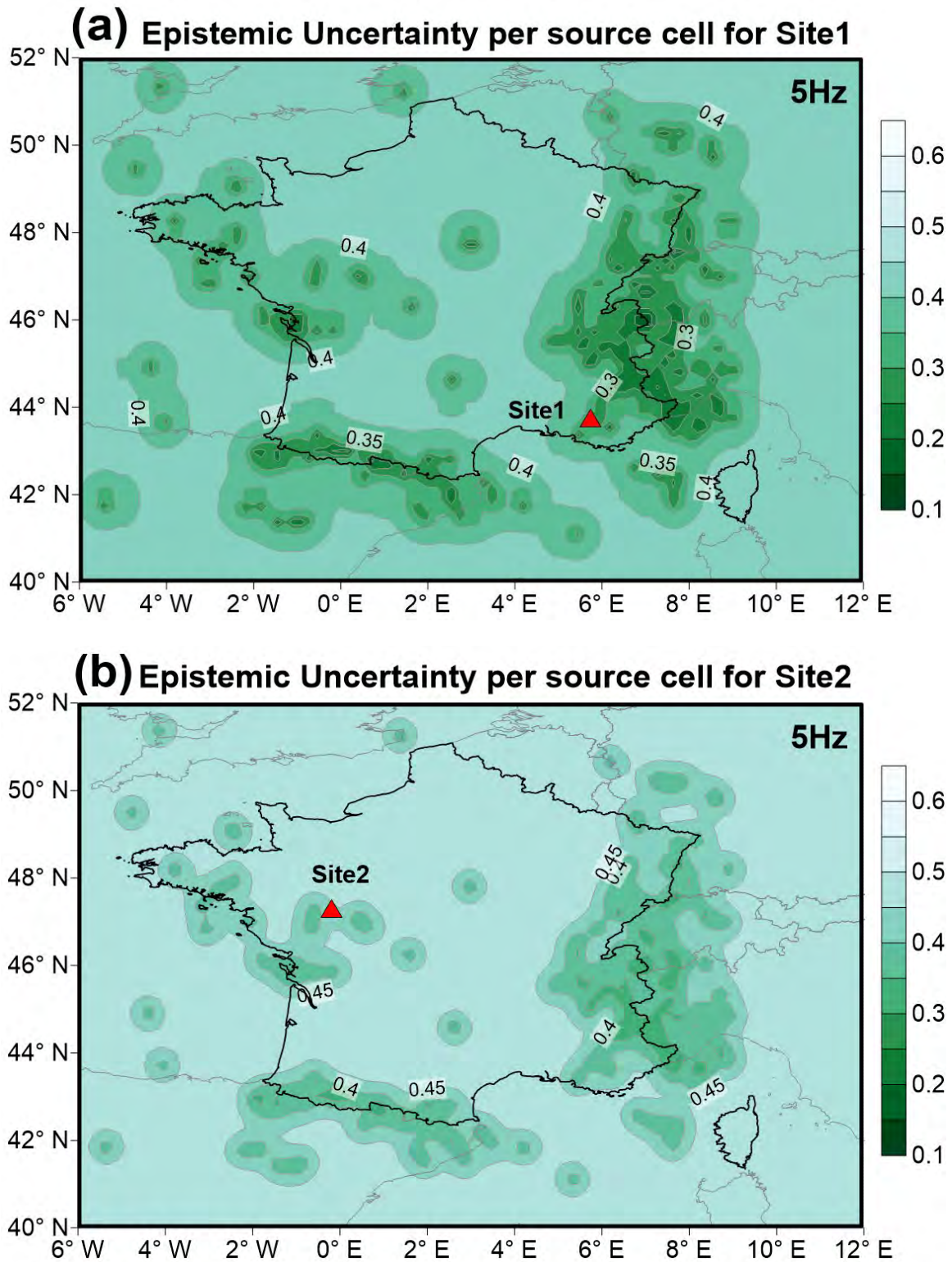
Figure 26. Epistemic uncertainty of a non-ergodic model per cell at 5.0 Hz for (1) Site1 and (2) Site2.
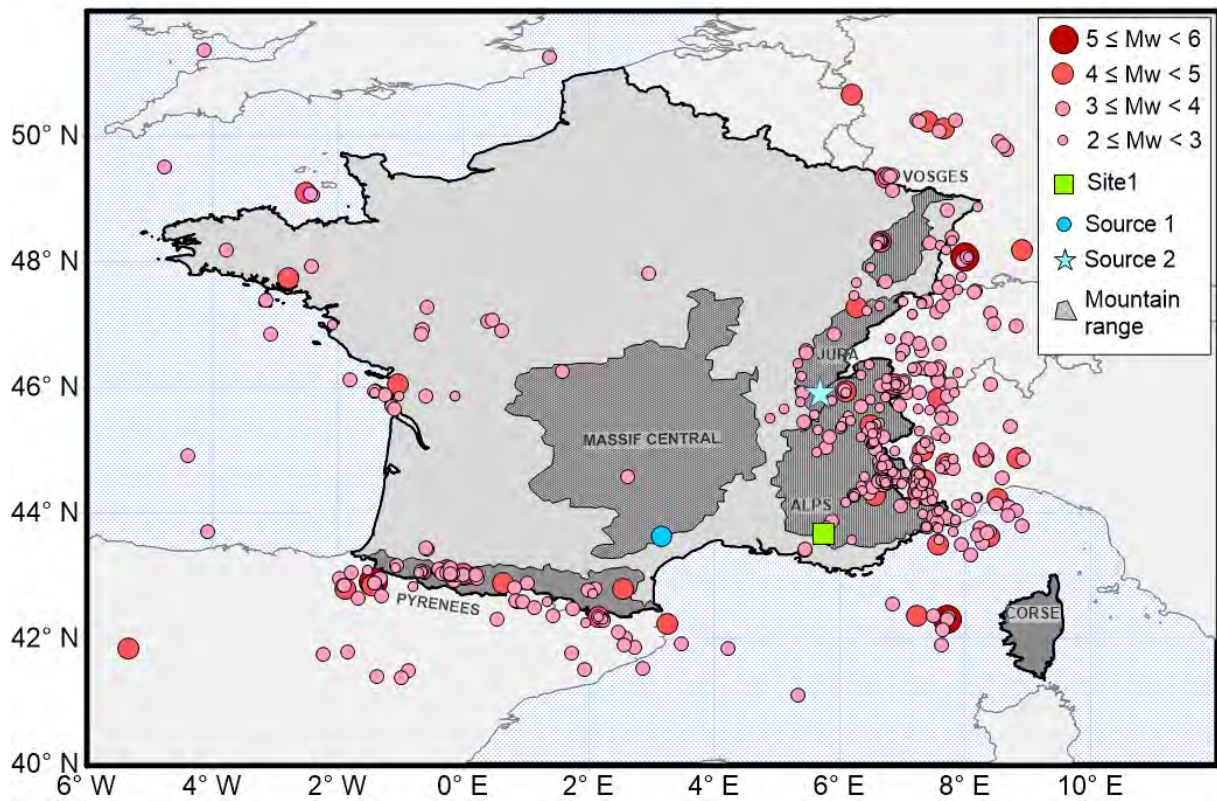
Figure 27. the distribution of the available data and two target sources for Site1.
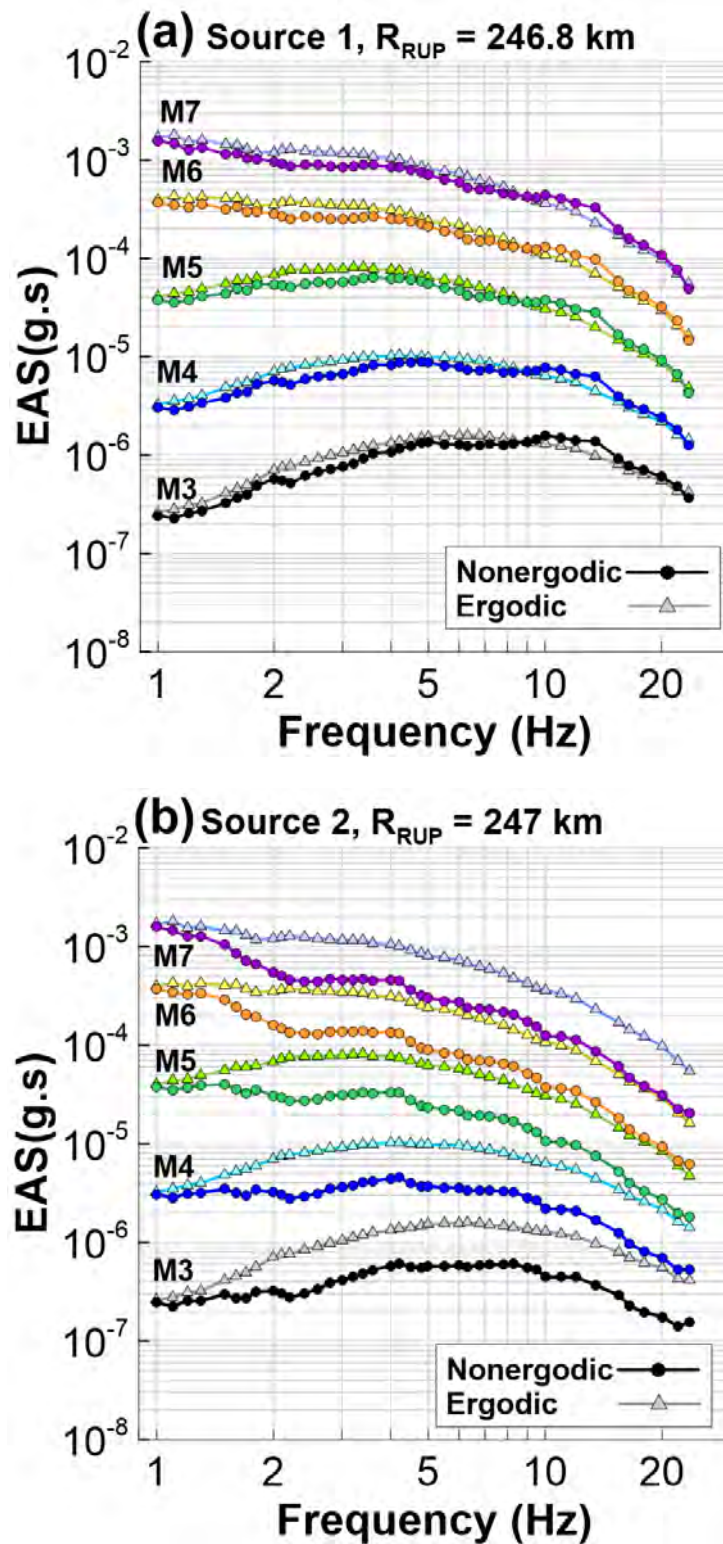
Figure 28. Median EAS spectra from the BA19, ergodic and non-ergodic models from M3 to M8 for each frequency, for (a) source1 and (b) source 2.
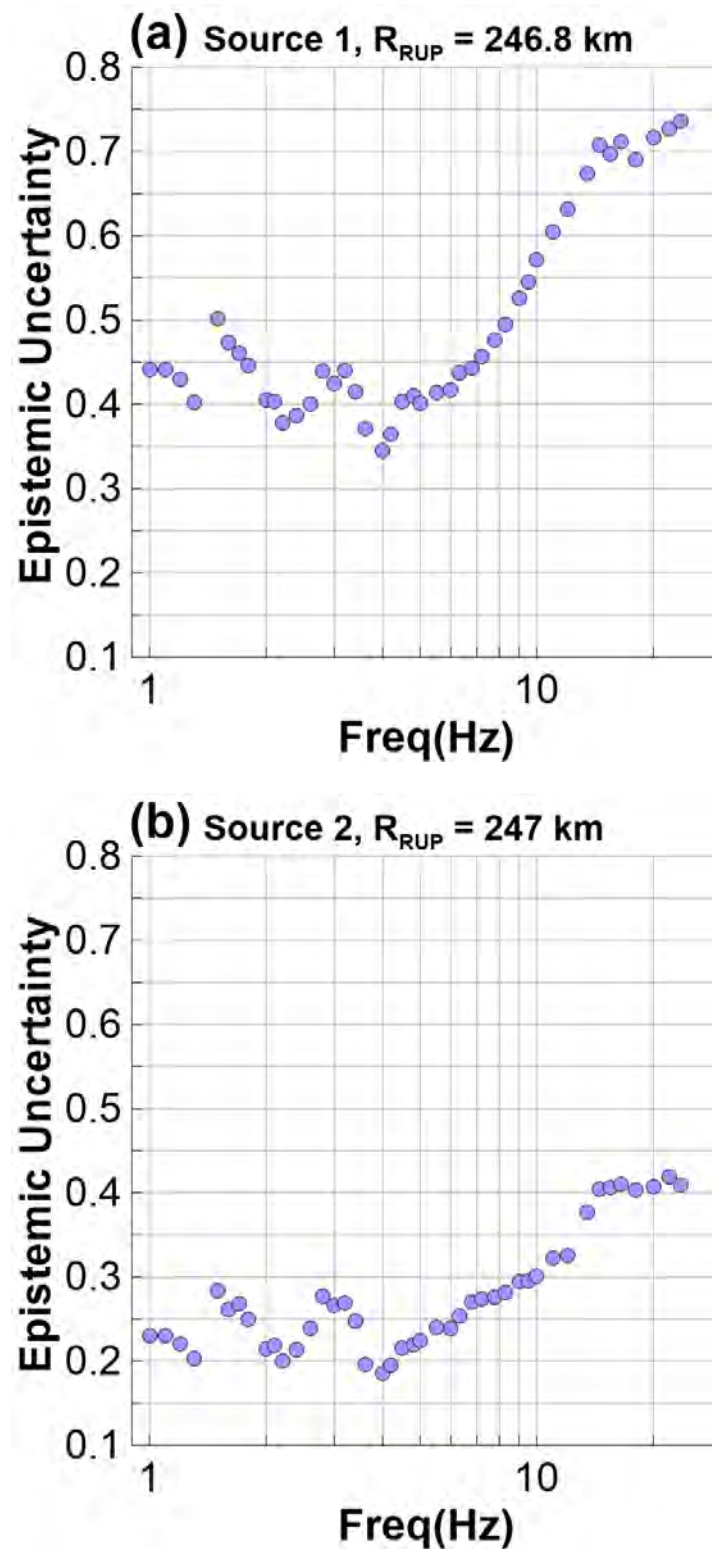
Figure 29. The epistemic uncertainty of the non-ergodic model for each frequency, for (a) source 1 and (b) source 2.
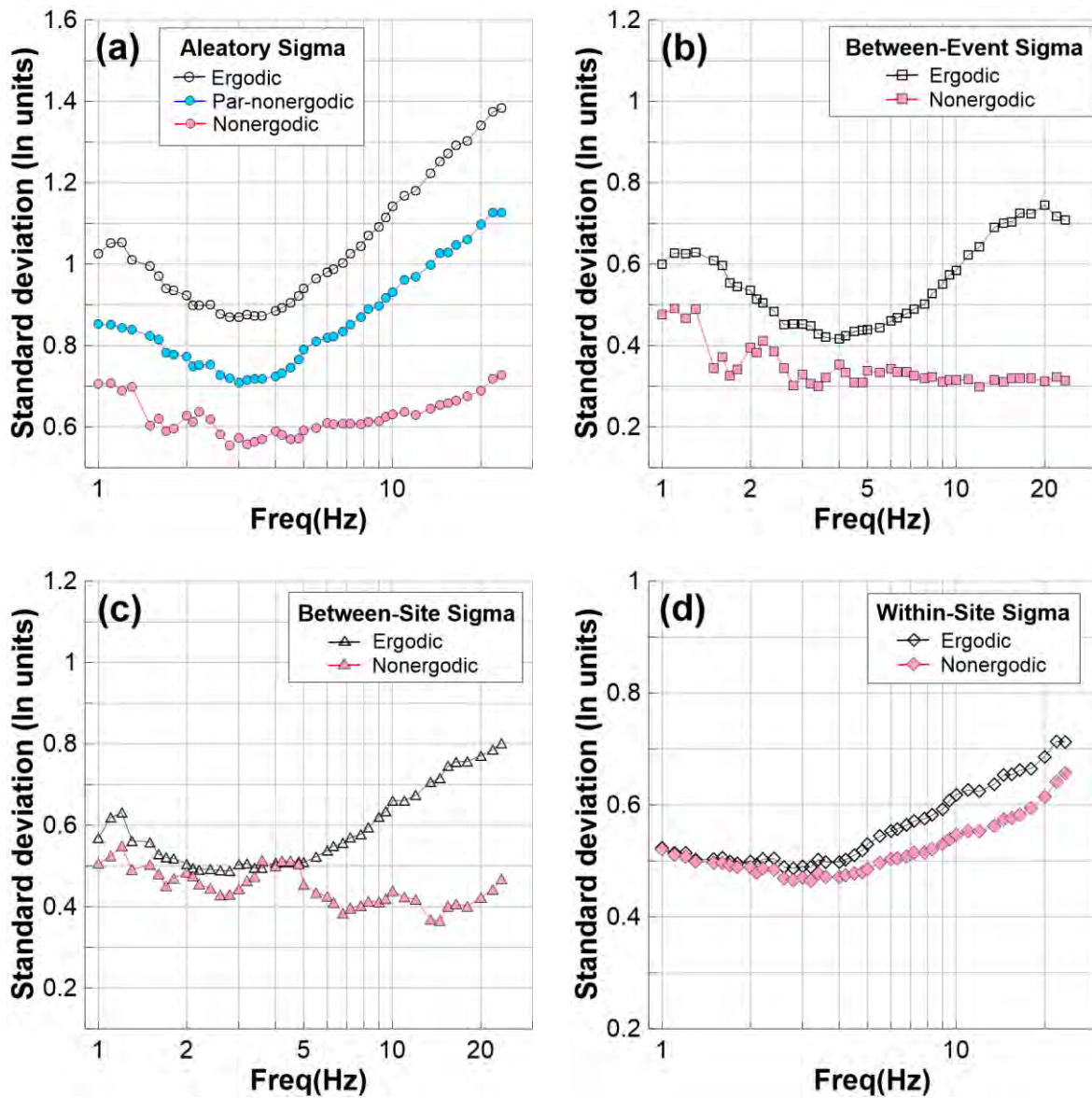
Figure 30. All kind of standard deviation of ergodic and non-ergodic GMMs. (a) aleatory, (b) between-event, (c) between-site, and (d) within-site standard deviations.
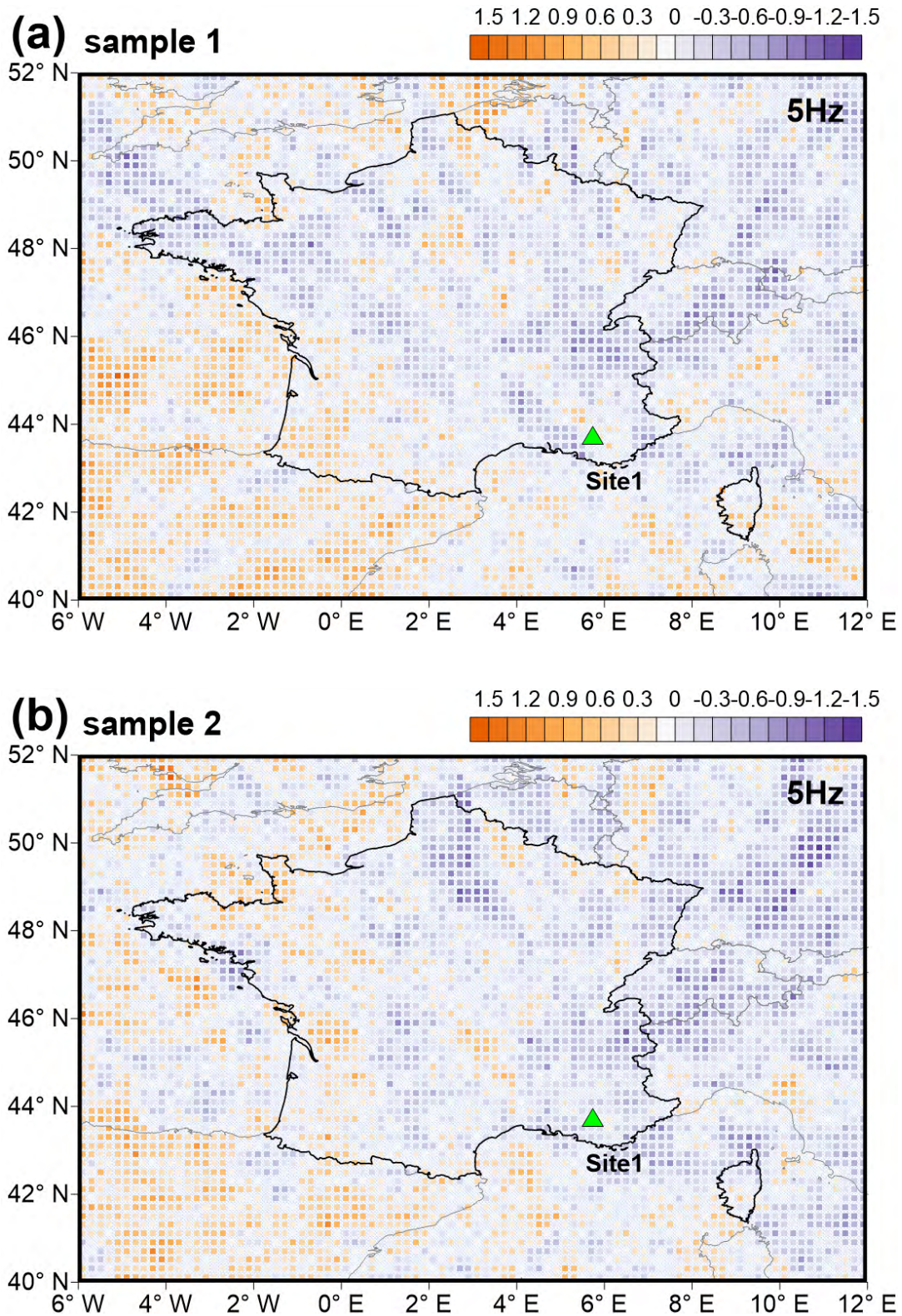
Figure 31. two samples of 100 maps for sampled adjustments for 5Hz at site1.
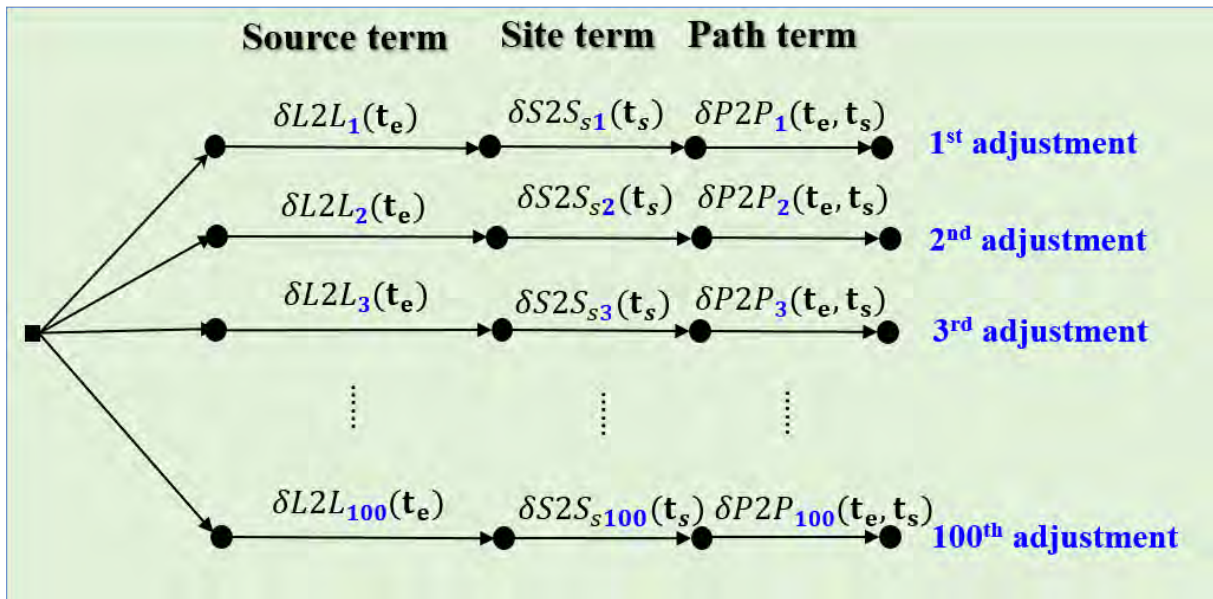
Figure 32. a logic tree with 100 branches of the non-ergodic terms for the GMM.
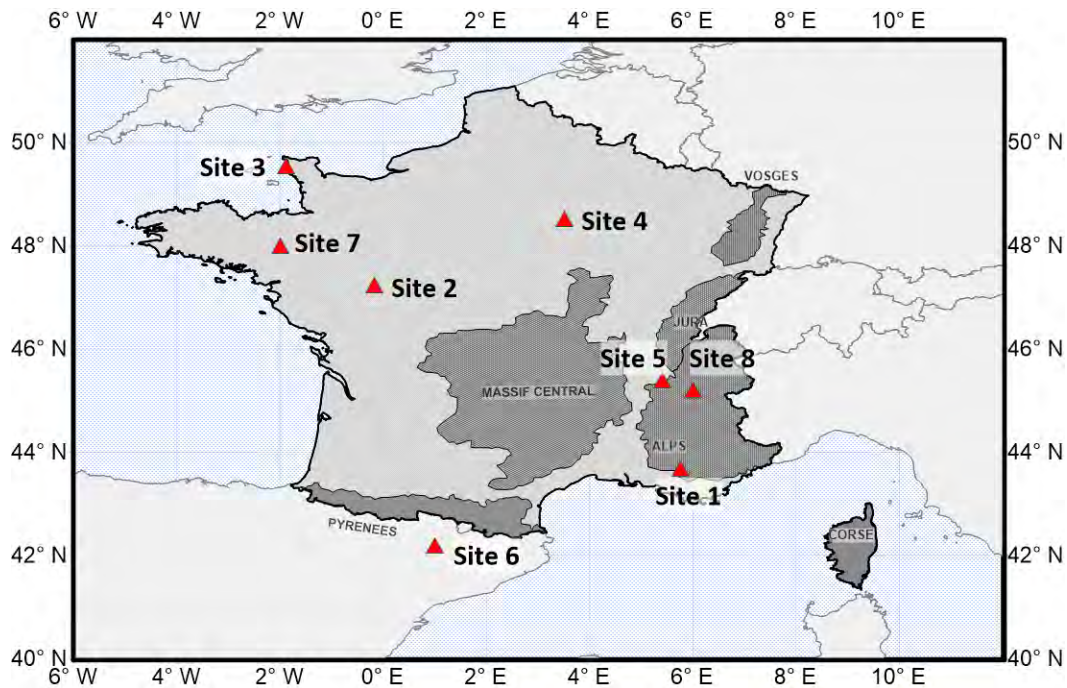
Figure 33. the locations of the selected sites in the PSHA calculation.

(a) Mean adjustment per source cell for Site1

(b) Mean adjustment per source cell for Site2
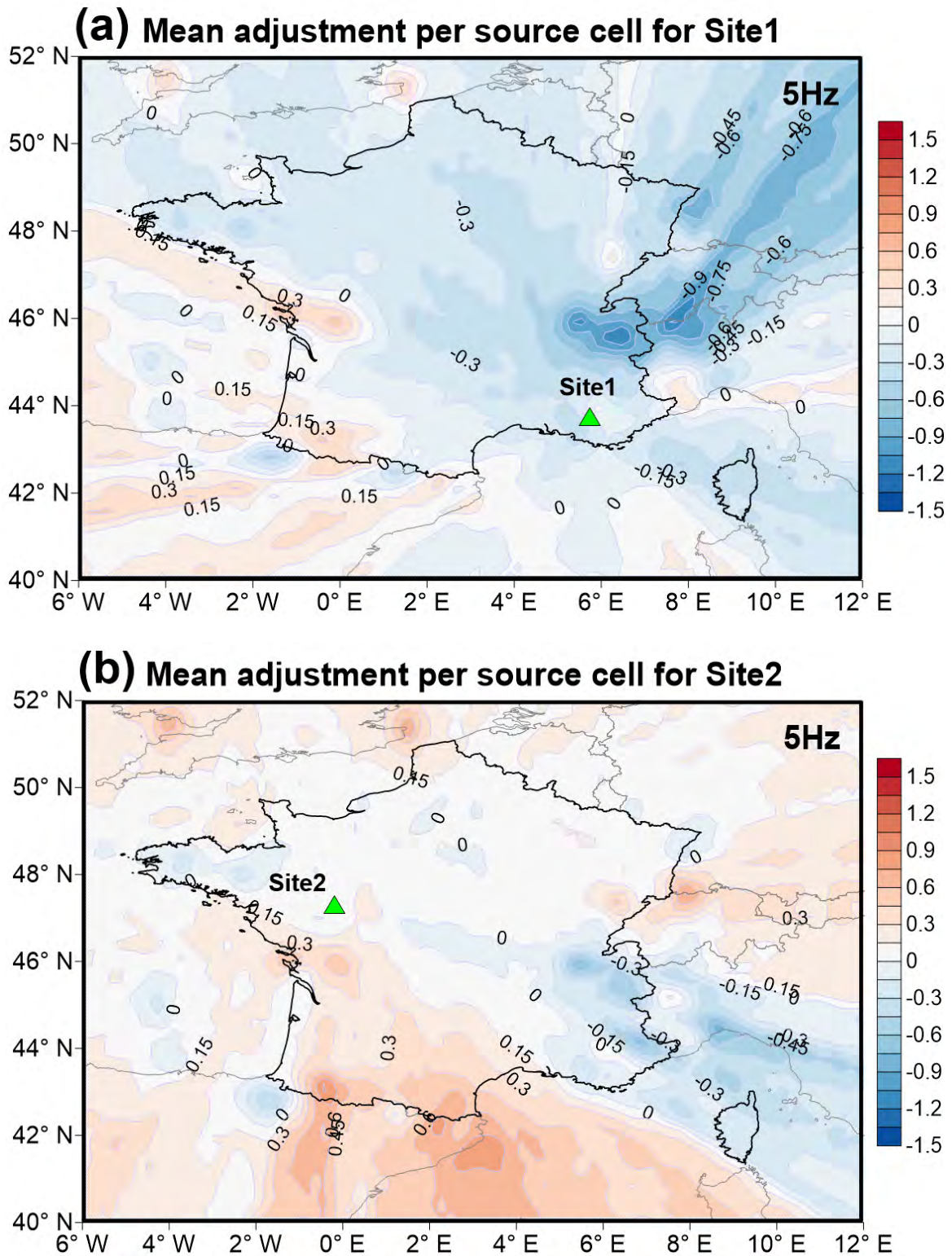
Figure 34 Mean residual of 100 residuals per cell, which are differences between an ergodic ln(EAS) and 100 non-ergodic ln(EAS) at (a) Site1 and (b) Site2 for 5.0 Hz.
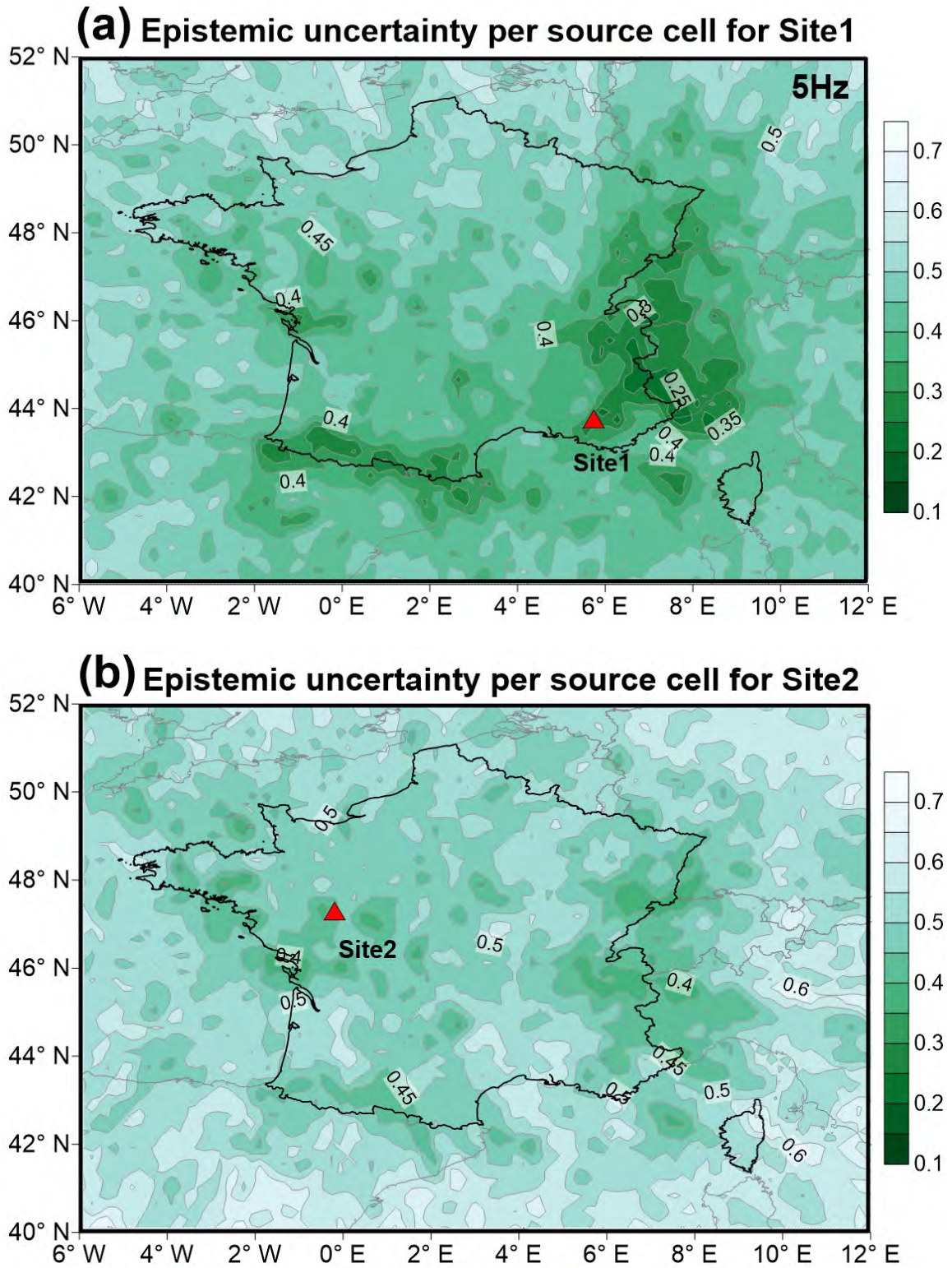
**Figure 35.** Standard deviation of 100 residuals per cell at (a) Site1 and (b) Site2 for 5.0 Hz.
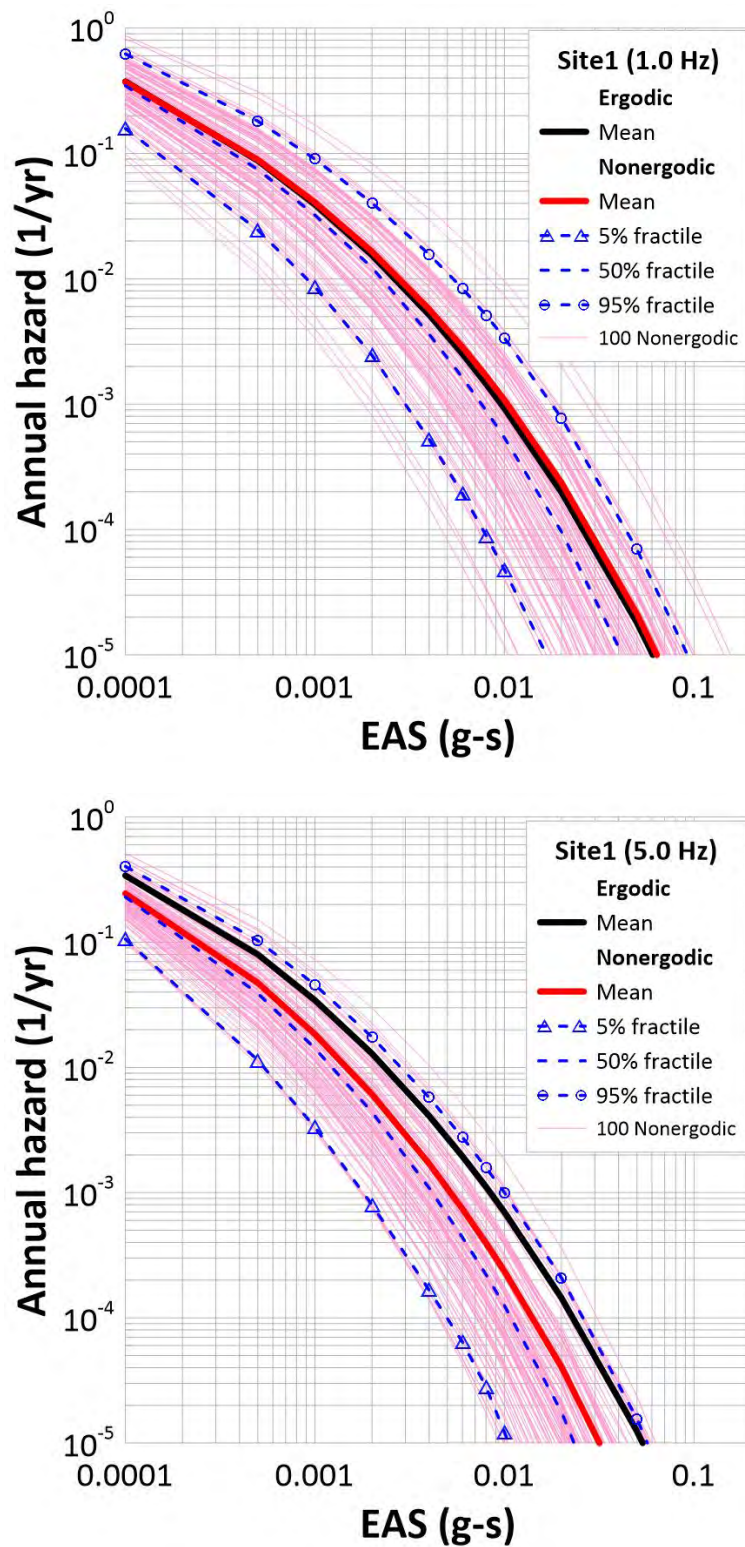
Figure 36. Mean hazard as well as 5%, 50%, and 95% fractiles of the resulting hazard curve distribution for Site1 for 1.0 Hz (upper) and 5.0 Hz (bottom)
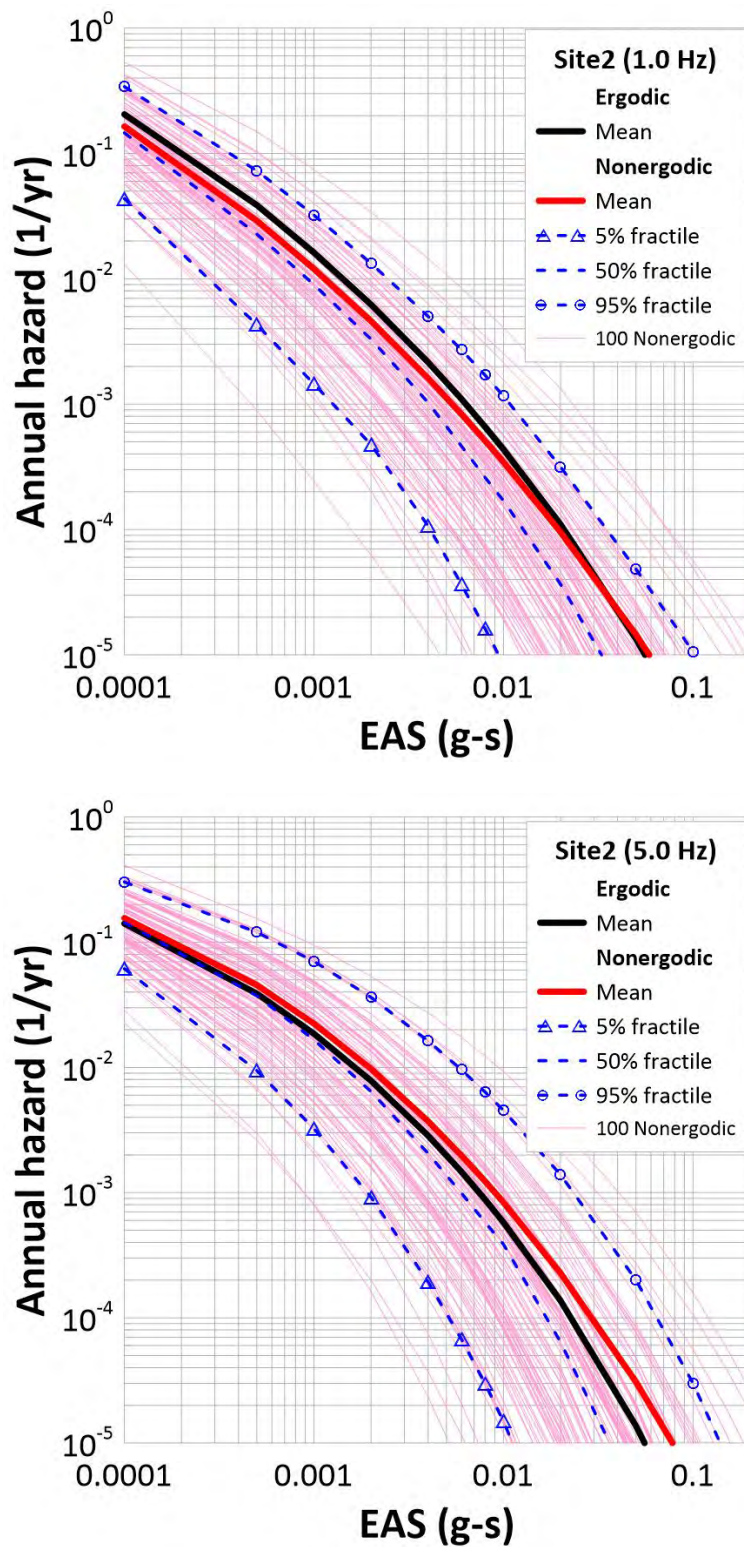
Figure 37. Mean hazard as well as 5%, 50%, and 95% fractiles of the resulting hazard curve distribution for Site2 for 1.0 Hz (upper) and 5.0 Hz (bottom).
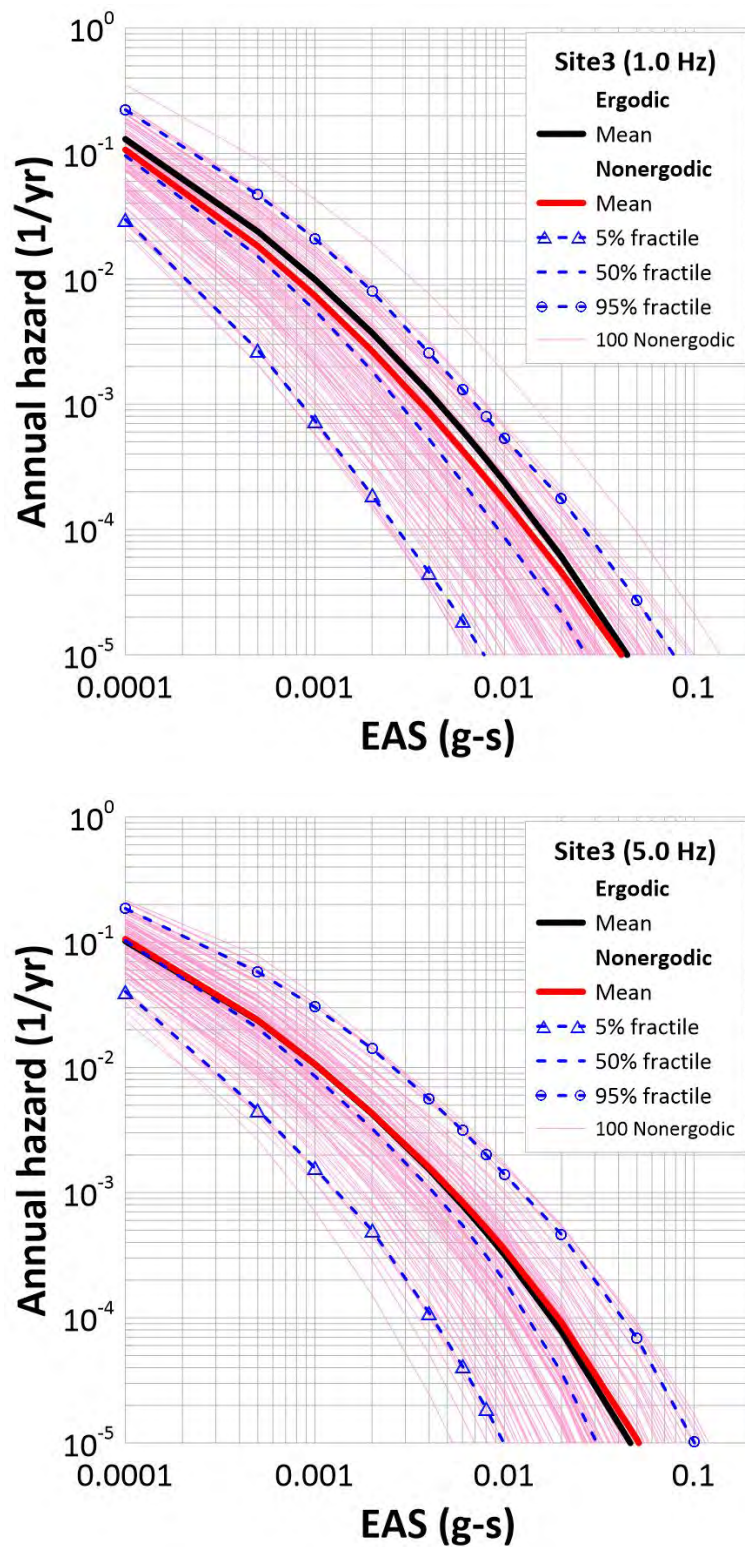
Figure 38. Mean hazard as well as 5%, 50%, and 95% fractiles of the resulting hazard curve distribution for Site3 for 1.0 Hz (upper) and 5.0 Hz (bottom).
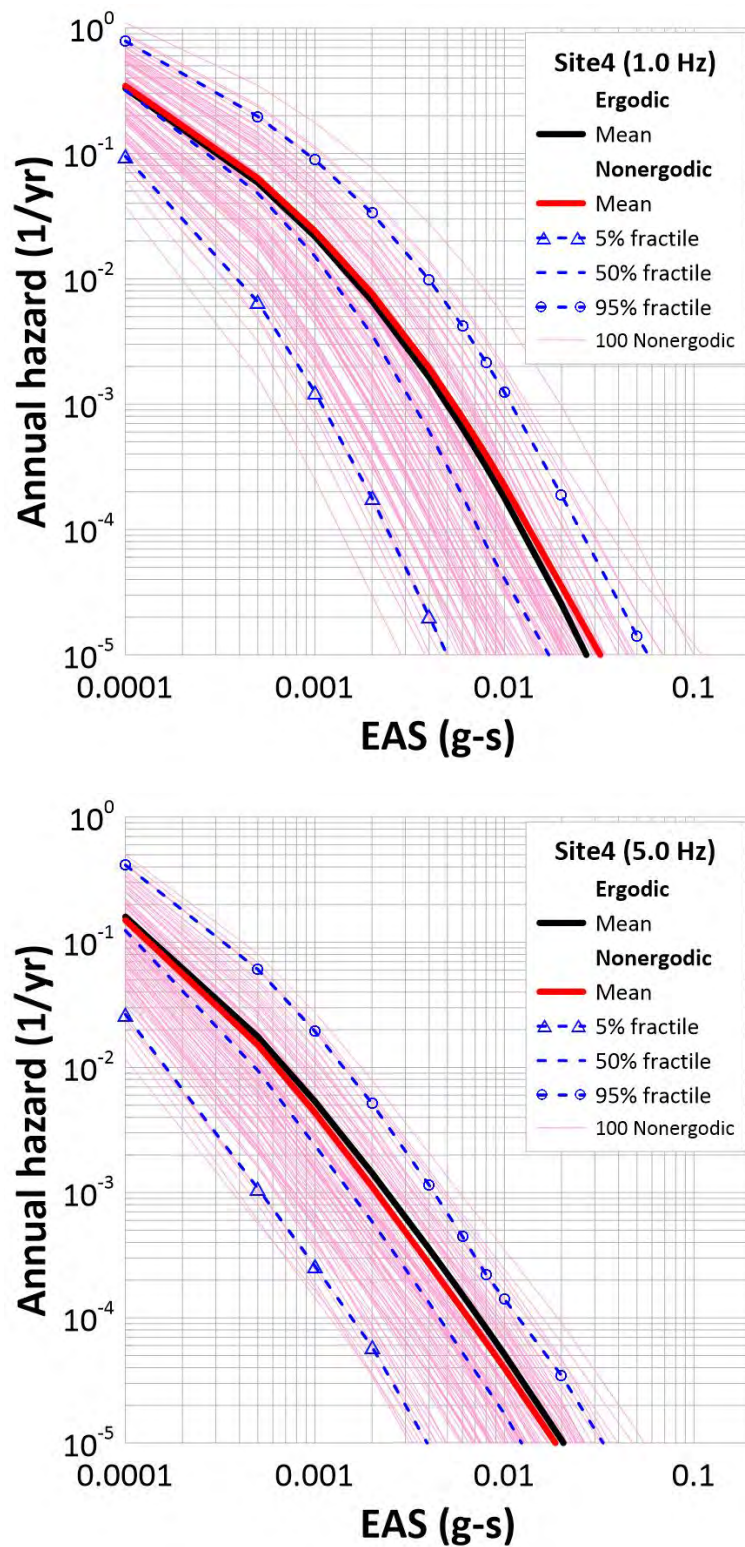
Figure 39. Mean hazard as well as 5%, 50%, and 95% fractiles of the resulting hazard curve distribution for Site4 for 1.0 Hz (upper) and 5.0 Hz (bottom).
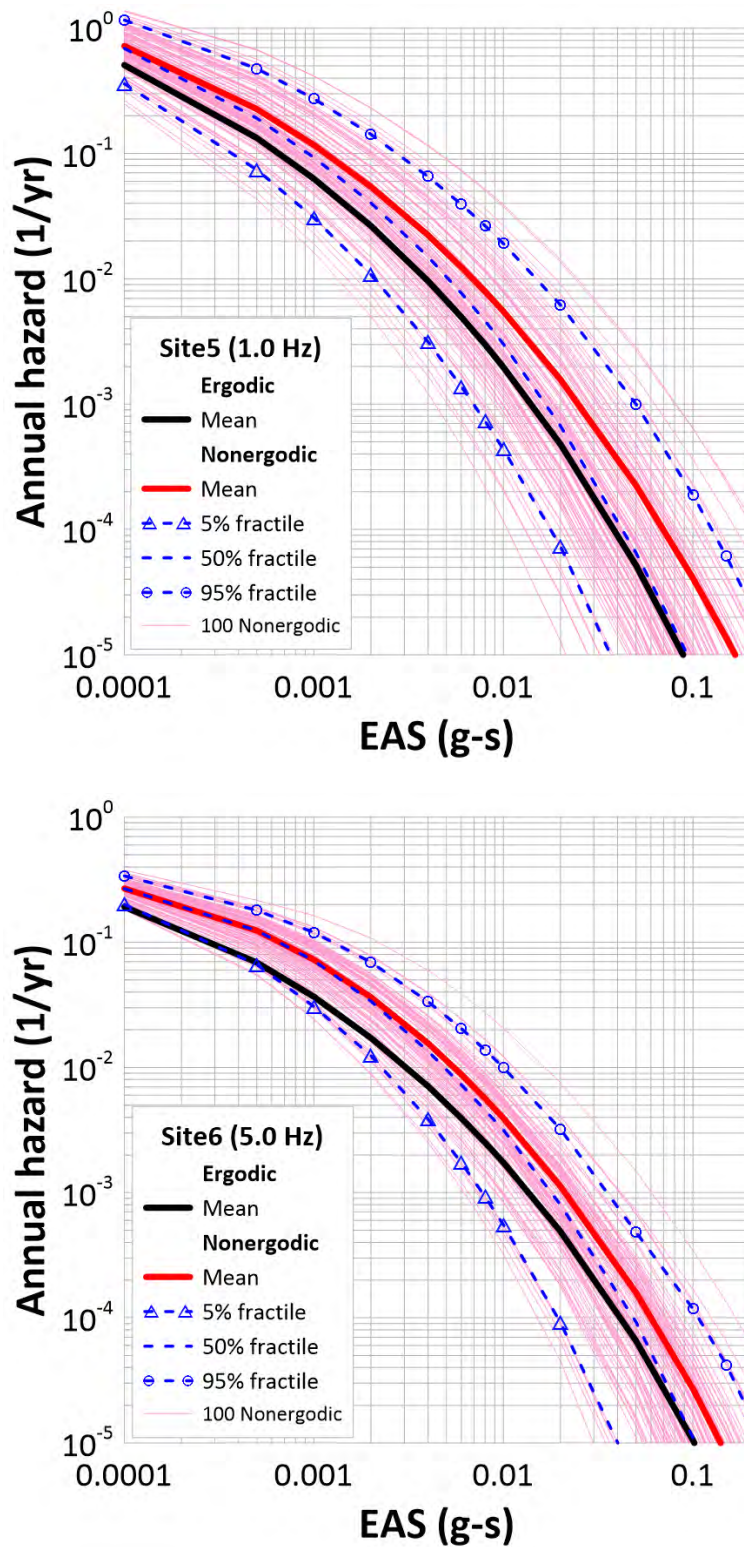
Figure 40. Mean hazard as well as 5%, 50%, and 95% fractiles of the resulting hazard curve distribution for Site5 for 1.0 Hz (upper), and for Site6 for 5.0 Hz (bottom).
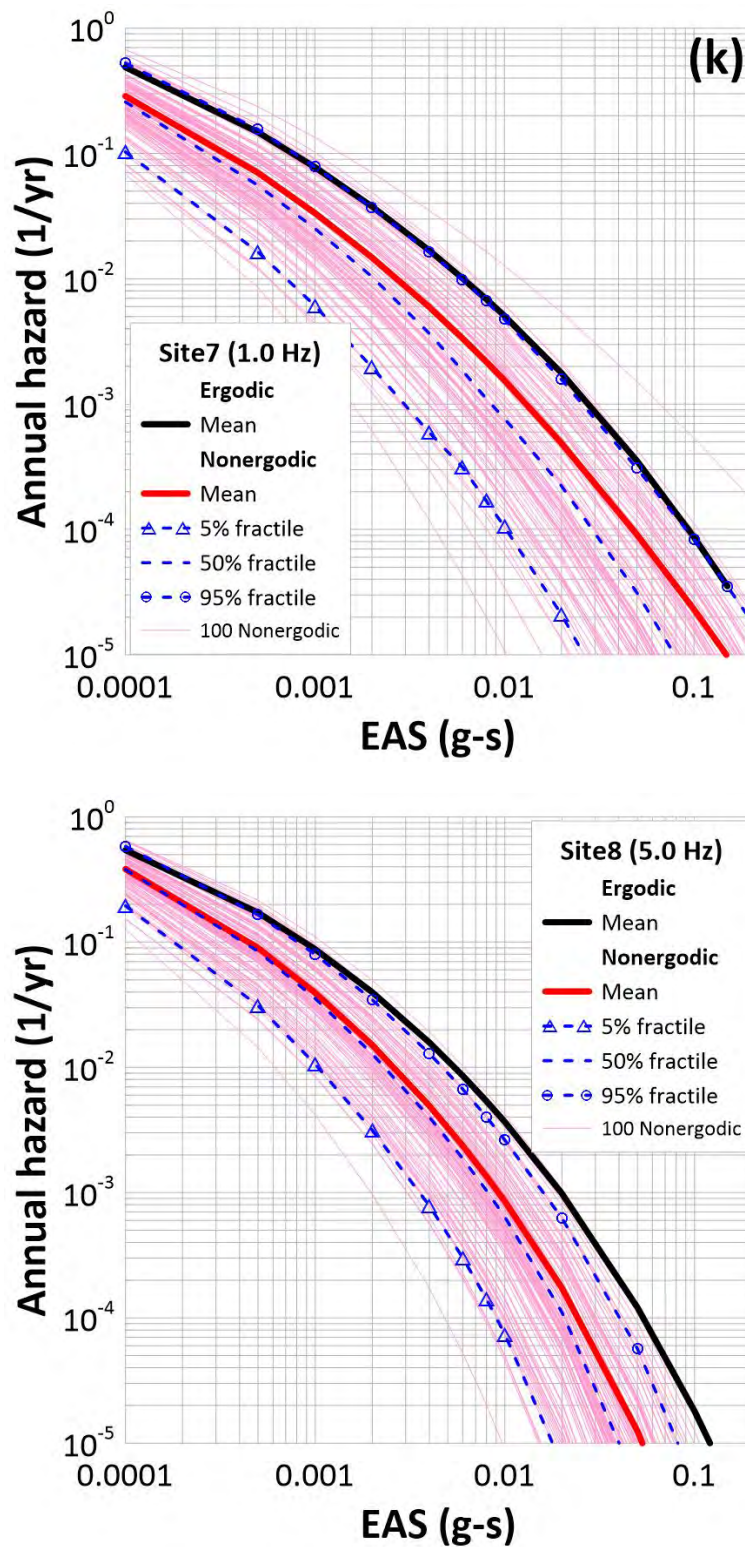
Figure 41. Mean hazard as well as 5%, 50%, and 95% fractiles of the resulting hazard curve distribution for Site7 for 1.0 Hz (upper), and for Site8 for 5.0 Hz (bottom).
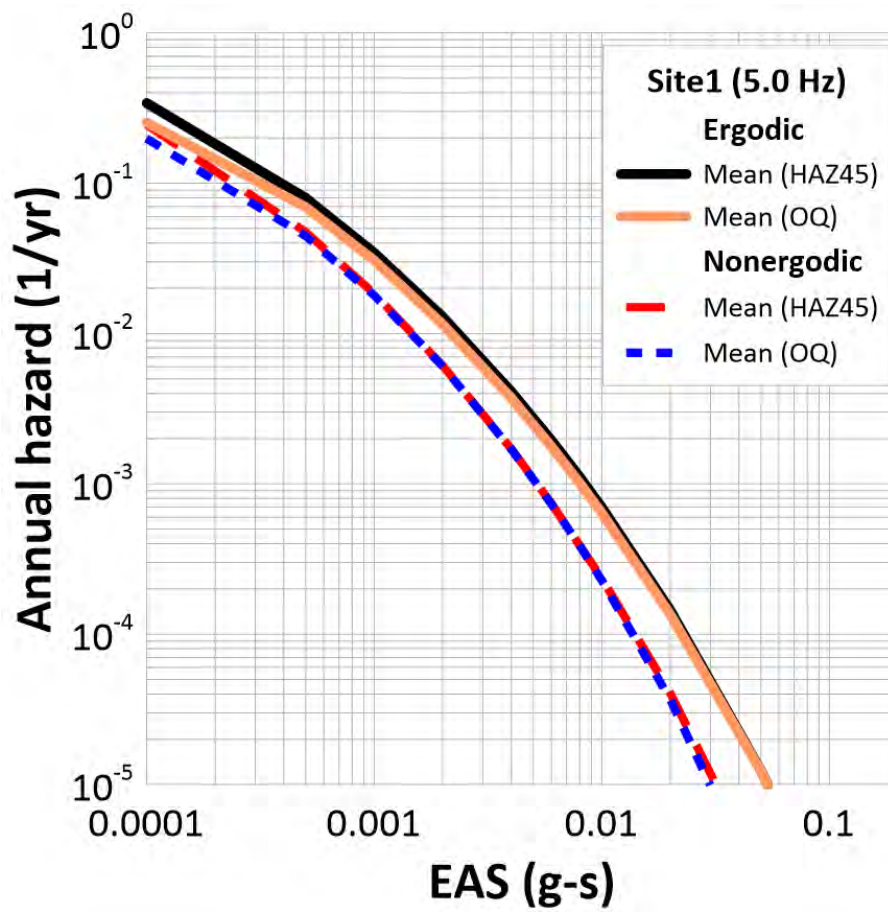
Figure 42. the verification of the ergodic and the non-ergodic PSHA codes by comparing the hazard results from OpenQuake with HAZ54.

APPENDIX A

Table A1. Coefficients of Ergodic Ground Motion Models from 0.1 to 0.9 Hz.

| Freq	N	c_1	c_2	c_3	c_4	c_5	c_6	c_7	c_8	c_9	c_n	c_m	c_{hm}	σ_T	τ	ϕ_{S2S}	φ_{SS}
0.1	49	3.645	0.27	1.402	1.86	0.5818	0.45	5.26E-05	0.755	0.0312	0.573	0.774	0.838	0.432	0.732	0.253	0.645
0.2	86	3.582	0.27	1.074	1.86	0.5818	0.45	0.0008	0.933	0.0315	0.928	0.432	0.837	0.184	0.240	0.200	0.652
0.3	498	3.541	0.27	0.881	1.86	0.5818	0.4501	0.0013	1.042	0.0303	0.228	0.220	0.836	0.117	0.935	0.366	0.599
0.4	077	3.514	0.27	0.763	1.86	0.5818	0.4502	0.0017	1.103	0.0256	0.474	0.072	0.834	0.114	0.795	0.445	0.599
0.5	659	3.494	0.27	0.681	1.86	0.5818	0.4503	0.0022	1.136	0.0193	0.680	0.963	0.833	0.065	0.731	0.453	0.579
0.6	303	3.474	0.27	0.604	1.86	0.5817	0.4505	0.0026	1.151	0.0116	0.900	0.861	0.830	0.072	0.708	0.497	0.551
0.7	699	3.460	0.27	0.555	1.86	0.5816	0.4507	0.0030	1.151	0.0066	0.060	0.798	0.827	0.065	0.693	0.521	0.546
0.8	081	3.447	0.27	0.506	1.86	0.5815	0.4511	0.0034	1.144	0.0022	0.243	0.735	0.822	0.061	0.688	0.517	0.53
0.9	459	3.435	0.27	0.466	1.86	0.5814	0.4514	0.0037	1.133	.0009	0.419	0.685	0.818	0.031	0.650	0.531	0.516

**Table A2.** Hyperparameters of Kernel Function from 0.1 to 0.9 Hz.

Freq	θ_{-1}	θ_0	θ_4	ρ_{-1}	ρ_0	ρ_4
0.1	6.73E-01	2.45E-01	1.50E-01	5.11E-01	10.64E-01	4.67E-01
0.2	3.60E-01	1.72E-01	1.49E-01	1.01E+00	7.14E-01	4.80E-01
0.3	2.30E-01	3.06E-01	1.50E-01	8.41E-01	1.79E-01	5.42E-01
0.4	4.80E-01	3.59E-01	1.50E-01	6.06E-01	3.80E-01	4.94E-01
0.5	4.48E-01	3.27E-01	1.51E-01	4.35E-01	5.87E-01	5.50E-01
0.6	5.93E-01	3.67E-01	1.50E-01	3.54E-01	3.62E-01	5.11E-01
0.7	4.33E-01	3.96E-01	1.50E-01	5.87E-01	7.06E-01	4.83E-01
0.8	4.27E-01	5.13E-01	1.47E-01	3.56E-01	1.30E+00	5.39E-01
0.9	4.87E-01	4.15E-01	1.49E-01	3.10E-01	1.03E+00	4.79E-01

Table A3. Mean and Standard Deviation of Posterior Distribution of θ_{ANTT}, standard deviation and the aleatory term for the fully non-ergodic models from 0.1 to 0.9 Hz.

| Freq	$\mu(\theta_{ANTT})$	$std(\theta_{ANTT})$	$\sigma_{T,non}$	τ_{non}	$\phi_{S2S,non}$	$\varphi_{SS,non}$	$\sigma_{alt,nonerg}$
0.1	-4.00E-03	1.05E-03	1.960	1.740	0.434	0.792	1.910
0.2	-2.90E-03	7.30E-04	1.397	1.140	0.349	0.729	1.350
0.3	-3.00E-03	7.34E-04	1.198	0.962	0.298	0.648	1.160
0.4	-2.97E-03	7.52E-04	0.981	0.676	0.334	0.628	0.23
0.5	-2.81E-03	7.04E-04	0.937	0.602	0.394	0.600	0.850
0.6	-2.94E-03	8.08E-04	0.810	0.430	0.394	0.562	0.708
0.7	-3.29E-03	8.84E-04	0.898	0.549	0.444	0.555	0.781
0.8	-3.44E-03	9.61E-04	0.831	0.466	0.433	0.535	0.710
0.9	-3.66E-03	1.09E-03	0.800	0.390	0.466	0.520	0.650

APPENDIX B
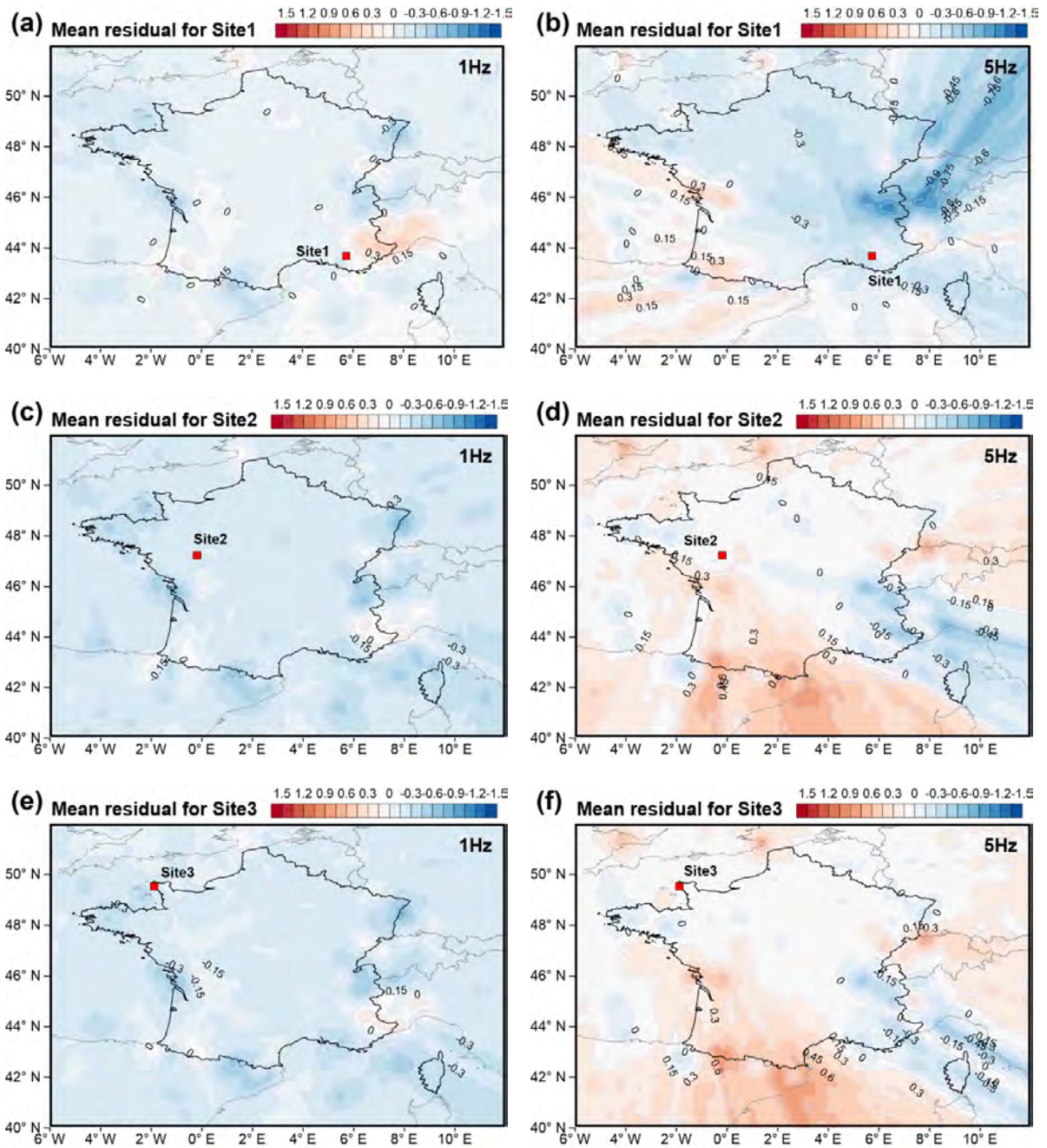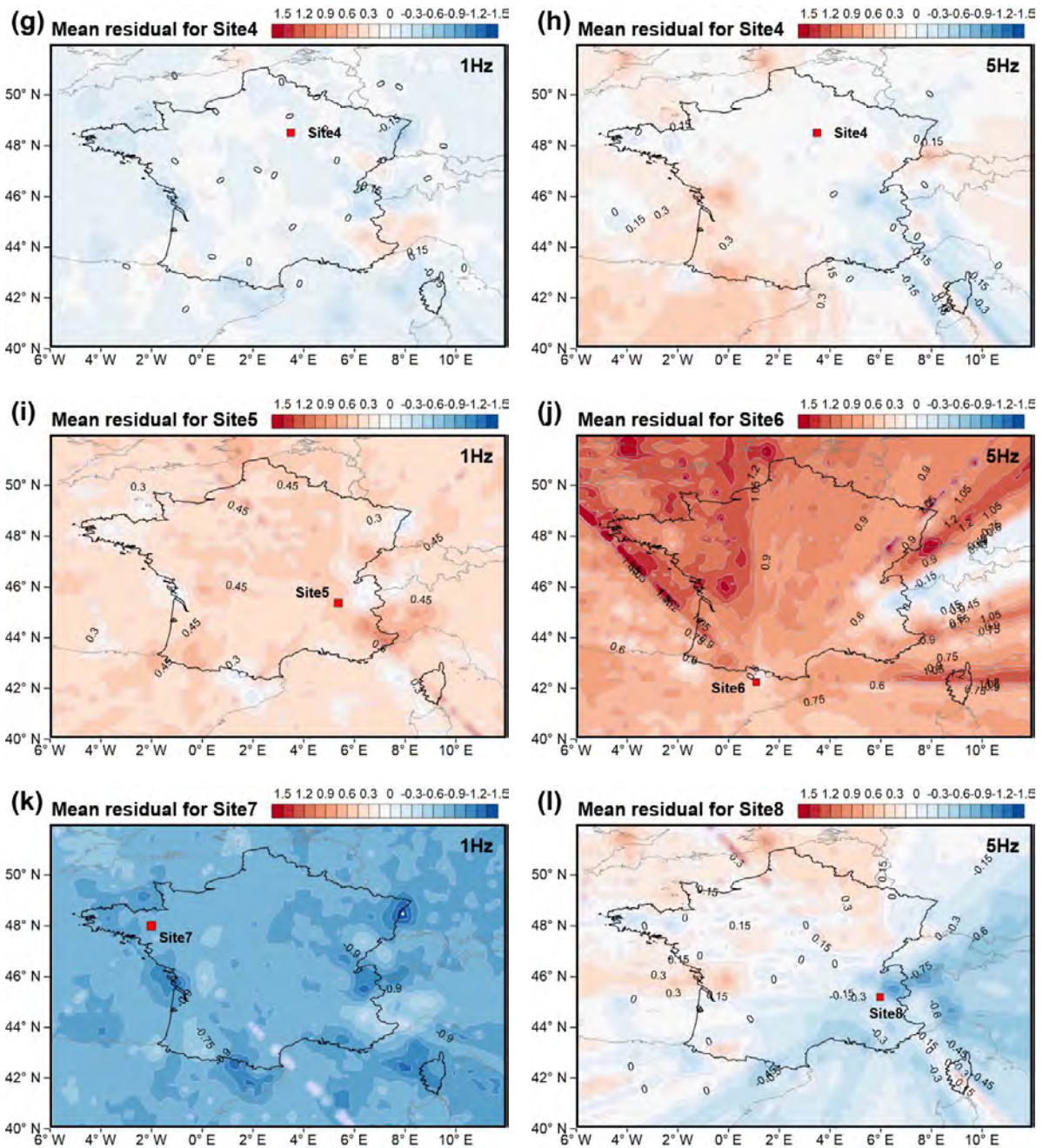
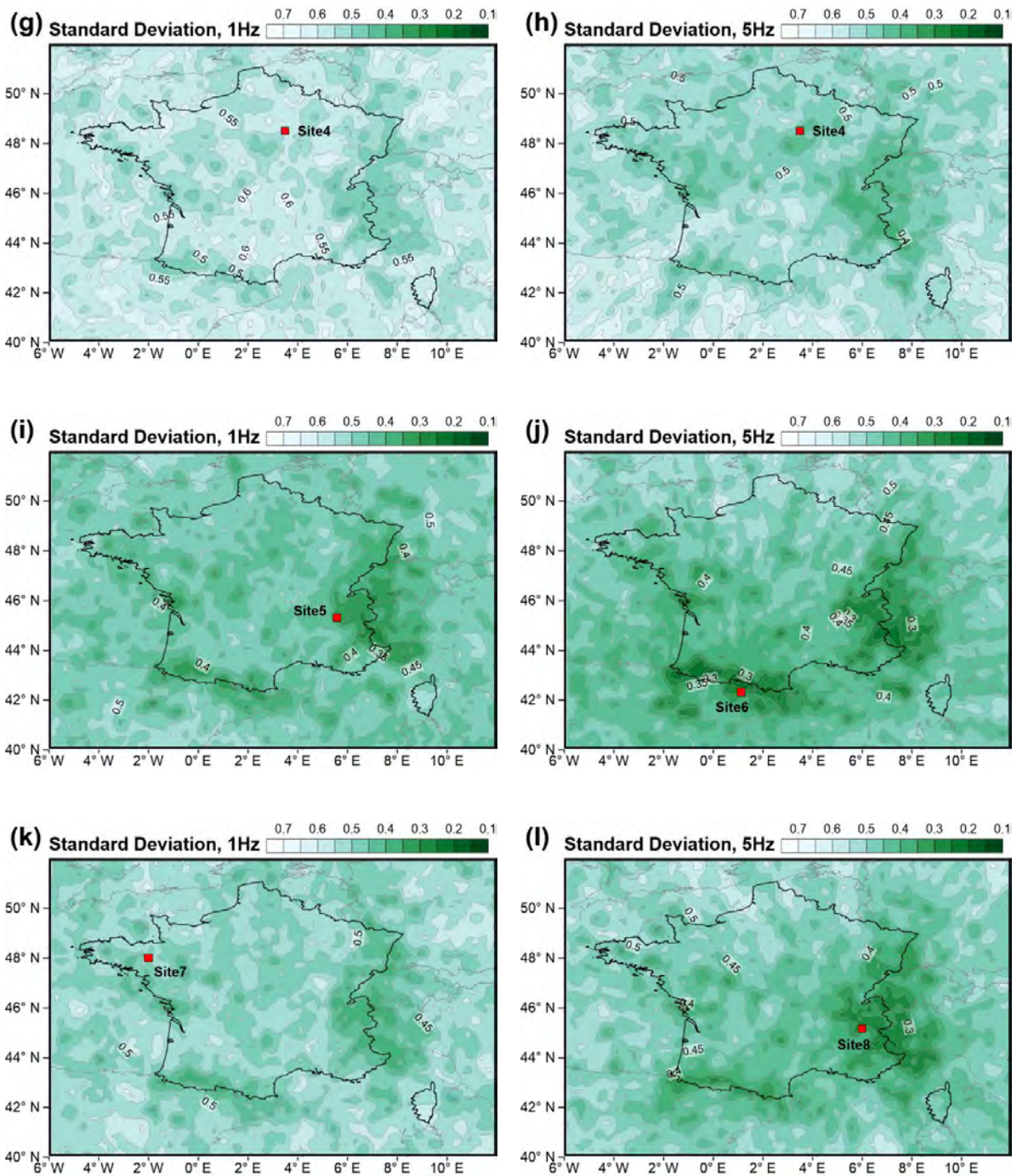**Figure B1.** Mean residual of 100 residuals per cell, which are differences between an ergodic ln(EAS) and 100 non-ergodic ln(EAS) at (a) Site1 for 1.0 Hz, (b) Site 1 for 5.0 Hz, (c) Site2 for 1.0 Hz, (d) Site2 for 5.0 Hz, (e) Site3 for 1.0 Hz, (f) Site3 for 5.0 Hz, (g) Site4 for 1.0 Hz, (h) Site4 for 5.0 Hz, (i) Site5 for 1Hz, (j) Site6 for 5Hz, (k) Site7 for 1Hz, and (l) Site 8 for 5Hz.

APPENDIX C
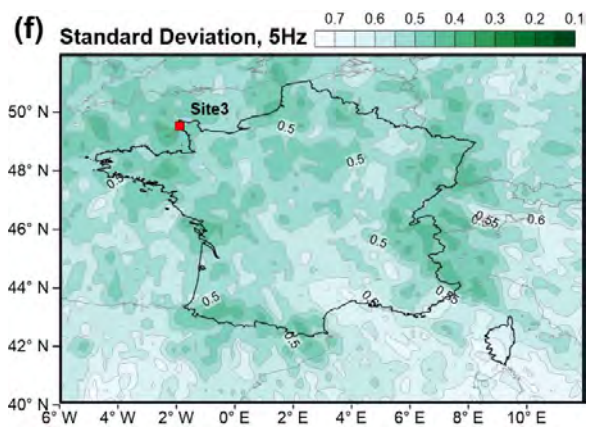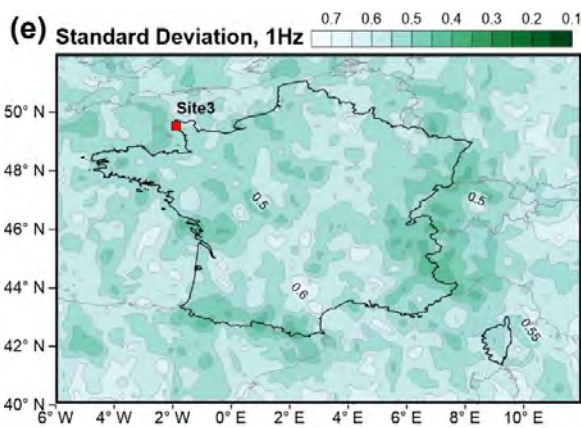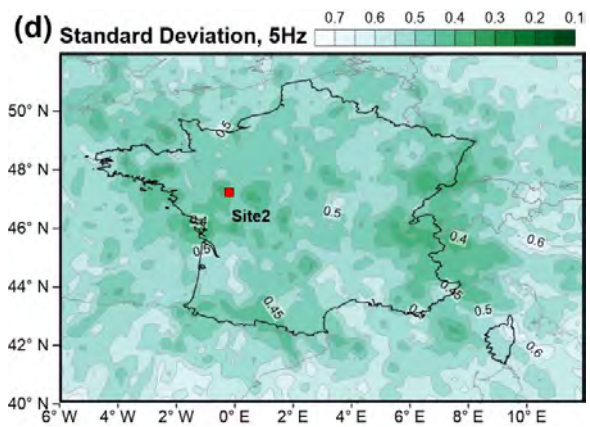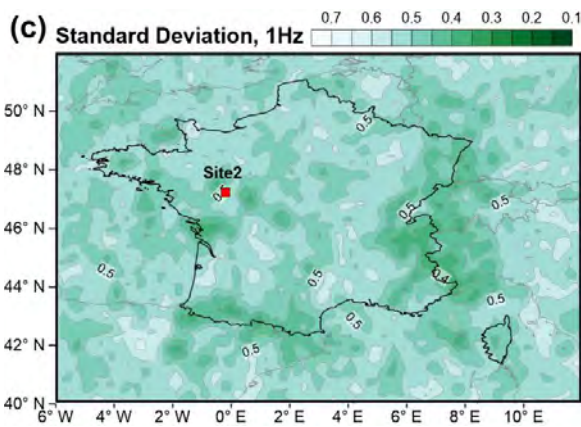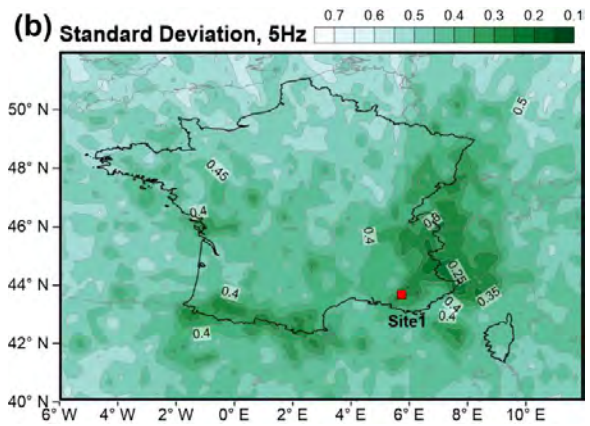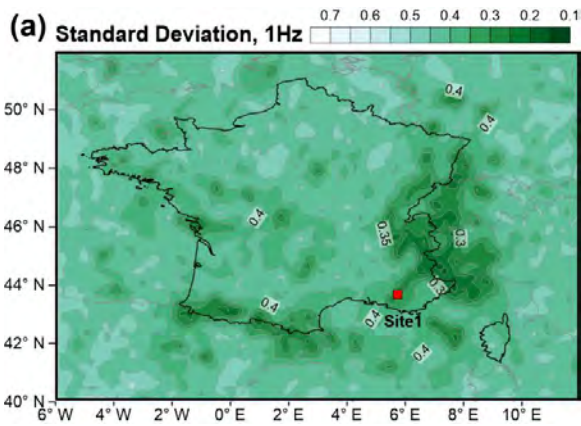
Figure C1. Standard deviation of 100 residuals per cell at (a) Site1 for 1.0 Hz, (b) Site1 for 5.0 Hz, (c) Site2 for 1.0 Hz, (d) Site2 for 5.0 Hz, (e) Site3 for 1.0 Hz, (f) Site3 for 5.0 Hz, (g) Site4 for 1.0 Hz, (h) Site4 for 5.0 Hz, (i) Site5 for 1Hz, (j) Site6 for 5Hz, (k) Site7 for 1Hz, and (l) Site8 for 5Hz.